UNIVERSITY OF TROMSØ UIT

FACULTY OF SCIENCE AND TECHNOLOGY
DEPARTMENT OF GEOLOGY

The Nussir copper deposit: petrology, mineralogy, geochemistry and distribution of ore mineralization

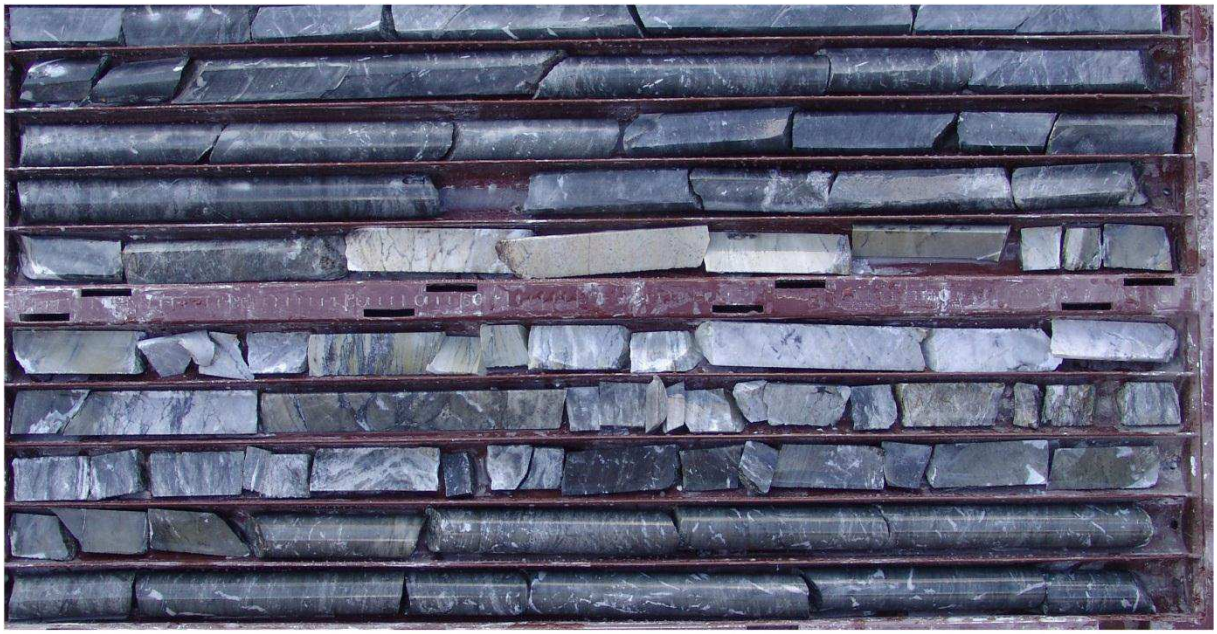

Yulia Mun

GEO-3900 Master's Thesis in Geology

August 2013

ABSTRACT

The geology, petrography, mineralogy and geochemistry of the Nussir copper deposit in Finnmark, Northern Norway were studied during writing this thesis. The Nussir deposit of copper is a sedimentary-hosted hydrothermal deposit affected by low grade methamorphism and ductile deformation. The copper mineralization includes chalcopyrite, chalcocite, bornite, covellite, and digenite. The deposit contains also economically interesting trace elements, such as silver, gold, and PGE. The deposit shows a vertical zonation of ore minerals, accordingly from top to bottom: pyrite, chalcopyrite, silver minerals, galena–bornite–digenite, chalcocite, and covellite.

Acknowledgments

This thesis would never be possible to be written without a financial support from SIU (Senter for internasjonalisering av utdanning) and "CPEA-2010/10105 - Cooperation in geology between Norway and Uzbekistan" project.

First I would like to thank my supervisor Kåre Vidar Kullerud for giving me the opportunity to do a master thesis at the University of Tromsø under his professional supervision.

My summer job in 2012 was provided and organized by Øystein Rushveldt (CEO of the Nussir ASA). I do appreciate his help and that he introduced me to new and extremely interesting people both from the company and local community of Kvalsund fylke. Many thanks to Magne Martinsen (chief geologist, Nussir ASA), Rasmus Blomqvist (former chief geologist, Nussir ASA, currently consulting geologist at Oy Atlas Geoconsulting Ab), Knut Emil Thommassen for providing me with samples, which were used during this study, and making my stay in the Repparfjord region comfortable and enjoyable. My special thank I would like to address to Kjell S. Nilsen for interesting and useful discussions, and wonderful field work period.

I am very grateful to José Perello and John Clifford for extensive scientific advice and directing me in my research.

I would like to express my gratitude to the laboratory assistants at the Department of Geology of the University of Tromsø for timely preparation of polished thin sections and Prof. Erling Krogh Ravna for his assistance during the work with XRF.

I would like to thank all my friends for nice time we have spent together in Tromsø, and special thanks to Nadya Priyatkina for her limitless enthusiasm in sharing her scientific experience and knowledge, and many pieces of good advice I have got from her.

And last but not least I thank my Italian-Uzbek-Russian family for support and believe in me.

Yulia Mun

August, 2013

Contents

Introduction 3
Chapter 1. Geological settings of the Baltic Shield 5
Chapter 2. Geological setting of the Nussir deposit 11
Chapter 3. Petrography 15
3.1. Method and technique 15
3.2. Lithology 15
Chapter 4. Geochemistry 21
4.1. Methods and technique 21
4.2. Major oxides 22
4.3. Trace elements 28
4.4. Ore elements 29
4.5. ICP-MS analyses 38
Chapter 5. Mineral chemistry 41
5.1. Analytical procedure 41
5.2. Mineral chemistry 42
Chapter 6. Discussion 49
Conclusion 53
References 55

Appendix 1

3.1. Drill hole NS-08/06

3.2. Drill hole BH60

Appendix 2

Introduction

The interest in finding and investigating mineral resources in Norway has been growing year by year during the last decade. The study of discovered deposits might contribute to enhancing the knowledge and understanding of ore deposit diagenesis, and the geological and tectonic settings of the Norwegian deposits.

The scope of this thesis is to understand the characteristics of copper mineralization distribution along a geological section of the Nussir copper deposit, and to investigate the variations in ore content depending on different lithologies of the deposit.

The Nussir deposit of copper was firstly discovered by Kjell Nilsen during his field work in Repparfjord area in 1979 (Kjell Nilsen, pers. comm. 2011). Recently the deposit has been drilled by the company Nussir ASA (established in 2005). Start-up of production is planned for 2015-2016. Figure 1 shows the territory that was claimed and pre-claimed by the Nussir ASA company for mineral exploration.

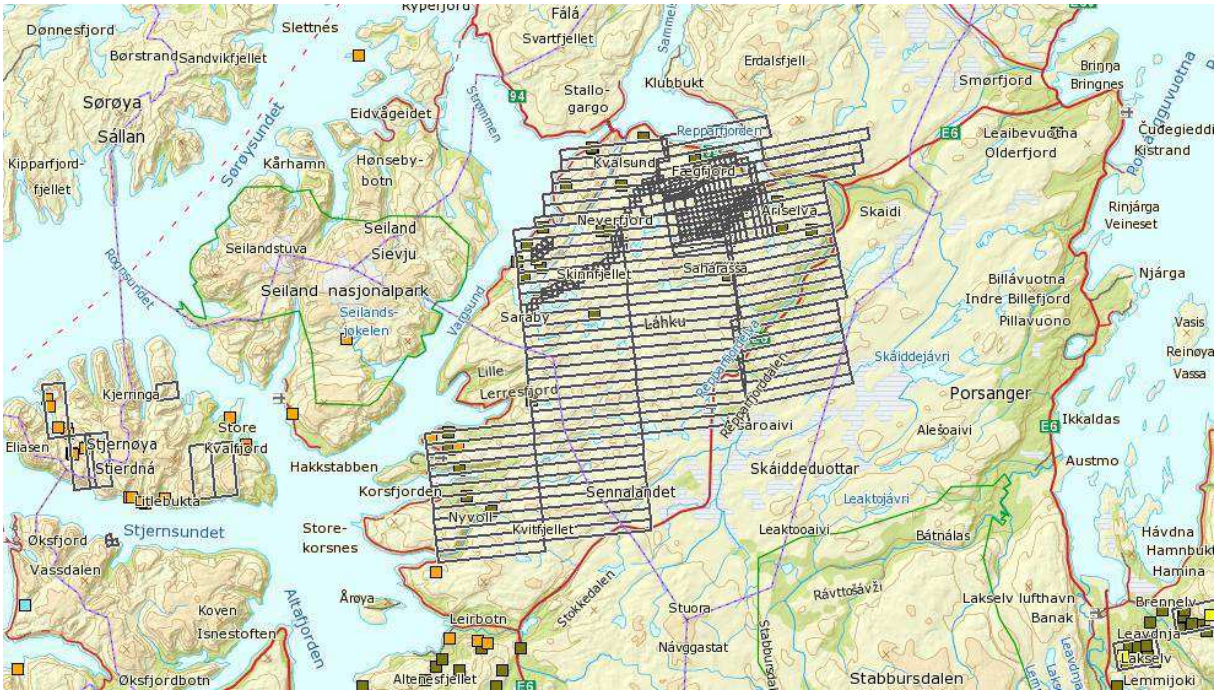

Figure 1. *Area claimed in order to conduct exploration and mining. Finnmark. Northern Norway. Source:* http://www.ngu.no/kart/mineralressurser/.

- Area claimed by Antaeus AS

- Area claimed by Nussir ASA

After the discovery of copper mineralization, research was conducted by the Geological Survey of Norway, and economically interesting trace elements such as Au, Ag and PGE (Platinum Group Elements) were found in the ore (Sandstad, 2010).

Administratively the Nussir deposit is located in the municipality of Kvalsund in Finnmark, Northern Norway.

The Nussir deposit is located in the Repparfjord Tectonic Window in Caledonides of West Finmark. The host rock is represented by Paleoproterozoic metasediments and metavolcanites that have been intruded by mafic, ultramafic and felsic intrusive rocks. The bedrock has undergone strong ductile deformation (Viola, 2008).

Chapter 1. Geological settings of the Baltic Shield

The Reppafjord Tectonic Window is a part of a huge domain that occupies the north-western part of Eurasia (Norway, Sweden, Finland, North-Western part of Russia and the territory under the Baltic Sea) and is called Baltic Shield (or Fennoscandian Shield) (Fig. 1.1).

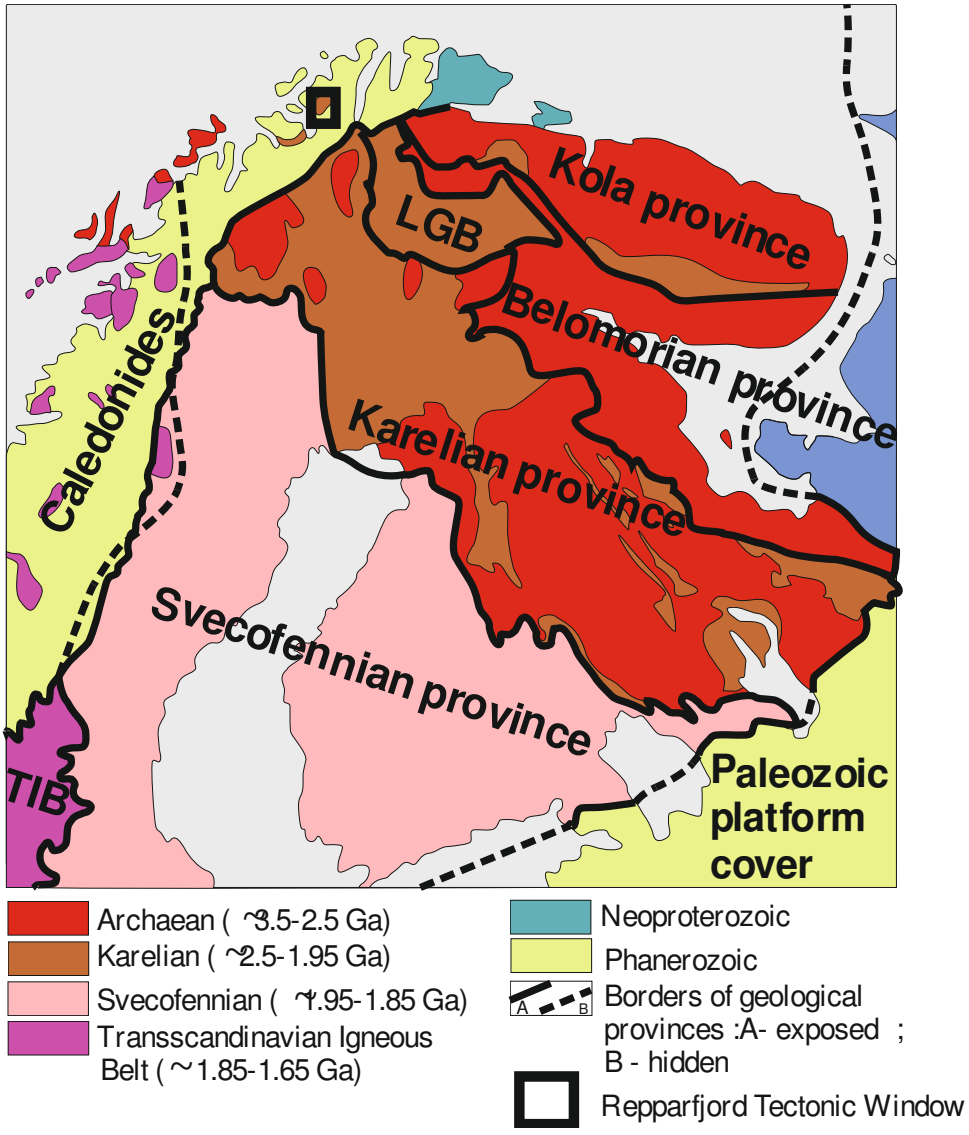

Figure 1.1. *Schematic geological map of the Baltic Shield. Simplified by Priyatkina (2013) after Koistinen et al. (2001), Gaal and Gorbatchev (1987)*

The oldest rocks of the Fennoscandian Shield are of **Archaean age**. They are found in the northeast, in Karelia (also called Fennokarelian Province), the Kola Peninsula, and northeastern Finland. They are mainly represented by gneisses and greenstone belts formed as a result of subduction (ensialic and ensimatic), spreading, continental rifting, mantle plumes, and collision with widely spread granitoids related to the mentioned

geodynamic setting (R.Gorbatschev et al., 1993, Slabunov et al., 2006). Indication of an early Archean cycle older than 2800 Ma are observed. They partly formed an ensialic basement for the greenstone belts. Slabunov et al. (2006) suggested that the formation of Archaean core took place between 3.1-2.5 Ga and was related to the accretionary and subduction geodynamic settings that were accompanied by continuous and intense mantle-plume activity. The Karelian and Kola provinces are separated by the early Proterozoic (~1.9Ma) collisional Lapland Granulite Complex (LGC) to the west. The Karelian Province is mainly composed by granitic gneisses (~3.1Ga) and Archaean greenstone belt sequences erupted between 2.9 and 2.7 Ga. (Slabunov, et al., 2006). The Kola Province predominantly contains granodioritic gneisses (2.9-2.6 Ga). The Lapland Granulite Complex has SW strike and was formed under medium pressure (P=7-8 kbar, T=800°C) (Pharaoh et al., 1990). In northeast, the Karelian Province is adjoined forming tectonic contact to the **Belomorian Belt**, which is characterized by high grade gneisses showing penetrative foliation and high pressure metamorphism. The geological settings are similar to those of the Karelian Province, in many cases, but differ by the presence of more abundant mafic volcanics and tonalitic-granodioritic plutonics (~2.8-2.7 Ga). Slabunov et al. (2006) supposed that the Belomorian greenstone belt is a metamorphosed tectonically disintegrated fragment of the Mesoarchean ophiolitic association.

Volcano-sedimentary deposits unconformably overlying TTG (tonalite-trondhjemite-granodiorite composition) gneiss complex divides the region into a binary structure and show the existence of the major tectonic event taken place in early crustal evolution which is called the Lapponian orogeny (2.5-2.3Ga). The age of this rifting event is still controversial and varies between Late Archaean and Early Proterozoic though relative observations proof more likely Late Archean age (Qian, 1997). The Lapponian greenstone belt is composed of felsic rocks occurring among predominantly basaltic-komatiitic volcanics of the Palaeoproterozoic riftogenic volcanic belts. 2.3-2.1 Ga ago the rifting of the Archaean craton continued with the Jatulian riftogenesis and the formation of widely spread mafic dike swarms accompanied by mafic volcanic rocks and sills (Mertanen, et al., 2005, Gorbatschev, et al., 1993).

The territories of Central Finland (Tampere), central and northern Sweden are covered with **Svecofennian** (called also **Svecokarelian**) rocks having an age between 1.92

to 1.87 Ga. They are distributed between the northeastern edge of the Archaean craton and the southern boundary of the Shield. In the western part the rocks of the province plunge under the Caledonides. From south-east the Svecofennian margin curves along a Proterozoic-Archaean boundary. Lithologically, the Svecofennian Domain is divided into two parts separated by the geological depression called the "Bothnian Basin" that is composed of greywackes and metapelitic rocks. The Bothnian Basin is enhanced between 2 belts of volcanic rocks. In the northern Sweden it is "Skellefte Field" and in south-central Sweden it is an area of "leptite" volcanics (fine-grained quartz-K-feldspar metavolcanic rock) referred as the "Bergslagen Field". All of the components of the Svecofennian Domain were deformed during at least two stages (Ehlers, 1993) and subjected to variable degree of metamorphism from greenschist and amphibolite to locally granulite facies. All over the rocks have been intruded by large massifs of syn-, late- and post-orogenic granite and granodiorite complexes (Pharaoh et al., 1990; Gorbatschev et al., 1993). They were most likely formed during the mantle differentiation related to subduction. Besides the features of high heat flow and more extensive melting in the mantle wedge above the subduction slab were discussed by Gaál (1987).

The northern part of the Svecofennian Domain is crosscut by the remarkable belt of porphyritic intermediate and felsic lavas erupted sub-aerially during the Svecofennian Orogeny, this belt is called Norrbotten Porphyry Arc (1.89-1.87 Ga) (Lundberg, 1980). The belt continues onto the Archaean craton and may extend in the north-western direction into the Lofoten Granulite Complex (Griffin et. al, 1978).

About 1.8-1.6 Ga ago, due to the resumption of subduction directed eastward beneath the recently accreted early Proterozoic and cratonized Archaean segments, an intrusion of granitic plutonic rocks took place in the western margin of Svecofennian province forming 1600 km-long and 20-150 km-wide **Transscandinavian Igneous Belt (TIB)** (Pharaoh et al, 1990, Ramberg et al., 2008). Porphyries were formed in at least three different episodes. It could be followed from southern Sweden (Småland) northward to Lofoten and then continues under much of the Caledonian mountain chain up to northern Scandinavia. Lithologically it is characterized by high alkali-calsic composition series of porphyritic volcanic rocks (mostly ignimbritic tuffs) and plutonic rocks of quartz-monzodiorites to granites.

Southwest of the TIB follows the **Southwestern gneiss province** (also known as the **Sveconorwegian orogenic belt**), which has a long and complex evolution ranging from c. 1700 to 900 Ma ago and was formed as a result of the collision between Fennoscandia and another plate, possibly Amazonia at the end of Mesoproterozoic (Bingen et al., 2008). The belt is subdivided into 5 parts from east to west. The eastern most part is traditionally called Eastern Segment and is followed by 4 terrranes being different lithotectonic units: Idefjorden, Kongsberg, Bamble and Telemarkia (Bingen, 2008). Lithologically, the Eastern Segment is a continuation of the Transscandinavian Igneous Belt and composed of various gneissic granitoids intruded by different uneven-aged mafic dykes and granitic dykes and plutons. The rocks were subjected to amphibolite-facies metamorphism that is dated as 1460-1410 Ma. The degree of metamorphism increases from north to south and from east to west (Johansson, 1991). The bedrock of the Idefjorden, Kongsberg and Bamble Terranes was originally formed during the Gothian orogeny that took place 1700-1550 Ma ago. They are mainly represented by calc-alcaline and tholeitic plutonic and volcanic rocks, associated with greywacke-bearing metasedimentary sequences that have been gone through amphibolite facies metamorphism. Supracrustal rocks of the Telemarkia series are dominating in the Telemarkia Terrane. They are represented by felsic and mafic volcanites, quartzites and quartz schists deformed and metamorphosed during Sveconorwegian orogeny (about 1130 Ma ago). Mineral associations typical for greenschist facies are observed in the central part while the degree of metamorphism increases southward. In the eastern and western parts the Telemarkia series rocks are represented by gneisses with remnants of supracrustal rocks and intruded by numerous granitoids (Bugge, 1982).

From the western side the Baltic Shield is covered by thick sequences of Cambrian-Devonian complex series of orogenic belts that runs down the north-west coast of Europe. Those are called Caledonides. The Caledonides were formed during tectonic events associated with the closure of the parts of the Iapetus Ocean that were situated between Laurentia (to the NW), Baltica and Avalonia (to the SE and E) and the Tornquist Sea (circa 570-360Ma) (Krawczyk et al., 2008). Together with slices of older basement, these rocks were thrusted several 100 km eastwards over the edge of the Fennoscandian Shield in several large thrust sheets known as nappes, when North America and Greenland collided with Scandinavia during the Caledonian orogeny c. 400 Ma ago. As the formation of

Caledonides took place between about 540 to 360Ma ago the term “Caledonian” could be used only for describing geological settings and not for age determination (McKerrow, 2000). Here, only the Scandinavian part of the Caledonian belt is described. The Caledonides of Greenland, Svalbard, and the parts belonging to Ireland, Scotland and Wales are not considered here.

The Scandinavian orogenic belt is distinctly bounded by allochtonous rocks covering the autochtonous Precambrian-Silurian series of sediments that in turn overly the peneplainized surface of the Baltic Shield rocks to the east and south-east. Within the Caledonian orogenic belt itself, Precambrian rocks are exposed in the tectonic windows (often with cupola structure).

According to Gee et al. (2008) the thrusts are subdivided into Lower, Middle, Upper and Uppermost allochthons located on the autochthonous crystalline basement. Lithologically, the allochthons are represented by metasedimentary and metavolcanic rocks with igneous complexes including ophiolites and island-arc series derived from the Iapetus Ocean. The difference in the degree of metamorphism is characteristic – it is increasing upwards from Middle Authochton.

Chapter 2. Geological setting of the Nussir deposit

The Nussir deposit is located in the Repparfjord Tectonic Window that is a basement culmination of Palaeoproterozoic rocks within the Caledonides of West Finnmark. Within the Reppafjord Tectonic Window 4 sequences are defined: the oldest is Holmvann Group and it is followed by Saltvann Group, Nussir Group, and the Porsa Group (Fig. 2.1).

The Holmvann Group in its turn is subdivided into 7 formations: they are (from oldest to youngest) Magerfjel, Båtdalselv, Båttajakka, Markfjell, Muvrassa, Aisaroaivi, Allavarri Formations. They are represented by metavolcanic (basaltic andesite, boninite, metabasalts, dacite, basalts) and metasedimentary rocks (metasandstones, carbonates, schist, quartzite) (Viola, 2008) subjected to greenschist to amphibolite facies of metamorphism about 1840 Ma ago (Pharaoh et al., 1982). It is observed a very well-developed schistosity that is generally parallel to the direction of the major fold axes (NE-SW) (Reitan, 1963). All over the rocks are intruded by mafic rocks.

The Holmvann Group rocks are overlain by 3 km thick Saltvann Group sequence with angular unconformity. The basal part of the group is composed by dolomites. In general the Saltvann Group in its turn is subdivided into 3 formations (Viola, 2008). These are: Ulveryggen Formation (meta-arenites with interbedded conglomeratic layers) overlain by Djupelv (greenstone conglomerate) and Stangvatn (porphyrite conglomerate) Formations. The orphyrite conglomerates of the Stangvatn formation are overlain by the dolomites and schistose siltstones hosting the copper mineralization of the Nussir deposit. According to Viola (2008) the Saltvann Group rocks are typical basin-infill deposits formed during tectonomagmatic events related to the onset of rifting. It is also confirmed by the metatholeites of the Nussir Group.

The Nussir Group (~1.8km thick) is subdivided into two formations: the Krokvatn and Svartfjell Formations. They are composed by mafic aquagene tuffs and submarine pillow basalts correspondingly. The Nussir Group is a typical greenstone sequence of Karelian (Early Proterozoic) supracrustal rocks that are widely spread in the northern Norway and northernmost Sweden (Pharaoh, 1985). Despite it was subjected to greenschist facies metamorphism that caused total recrystallization of the primary igneous mineralogy, the sequence is comparatively little deformed and contains well preserved textures.

The Saltvann and Nussir Groups are concordant with the Porsa Group and represent a continuous volcano-sedimentary sequence. The basal part of the Porsa Group is

composed by carbonates associated with quartzitic sandstone, schists, and/or shales. This group was described as mélanges and mélange-like rocks. Pharaoh et al. (1983) divided the Porsa Group into three formations. These are the Vargsund, Kvalsund, and Bierajav'ri Formations. Dolomites, which occur as discontinuous, intraformational lenses in the black shales of the Kvalsund Formation, are present in all three formations. The Group was formed in subtidal depositional environment interrupted by volcanic activity (interbedding with tuffs and tuffitic rocks). Reitan (1963) observed that the Vargsund metasediments are crosscut by several N-Ne/S-SW oriented faults.

The supracrustal rocks of the Repparfjord Window have been intruded by a suite of rocks ranging in composition from peridotites to gabbros (Raudfjell suite). In addition, a large tonalite body has intruded in the southwestern part of the Repparfjord Tectonic Window (Kvitfjell suite). Gabbro-peridotite-pyroxenite complex of the Raudfjell suite form sheet or podiform intrusions. Some gabbro intrusions, associated with ultramafic rocks, are rythmically layered and have cumulus textures. The suite consists of at least two generations of gabbro intrusions.

Kvitfjell suite represents pod-shaped tonalite intrusion in the southwestern part of the Repparfjord window. In the southwestern part of the Holmvann Group a dike swarm is present.

The Raudfjell suite of metagabbro is crosscut by mafic and intermediate composition dykes, which in turn are cut by tonalitic dykes. Viola (2008) has cited Jensen (1996) who considers them as an indicator of subduction-type magmatism.

Overall the stratigraphy of the Reparfjord Tectonic window is illustrated in Table 2.1.

The rocks of the Repparford tectonic window were moderately subjected to Caledonian deformation. Caledonian faults can be found in Nussir and Porsa groups in the western part of the window (Pharaoh, 1983).

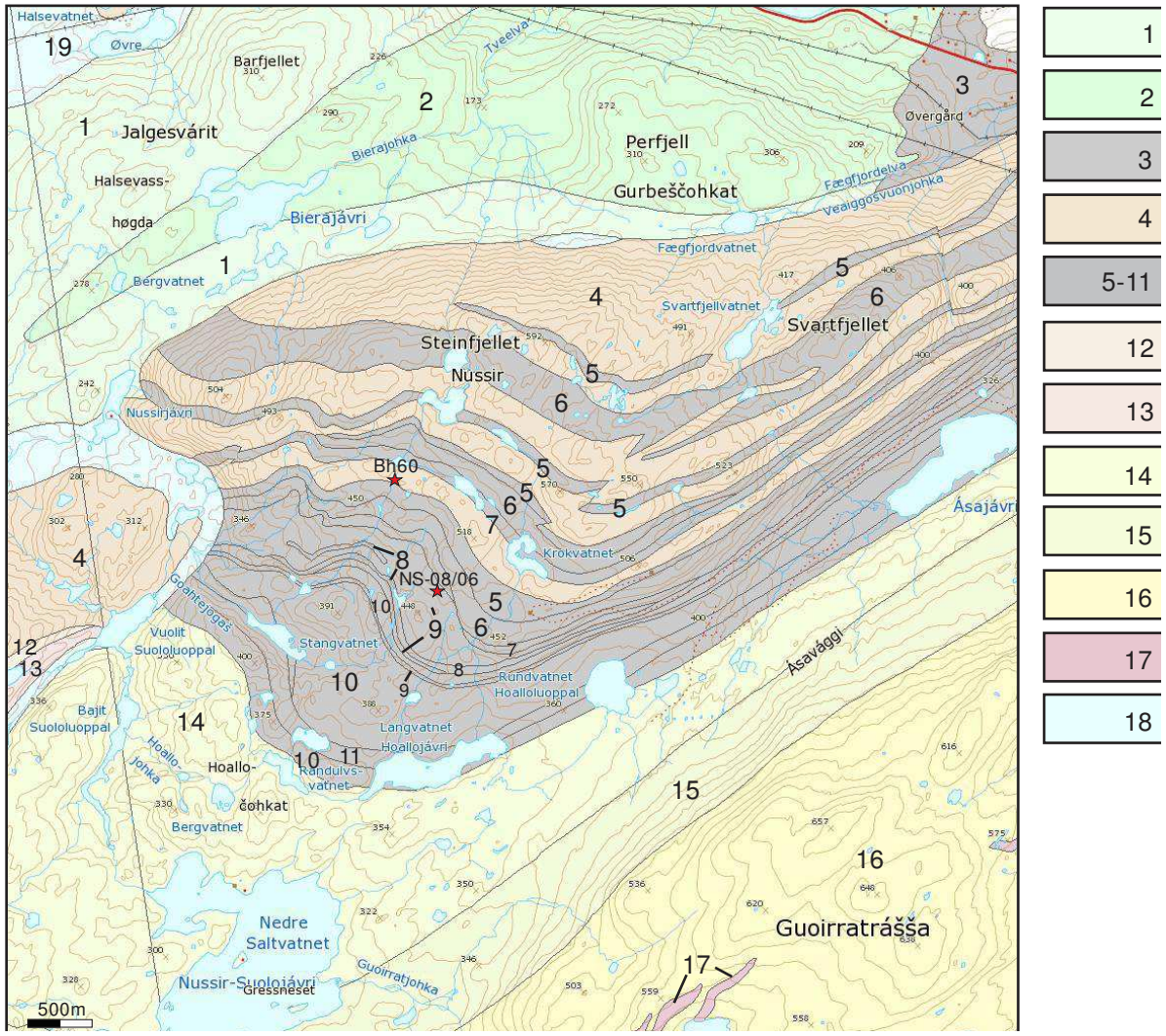

1
2
3
4
5-11
12
13
14
15
16
17
18

Figure 2.1. *Geological map of the Nussir deposit. Modified after Pharaoh (1984), Viola (2008), and http://geo.ngu.no/kart/arealisNGU/*

1. Kvalsund formation. Graphite schist, calcareous siltstone; 2. Bierajávri formation. Porsa Group. Schist, sandstone, tuff, carbonate layers; 3. Lomvass formation. Kalak thust (Kalak Nappe). Schist, siltstone; 4. Svartfjell formation. Nussir Group. Pillow metabasalt; 5. Krokvatn formation. Bedded mafic tuff. 6. Krokvatn formation. Massive metabasalt, massive tuff, tuffite; 7. Krokvatn formation. Tuff, tuffites, serpentine/magnetite rich. Mafic volcanic conglomerate at basement; 8. Stangvatn formation. Copper-bearing dolomite, claystone-siltstone; 9. Calcareous siltstone, claystone, thin dolomite-cherty layers; 10. Stangvatn formation. Dacite-porphyries conglomerate; 11. Sandstone, fuchsite-bearing layers; 12. Krokvatn formation. Tuffite, tuff, mafic volcanite-conglomerate with quartzitic pebbles; 13. Krokvatn formation. Metamorphic mafic and ultramafic (serpentinized) tuff, massive and pillow metabasalt, 14. Salvatn Group. Arkosic, lithic and quartzitic sandstones, conglomerates; 15. Quartz-, jaspis conglomerate with sandstone; 16. Quartz-feldspar sandstone with conglomerate, siltstone, sandstone, mice schist; 17. Raudfjell Suite. Gabbro; 18. Vargsund formation. Dolomite, quartzitic conglomerate at the bottom. Red stars show the location of sampled drill holes.

Table 2.1.

Scheme of the Repparfjord Tectonic Window (modified after Pharaoh et al., 1983, Jensen, 1996, Viola, 2008)

Group	Formations	Lithology
Porsa Group	Bierajav'ri Formation Kvalsund Formation Vargsund Formation	Quartzite, dolomite, schist
Nussir Group	Svartfjell Formation	Metabasaltic pillow lavas
	Krokvatn Formation	Volcaniclastic sediments interbedded with subordinate metabasaltic lava flows
Saltvatn Group	Stangvatn Formation	Porphyrite conglomerate
	Dypelv Formation	Greenstone conglomerate
	Ulverygg/Dåg'gejåkka Formation	Meta-arenites with interbedded conglomeratic layers
Holmvatn Group	Allavarri Formation	Amygdoidal basalt and volcaniclastic rocks
	Aisaroaivi Formation	Boninites, basalts and basaltic andesites, and calcaerous schist
	Muvrarassa Formation	Rhyolite
	Markfjell Formation	Greenstone/gneiss conglomerate, basalt and porphyritc basalts, tuff, calcaerous schist
	Båttajåkka Formation	Basaltic andesite, andesite, tuffite
	Breidalsvann Formation	Quartzite, dolomite
	Båtdalselv Formation	Quartzite, quartzofeldspathic metasandstone, mafic and felsic tuffites
	Magerfjell Formation	Pillow, massive basalts, andesitic basalts, volcaniclastic rocks
Pre-Karelian basement not exposed		

Discordant bedding
Concordant bedding

Chapter 3. Petrography

3.1. Method and technique

The petrology is described based on drill core samples from well NS-08/06 drilled from 0m to 235m by Nussir ASA in 2006. Polished thin sections were made from intervals of changes in lithology along the drill hole from 65.46m to 234.69m. Besides, samples from BH60 drill hole from the 28.45-28.92m interval that were earlier described (Mun, 2011) will be also included and presented in the Appendix.

Polished thin sections were produced in the laboratory of the Department of geology at the University of Tromsø. The thin sections were then studied using a Leica DM LM microscope. Each sample was firstly examined using polarized light in order to describe petrology. This examination was followed by using of reflected light with the aim to observe and describe ore minerals.

The Leica DML microscope was equipped with a Canon camera that allowed making photos presenting the polished thin section under different magnification. Objectives of the microscope allowed magnification of x2.5, x5, x10, x20, x63 times.

Detailed description of thin polished sections is represented in Appendix and only a short description will be given in this chapter.

3.2. Lithology

The geological section along the NS-08/06 drill hole is represented by a sedimentary-volcanogenic subsequence. The rocks were subjected to green-schist facies metamorphism and hydrothermal reworking. Evidence for the degree of metamorphism is widely spread chlorite and actinolite as well as observation of secondary processes such as sericitization of K-feldspar and plagioclase (Fig.3.2.2).

All around, the country rock is crosscut by quartz veins, carbonate veins and quartz-carbonate veins. Evidence shows that carbonate veins are later than quartz veins (Fig. Ap.3.2.1.7, Ap.3.2.1.28, b). A hydrothermal origin of the quartz, carbonate, and quartz-carbonate veins is considered by numerous examples and observation of the shape of veins, presence of stylolitic veins, and veinlets.

The lithological section was constructed based on the description of the thin polished sections (Fig.3.2.1).

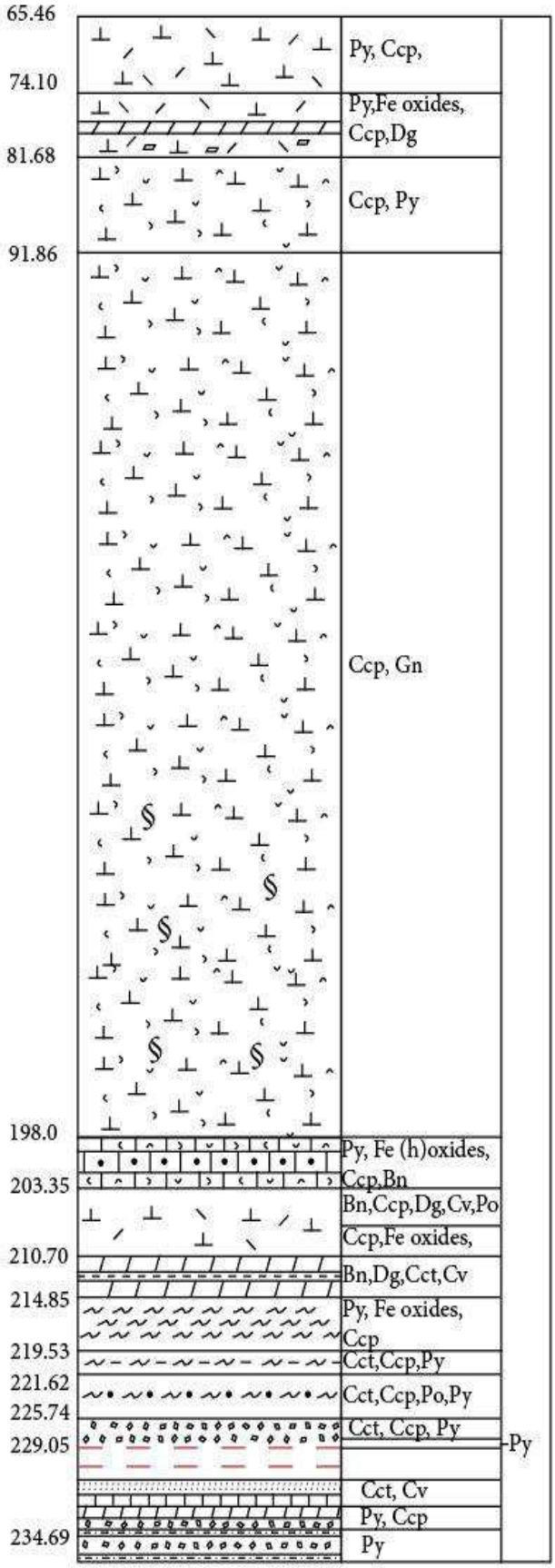

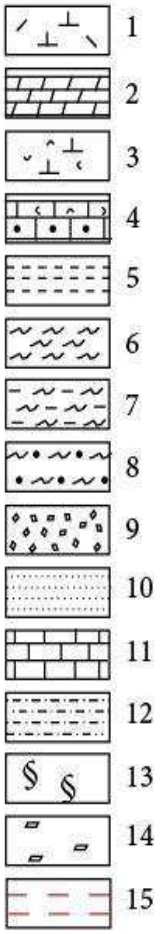

Figure 3.2.1.

Lithological section along the drill hole NS-08/06.

1. Mafic volcanite; 2. Dolomite; 3. Tuffite; 4. Carbonatized tuffite; 5. Pelite; 6. Schist; 7. Pelitic schist; 8. Quartzitic schist; 9. Breccia; 10. Sandstone; 11. Limestone; 12. Siltstone; 13. Chlorite-rich layers, chloritization; 14. Carbonatization; 15. Shear zone; Py-pyrite; Ccp-chalcopyrite; Cct-chalcocite, Bn-bornite; Cv-covellite; Dg – digenite; Gn – galena. Abbreviations of mineral names are given after Whitney and Evans (2010).

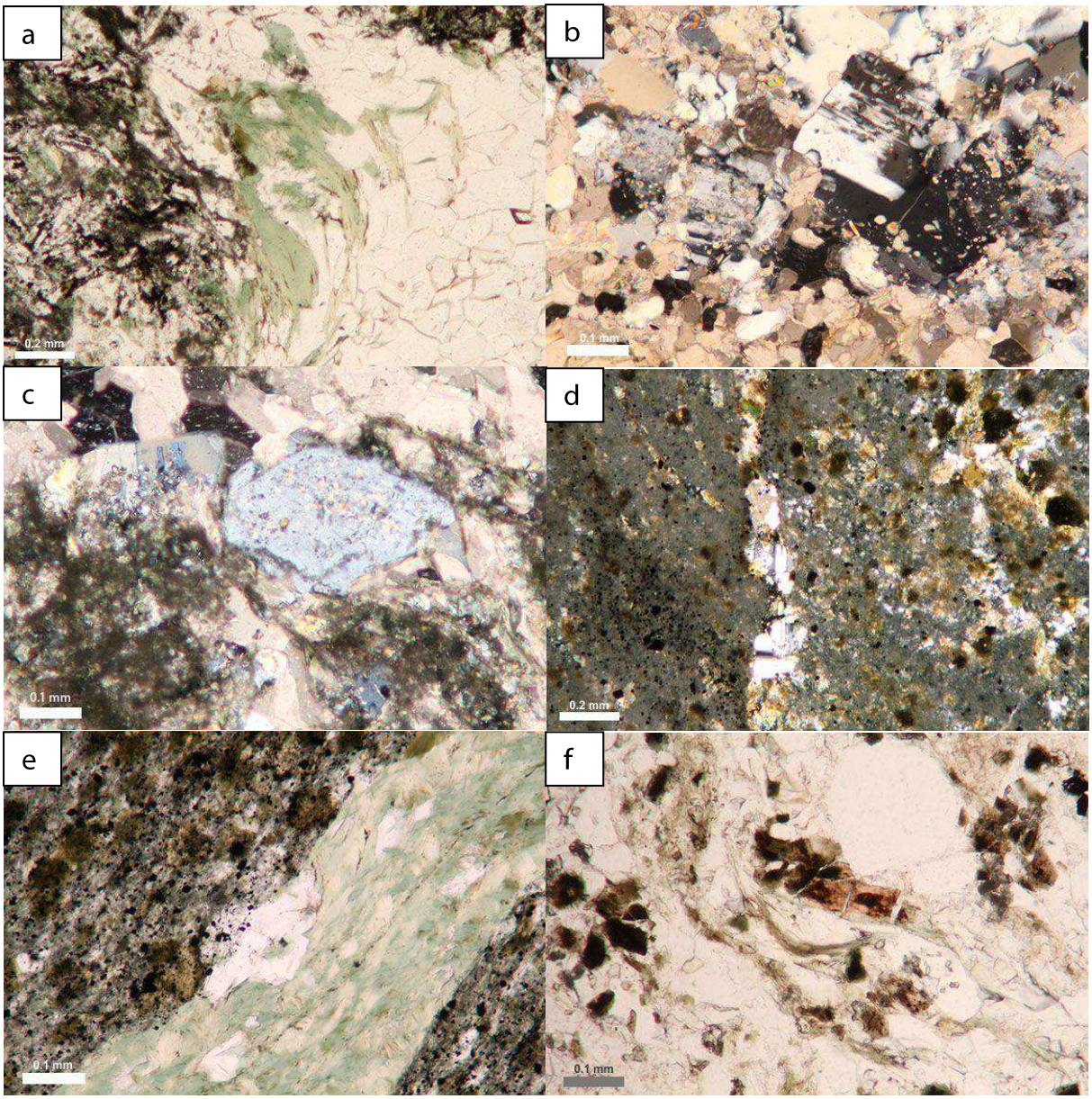

Figure 3.2.2. *Secondary minerals appearance in the country rocks. a) chlorite forms both in the country rock and vein. PPL. NS-10; b) sericitization of K-feldspar. XPL. NS-15; c) sericitization of alkali feldspar. XPL. NS-11; d) sericitization of plagioclase. XPL. NS-9; e) chlorite layer within the host rock. PPL. NS-12; f) replacement of biotite by chlorite. PPL. NS-15.*

In the upper part of the strata, volcanites and tuffite of mafic composition are observed. They form strata of a great thickness, more than 145m. Along the whole subsequence the country rocks are intensively chloritized and in some places carbonatized. The rocks show a massive texture, but over some intervals they are layered. The layers are made of chlorite (Fig. 3.2.2, e).

The volcanite is mainly composed of quartz, plagioclase, alkali feldspars, and biotite grains. Quartz is represented by grains of the size not exceeding 0.05mm, and mostly of anhedral shape. Observed biotite has a tabular shape. It is often replaced by chlorite. The grain size of biotite varies dramatically from 0.1mm to 1mm. Plagioclase and alkali feldspars have a tabular shape, and almost in all cases they are sericitized.

The country rocks are intruded by quartz-carbonate veins and veinlets. Carbonate is mainly represented by dolomite (rhomboidal crystals showing zonation). Dolomite shows both elongated and deformed grain shapes (Fig.3.2.3, a) with the length of up to 5 mm, and euhedral and subhedral crystals (Fig.3.2.3, b,c) of the size from 0.1mm to 0.2-0.3mm. Carbonate (dolomite) veins developed after the quartz veins were intruded. The evidence for this is that carbonate veins crosscut quartz veins, and recrystallization of quartz in the quartz veins (Fig.3.2.3 b,c). Quartz shows an anhedral shape. The grain size varies significantly from 1mm in diameter to very small ones with diameter less than 0.1mm. The length and extension of quartz-carbonate veins differs from one sample to another, and they can reach 2-2.5mm long. Quartz-carbonate nests are also observed within the host rocks and their diameter is approximately 1.2-1.5mm (Fig.3.2.3 c,d).

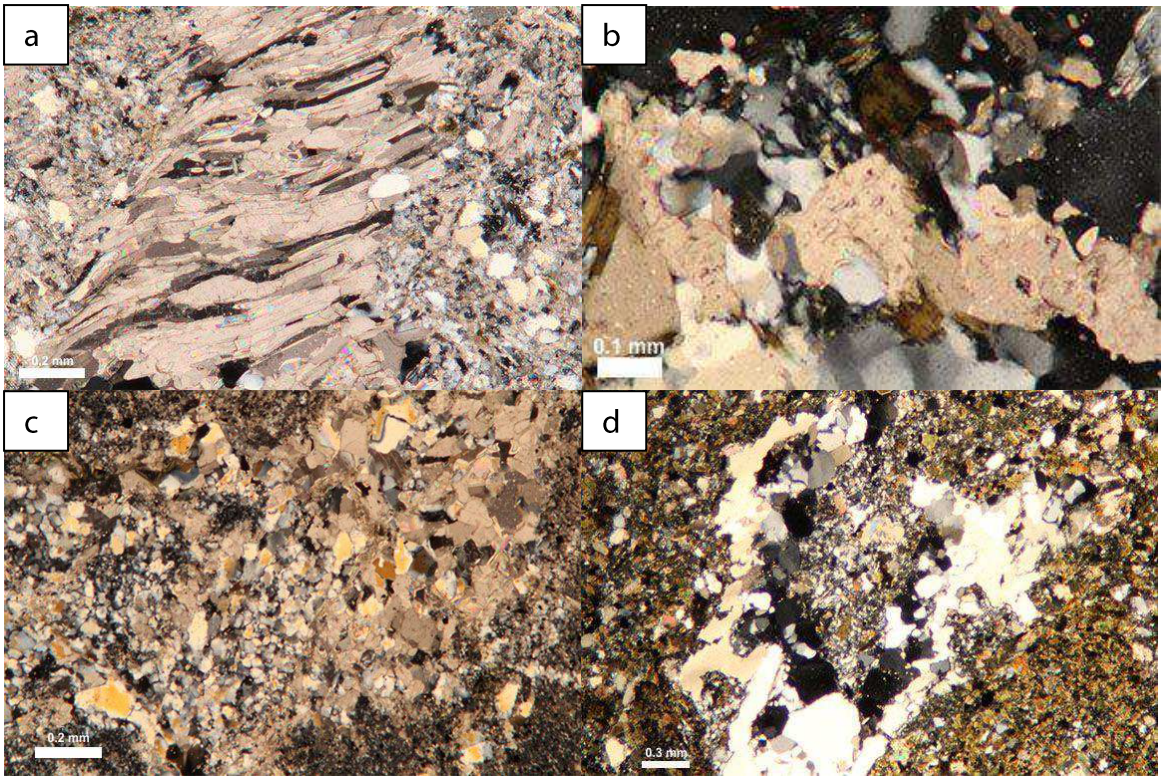

Figure 3.2.3. *Microphotographs of hydrothermal quartz-carbonate veins (a,b) and aggregates (c,d). XPL. a) NS-14.; b) NS-6.; c) NS-8.; d) NS-13.*

At the depth of 210.70m (thin polished section NS-16) the lithology of the sequence changes and dolomite interlayered with semipelite appears. They are followed by alternating layers of pelitic schist, quartzitic semischist, siltstone, and breccia. Greenschist was formed on behalf of mafic rock since chlorite and actinolite are widely spread. At the depth of 219.53-219.63m the greenschist is interlayered with dolomite and the contact zone is composed predominantly of chlorite. A breccia forms a layer of about 2m thickness (225.74-227.05m). The fragments of the breccia are constituted of quartz and sericitized feldspars. The quartz grain size varies from 0.1mm to 0.6mm, and the shape is often rounded but there are also more irregular varieties. Feldspars have euhedral shape and up to 1.2mm in diameter. The breccia is cemented by chlorite-muscovite cement.

From 229.64m to 231.90m the rock is intensively crushed, chloritized, schistose, and it has all features characterizing a shear zone.

Below the shear zone, strata of frequent interlayered sandstone, limestone, dolomite, and siltstone is observed. In their turn sediments of rather quiet geological environment are substituted and interlayered with breccia layers. This sequence is about 3m thick.

Similar to the volcanogenic-sedimentary part, the sedimentary part of the section is crosscut by quartz-carbonate veins. The carbonate is represented by dolomite that has an euhedral shape and sizes of 0.05mm to 1mm and bigger in diameter. Figure 3.2.1.28b from the appendix shows how carbonate vein crosscuts quartz vein. Quartz shows smaller grain sizes that mostly vary from 0.3 to 0.6mm. The shape of crystals is anhedral.

Samples from drill hole BH60 from the 28.45-28.92m interval were also examined under optical microscope. The microscopic study presented here shows that the studied samples from the Nussir deposit represent sedimentary rocks that have undergone deformation and low grade metamorphism. Deformation structures including crenulation cleavage in mica-rich layers, sigmoidal shaped aggregates of quartz and carbonate, as well as elongated grains of quartz in the veinlets and recrystallization of quartz grains, suggest that the rock was exposed to contractional forces after its formation. Otherwise, the rocks can also obtain these features during hydrothermal invasion of quartz-carbonate veins. Most likely, the alteration of the host rocks resulting in low-grade metamorphism took place during formation of the veinlets and during the subsequent deformation processes. Veins of deformed and undeformed carbonate grains indicate at least two generations of carbonate veins, and that the last generation of carbonate was formed after compressional deformation occurred.

Chapter 4. Geochemistry

4.1. Methods and technique

Whole-rock analysis of the samples was performed by the author using a "Bruker S8 TIGER" XRF at the Department of Geology, University of Tromsø. Major, trace and ore element contents were determined.

Samples were analyzed with optimum excitation using a Rhodium tube with an acceleration voltage of 60 kV and tube current of 67 mA. The analyzer crystal LiF220 ensures that in combination with the 0.23° collimator, the best separation is achieved for adjacent elements (Lab Report XRF 90).

ICP MS analysis of one sample was performed as a test in the Central Laboratory of the Republic of Uzbekistan on an Elan DRC II ICP-MS (Perkin-Elmer, USA-Canada). This method allows determination of all major, trace and ore elements with a detection limit of 10^{-9} %. The Elan DRC II is equipped with a by LSX-200 laser sampling system (Cetac, USA). The intensity of the masses was registered in a regime of semi-quantitative analysis along the whole range of masses from 6 (Li) to 238 (U). Laser operating conditions: diameter – 200 µm, power - 5mJ, impuls frequency – 5/sec.

For analysis of major, trace and ore elements the samples were crushed to the powder. In order to perform this they were firstly crushed to pieces with <1cm size in a jaw crusher. Afterwards the material was transferred to a swing mill and crushed to a grain size <0.25mm. The swing mill was carefully washed and dried after each sample was crushed.

Major element analyses were obtained from glass beads. Fused glass beads prepared from the rock powder and Li-tetraborate ($Li_2B_4O_7$) that were mixed in 1:7 weight proportions. Weighing was performed using Mettler AE160 balance. 4.2 g of Li-tetraborate was mixed with 0.6 g of rock powder. The mixture was shacked in a glass container until it was homogenized.

The mixture afterwards was melted in Pt-crucible covered with Pt mold over a "Turbotorc" gas burner at approximately 1200°C for about 6-7 min. The crucibles were initially cooled down on a slab of ultramafic rock. Crucibles and molds were cleaned in a warm solution of water with citric acid and rinsed in running water after each sample.

Trace and ore elements were analyzed in pressed pellets. 9 grams of rock powder were weighted and mixed with 9 wax tablets of POLYSIUS PROLAB® Mahlhilfe in an agate

mortar during 8-10 min until complete homogeneity was obtained. The mixture was then put to a double cylinder + piston device and then inserted into a hydraulic press for 3 minutes. Afterwards, the sample was carefully removed, labeled, and placed into a plastic container.

It has not been possible to get analytical procedure from the laboratory.

4.2. Major oxides

Whole-rock analysis of all analyzed samples is shown in table 4.2.1 and Fig. 4.2.1. Due to the fact that the upper part of the studied drill core is composed of mafic volcanites and tuffites (see chapter 3), MgO was chosen as horizontal axis in Fig.4.2.1.

As shown in the table, the MgO content varies dramatically between different lithologies (0.87-14.84 wt.%). The bivariate plots in Fig.4.2.1 show how MgO varies with the variations of the major oxides. It can be observed that MgO shows a negative correlation with SiO_2, Al_2O_3, Na_2O, K_2O, which contents are as follow: SiO_2=46.99-71.45 wt.%; Al_2O_3 = 10.52-15.81 wt.%; Na_2O = 0.10-6.15 wt.%; K_2O = 0.60-7.76 wt.%. Furthermore, MgO shows positive correlations to TiO_2 (0.37-2.14 wt.%), P_2O_5 (0.10-0.50 wt.%), and Fe_2O_3 (1.80-18.05 wt.%).

The samples from the drill core can be subdivided into a mafic part (samples NS-6-NS-14 with exception of NS-11), and a felsic part (samples NS-15 - NS-25). In the volcanite-tuffite subsequence major oxide contents show a range of variations. Thus, Al_2O_3 varies from 11.97 to 15.36 wt.%; SiO_2=46.99-56.47 wt.%; P_2O_5 = 0.14-0.50 wt.%; K_2O = 0.60-2.22 wt.%; TiO_2 = 1.51-2.14 wt.%; MnO = 0.11-0.35; Fe_2O_3 = 5.58-18.05 wt.%. MgO, Na_2O and CaO, however, shows relatively much larger variations with MgO = 1.73-14.84 wt. %, Na_2O= 0.10-6.15 wt.%, and CaO = 1.79-12.60 wt.%.

The felsic part shows lower content of Fe_2O_3 (1.80-6.82 wt.%); slightly lower TiO_2 = 0.37-0.59 wt.%; higher average CaO = 1.62-9.93 wt.%; higher K_2O = 2.31-7.76 wt.%; markedly higher SiO_2 = 64.24-71.45; considerable lower MgO = 0.40-2.39 wt.%; slightly lower Na_2O = 0.87-3.63 wt.%. The contents of Al_2O_3, P_2O_5, MnO is similar as for the mafic part, with Al_2O_3 = 10.52-15.81 wt.%; P_2O_5 = 0.10-0.15 wt.%; and MnO = 0.05-0.24 wt.%.

Figure 4.2.2 shows the TAS diagram after Le Bas (1986), which is based on SiO_2 vs Na_2O+K_2O ratios of the studies samples. Only samples NS-6-NS-13 is shown in the diagram, because the lower part of the drill core is represented by metasedimentary rocks and are

not suitable for the diagram. However, the samples NS-6 - NS-13 show compositions corresponding to basic to intermediate volcanites. Thus, the varieties of rocks are basalt, basaltic andesite, basaltic trachyandesite, and trachybasalt.

In the AFM diagram after Irvine and Baragar (1971), samples NS-6 - NS-13 plot in the field corresponding to the tholeitic series (Fig.4.2.3). Sample NS-14 plots in the field of the calc-alkaline series.

Figure 4.2.4 shows the ternary MnO - TiO_2 - P_2O_5 discrimination diagram after Mullen (1983). Only samples NS-10 - NS-13 are shown in the diagram, since they are the only ones that are suitable for plotting in the diagram (45wt.% < SiO_2<54 wt.%). According to this diagram, the samples scatter between mid-ocean ridge basalts, ocean island-tholeite, and island arc tholeite. In order to get a more unambiguous tectonic setting of the samples, the diagram proposed by Pearce et al. (1977) was applied (Fig.4.2.5). However, in this diagram, the data plot in the fields of ocean-island, continental, and spreading center island. According to Pearce et al. (1977) continental environment describes subalkalic basaltic-andesites erupted on continents as traps, flood basalts and plateau basalts. Spreading center island includes basalts having higher content of Fe and Al compared to basalts from sea floor and intra-plate islands (Pearce et al, 1977).

Sample	Na_2O	MgO	Al_2O_3	SiO_2 (%)	P_2O_5	K_2O	CaO	TiO_2	MnO	Fe_2O_3
NS-6	3.08	6.50	15.36	55.42	0.14	1.59	1.79	1.51	0.17	14.45
NS-8	6.15	3.06	14.60	54.02	0.23	0.78	4.31	1.93	0.13	14.78
NS-9	1.57	7.15	12.24	56.47	0.13	2.05	4.93	1.71	0.26	13.49
NS-11	2.79	5.67	11.97	51.55	0.50	0.60	12.60	2.14	0.35	11.83
NS-10	4.85	4.07	13.48	48.70	0.15	0.92	7.48	2.09	0.21	18.05
NS-12	4.15	4.56	15.10	53.10	0.20	1.86	1.98	2.14	0.11	16.80
NS-13	0.10	14.84	12.95	46.99	0.20	1.79	5.52	1.78	0.25	15.58
NS-14	3.98	1.73	12.01	63.91	0.15	2.22	9.42	0.76	0.24	5.58
NS-15	3.63	1.50	11.88	67.36	0.15	2.31	9.93	0.56	0.25	2.45
NS-17	2.06	0.87	10.88	69.99	0.12	4.65	8.42	0.47	0.24	2.30
NS-18	1.04	2.39	15.81	64.24	0.12	7.76	1.62	0.59	0.05	6.38
NS-19	2.06	1.01	12.17	70.49	0.11	5.64	6.18	0.37	0.16	1.80
NS-20	1.44	1.00	10.63	70.71	0.10	6.02	5.03	0.47	0.13	4.46
NS-21	1.85	1.33	13.58	64.41	0.11	6.46	6.64	0.48	0.17	4.97
NS-23	0.87	1.57	10.52	66.59	0.12	6.53	6.25	0.53	0.20	6.82
NS-25	1.44	0.40	10.87	71.45	0.11	6.49	2.29	0.55	0.05	6.35

Table 4.2.1. *Whole-rock chemical analysis recalculated to volatile-free basis. The contents are in weight %.*

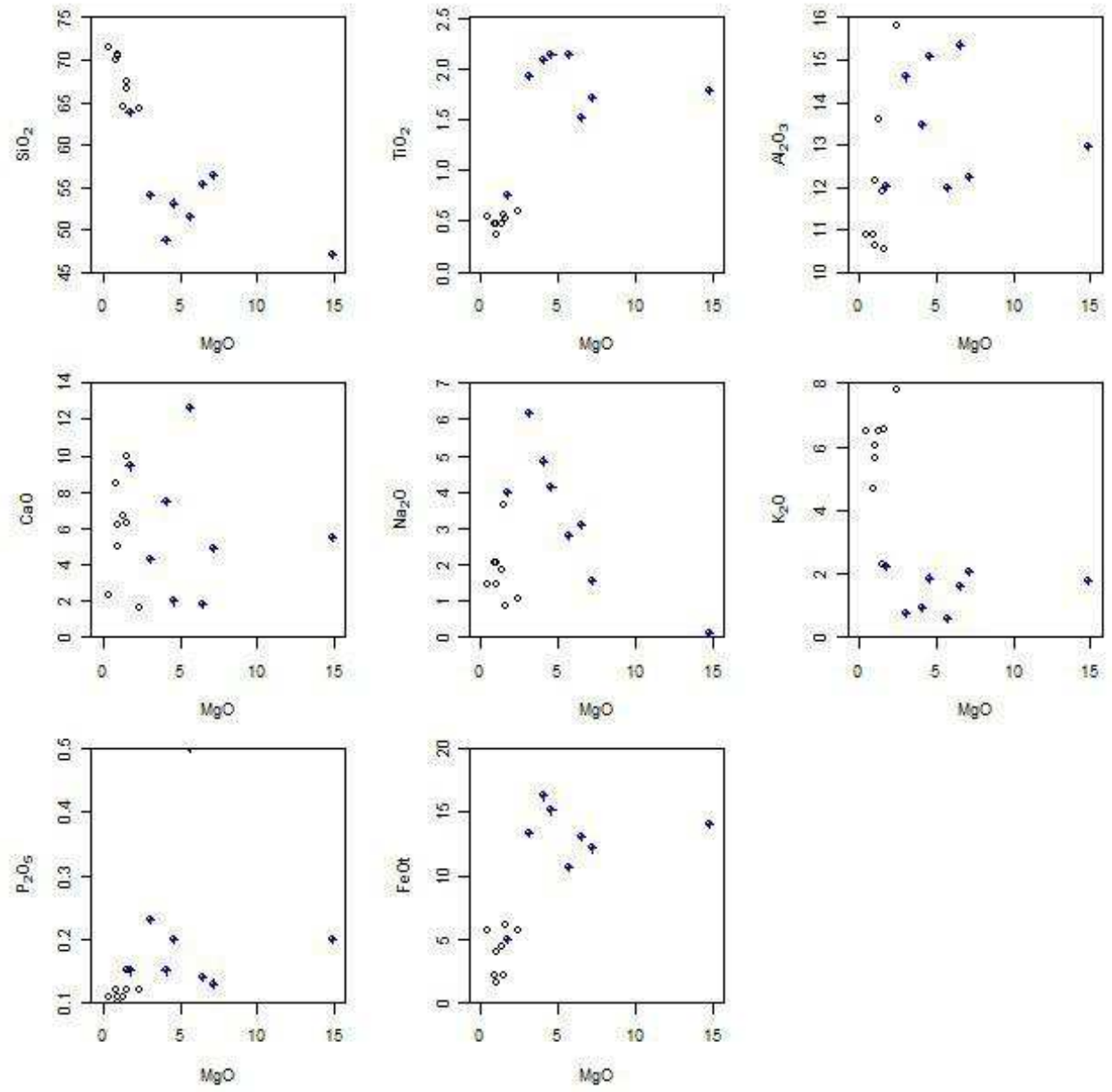

Figure. 4.2.1. *Bivariate plots demonstrating distribution of major oxides versus MgO. Blue spots – samples NS-6-NS-14, white – samples NS-15-NS-25.*

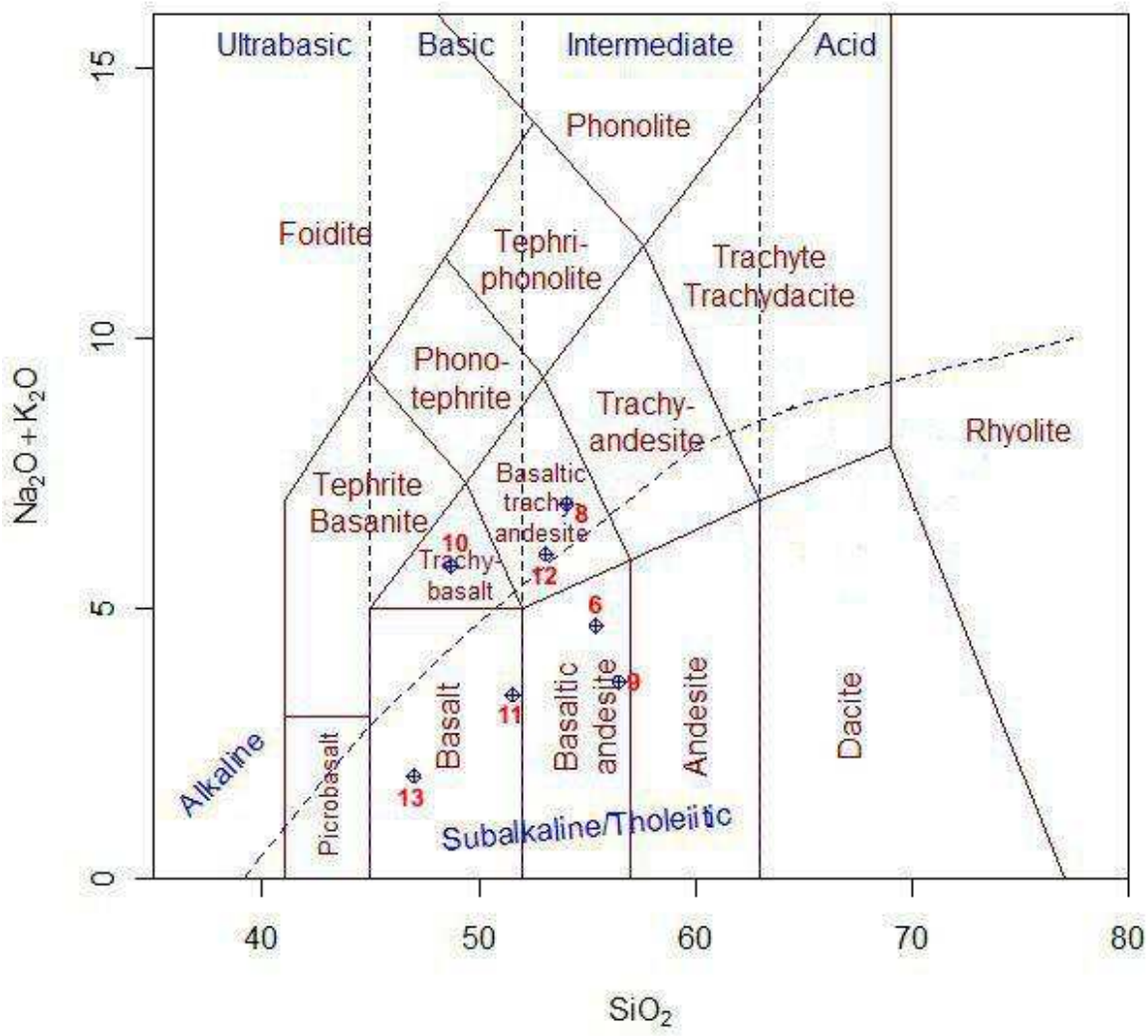

Figure 4.2.2 *Composition based distribution of samples on the TAS diagram after Le Bas (1986). Numbers 6-13 correspond to sample numbers NS-6 - NS-13.*

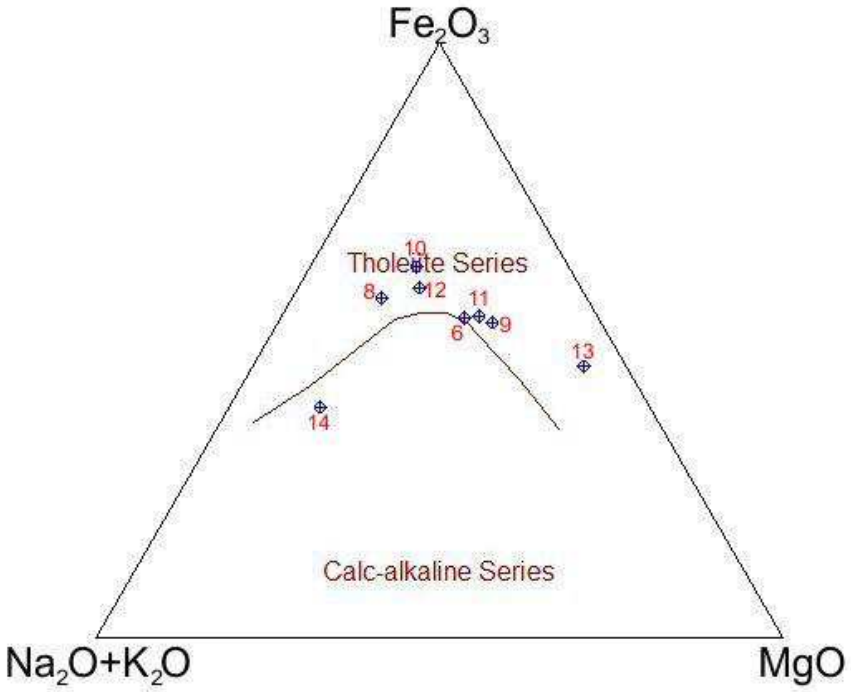

Figure 4.2.3. *Compositional data of samples in the AFM diagram after Irvine and Baragar (1971).*

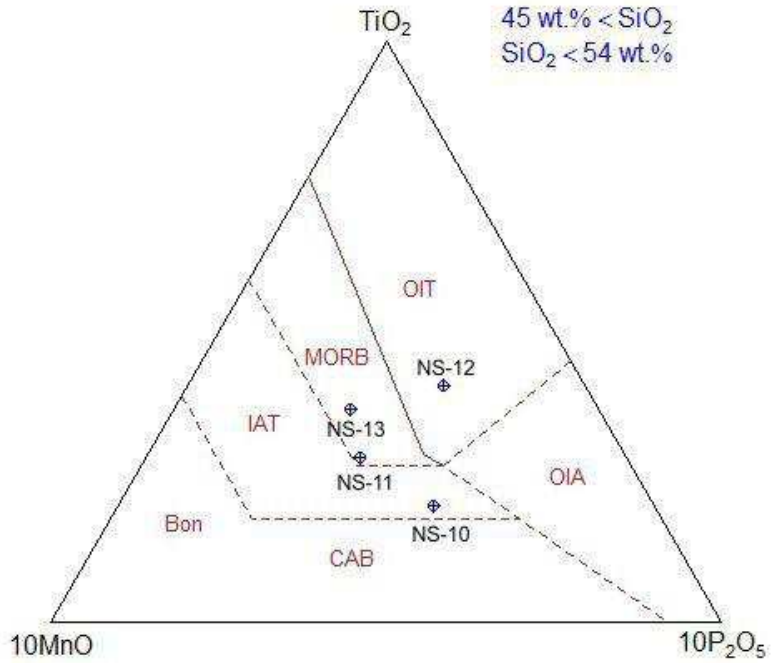

Figure 4.2.4. *Ternary plot showing geodynamic position based on composition of samples (after Mullen, 1983). OIT – ocean island tholeiite, MORB – mid-ocean ridge, IAT –island arc tholeiite, Bon - boninite, CAB – calc-alcaline basalts, OIA-ocean island alcalic basalts.*

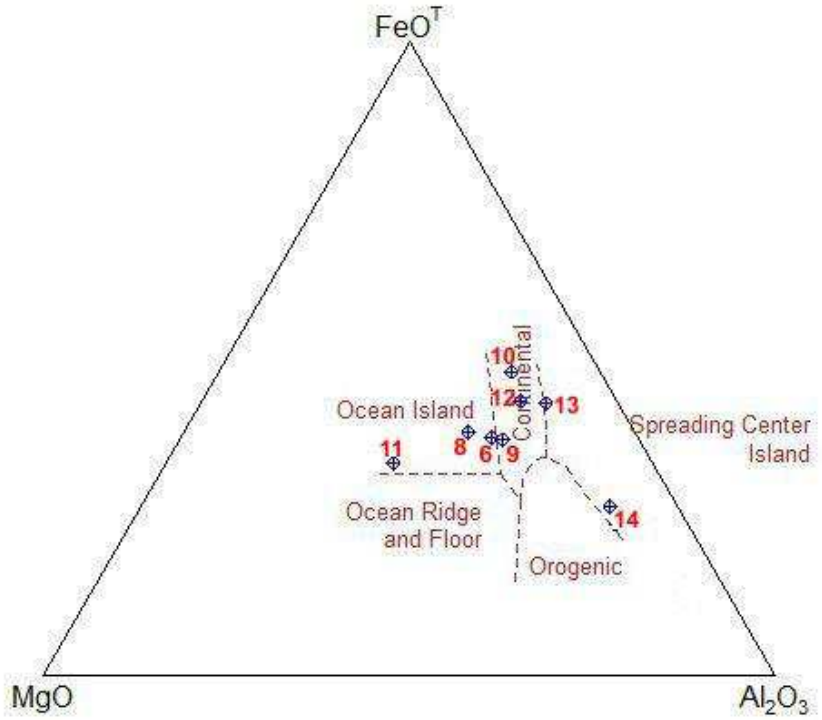

Figure 4.2.5. *Ternary plot showing tectonic environment based on MgO – FeO - Al_2O_3 composition (after Pearce et al., 1977). Symbols are the same as in Fig.4.2.2.*

4.3. Trace elements

Trace element and rare earth element (REE) compositions normalized to chondrite are given in table 4.3.1. The values are in ppm. The chemical compositions of the samples vary significantly along the drill core. Thus, La content changes from 24.7 pp to 109.8 ppm; Y=2.2-13.6ppm; Ce=22.3-88.9ppm; Rb=10.4-143.4ppm; Th=130-375ppm; Nb=5.7-24.8ppm; Ba=31.6-942.8ppm; Sr=2.5-25.3ppm; Zr=11.2-28.0ppm; V=0.6-10.3ppm; Cr=0.1-0.7ppm; Y=1.6-13.6ppm.

Bivariant diagrams of MgO vs. REE and trace elements (Fig.4.3.1, 4.3.2) show that MgO is negatively correlated to Ba, Rb, Y, Sr, Zr, La, and positively correlated to Cr, Ni, Ce.

Based on the fact that Zr, Y, Nb, and Ti are considered to be immobile elements during most geological processes, they have been used for determination of the tectonic setting of a rock. Figure 4.3.3 shows the composition of the samples plotted in the diagram proposed by Winchester and Floyd (1977). Some samples plot outside of the fields given in the diagram and have not been included. As it is seen from the figure, two of the samples plot in the field of alkali basalts.

Diagrams after Pearce (1982) (Fig.4.3.4) and Pearce and Cann (1973) (Fig. 4.3.5) have been constrained using Ti, Zr, Y, and Sr. As shown in Fig. 4.3.4., the composition of one

sample (NS-14) corresponds to island-arc volcanite while some samples plot outside the fields that are indicated. Moreover, the discrimination diagram after Pearce and Cann (1973) (Fig.4.3.5) shows that samples NS-6/8/9/10/12/13 plot outside the indicated fields while NS-14 corresponds again to island-arc tholeitic basalt. .

4.4. Ore elements

XRF analysis (UiT) allowed determination and evaluation of following ore elements: Ag, Cu, As, Bi, Sb, Se, Zn, Sn, Co, and Ni. Their compositional variations along the drillcore are shown in table 4.4.1. As it can be observed, the Cu content varies from 0 ppm to 10030 ppm; Ag=0.7-9.2 ppm; As=9-19 ppm; Bi=0-1 ppm; Sb=1.3-7.8 ppm; Zn=30-210 ppm; Sn=1-16.1 ppm; Co and Ni occur in minor amounts and their content varies from about 0.01 ppm to 0.2 ppm, and 0.001-0.07 ppm correspondingly.

The plots of the compositional variations of the ore elements toward the depth of the drill core are given in figure 4.4.1. As it is demonstrated, the concentrations of the ore elements are low through most of the drill core; only at a depth of about 210.75 m an anomal zone can be observed. Here the contents of all elements are significantly higher than elsewhere along drill core NS-08/06. Notice that the lithology at this interval is represented by sandstone with dolomite, and the rock is hydrothermally altered (See appendix 3, NS-16).

Sample	Sc	Y	La	Ce	Rb	Th	Nb	Ba	Sr	Zr	V	Cr	Co	Ni
NS6	5,278	10,250	64,634	56,069	27,606	220,000	22,679	105,833	5,371	20,556	5,639	0,383	0,156	0,035
NS8	4,530	9,550	71,037	54,682	12,181	162,500	20,714	64,417	5,171	15,656	5,263	0,256	0,103	0,018
NS9	5,854	4,600	44,512	38,150	37,394	187,500	16,071	116,944	3,829	13,533	5,571	0,483	0,164	0,039
NS11	4,511	13,550	100,915	87,630	10,426	225,000	22,857	31,556	9,248	18,100	5,757	0,172	0,084	0,021
NS10	5,048	7,900	42,988	22,775	15,479	157,500	13,929	58,556	6,305	11,244	10,263	0,037	0,110	0,004
NS12	5,950	7,700	76,524	50,289	35,160	247,500	24,821	121,694	2,838	18,667	6,290	0,395	0,134	0,026
NS13	5,739	8,550	42,378	22,312	31,170	130,000	15,357	245,139	6,610	12,667	5,161	0,773	0,161	0,073
NS-14	2,303	9,050	39,634	36,879	35,745	290,000	13,393	309,056	14,200	23,756	1,647	0,088	0,031	0,003
NS15	2,169	9,400	24,695	24,624	36,383	177,500	10,536	926,417	25,286	19,122	1,169	0,075	0,020	0,003
NS16	3,052	3,000	109,756	82,081	27,713	215,000	5,714	101,361	24,076	10,733	0,982	0,061	0,006	0,001
NS-17	1,497	6,150	51,524	47,052	63,245	332,500	7,679	340,750	10,676	32,556	0,635	0,179	0,011	0,002
NS-18	2,284	1,600	62,195	44,855	143,404	320,000	9,821	509,222	3,543	15,800	2,978	0,084	0,041	0,005
NS-19	1,209	6,550	55,488	39,653	71,809	277,500	8,214	337,750	7,248	20,789	0,806	0,096	0,012	0,003
NS-20	1,094	5,450	51,829	35,607	69,149	352,500	11,607	942,750	10,200	28,033	1,402	0,101	0,019	0,002
NS-21	1,843	2,150	71,951	49,595	86,543	297,500	11,429	318,250	7,019	14,967	1,467	0,110	0,021	0,003
NS-23	1,401	6,100	95,122	88,902	79,096	300,000	12,500	254,500	4,962	24,044	1,708	0,101	0,030	0,003
NS-25	1,190	5,850	71,341	58,497	63,457	375,000	13,750	375,583	2,533	27,144	1,331	0,144	0,020	0,001

Table 4.3.1. *REE and trace elements composition normalized to chondrite (Rollinson H.R., 1994), the contents are expressed in ppm.*

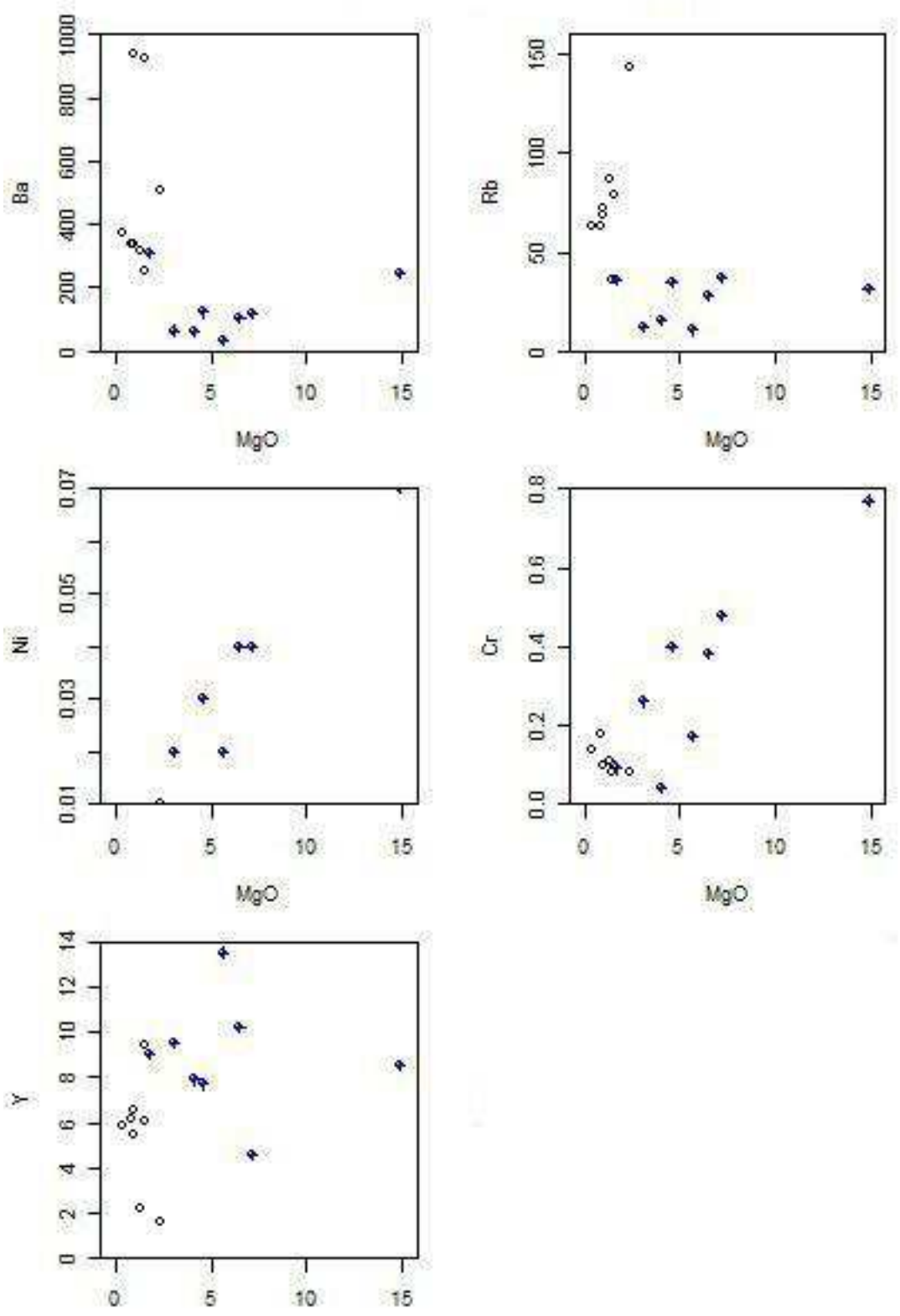

Figure 4.3.1. *Element vs. MgO bivariate plots of various samples from drill core (NS-08/06 MgO in wt.%, trace elements are in ppm). Blue spots: samples NS-6-Ns-14; white spots: samples NS-15-NS-25.*

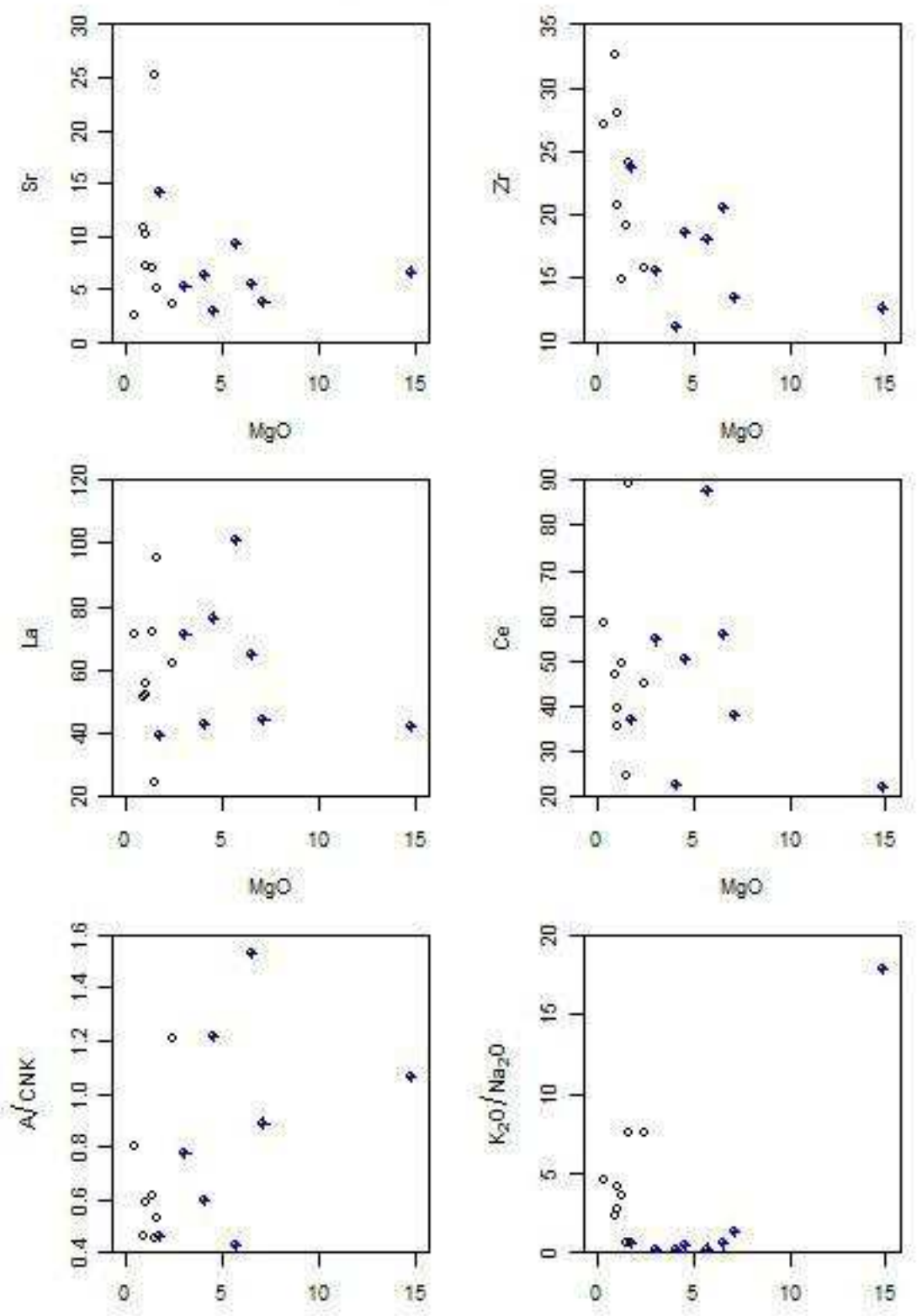

Figure 4.3.2. *Element vs. MgO bivariate plots of various samples from NS-08/06 drill hole (MgO and major oxides in wt.%, trace elements are in ppm). Blue spots: samples NS-6 - Ns-14; white spots: samples NS-15 - NS-25.*

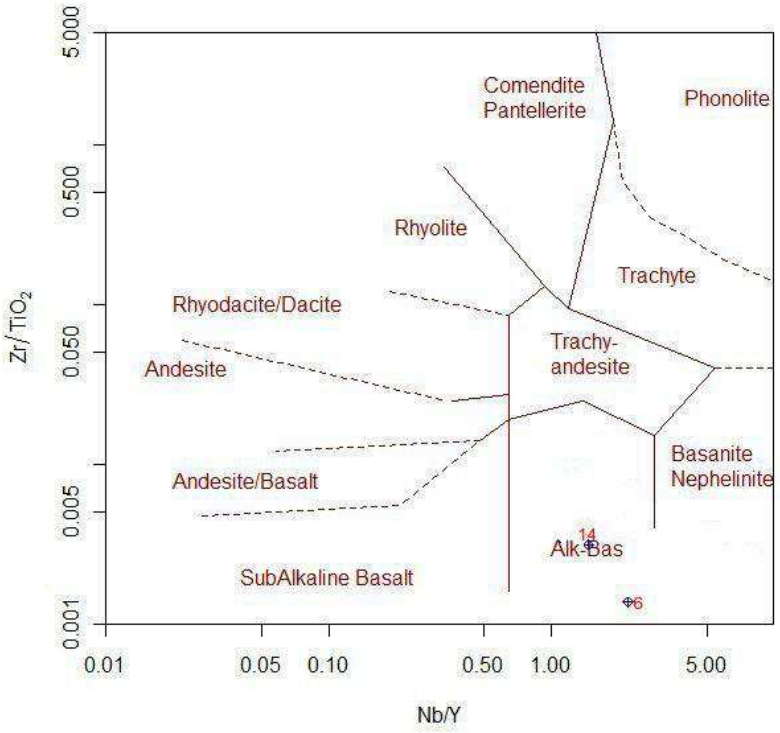

Figure 4.3.3. *Compositional data of samples in the diagram proposed by Winchester and Floyd (1977).*

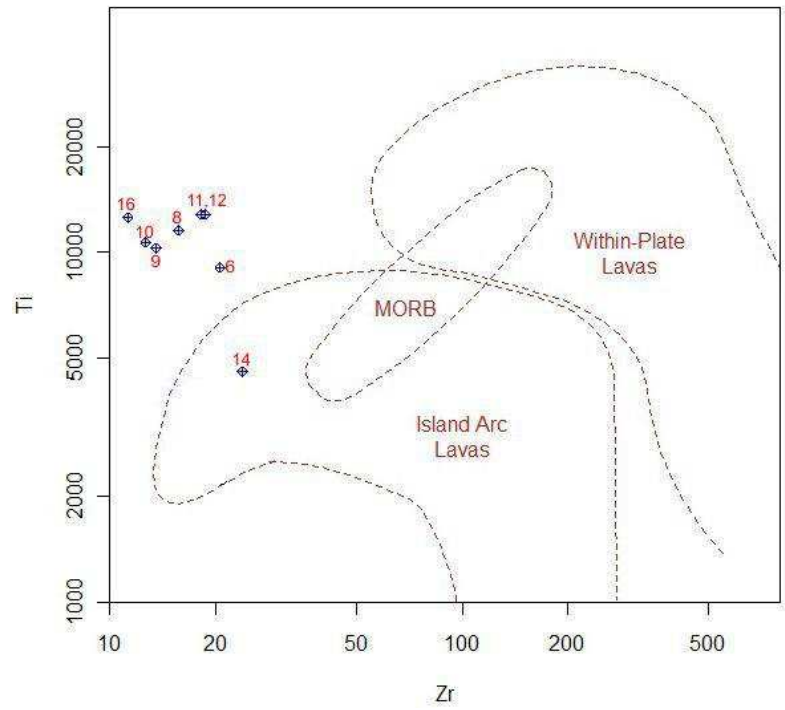

Figure 4.3.4. *Discriminative diagram for NS-6-NS-25 samples after Pearce (1982)*

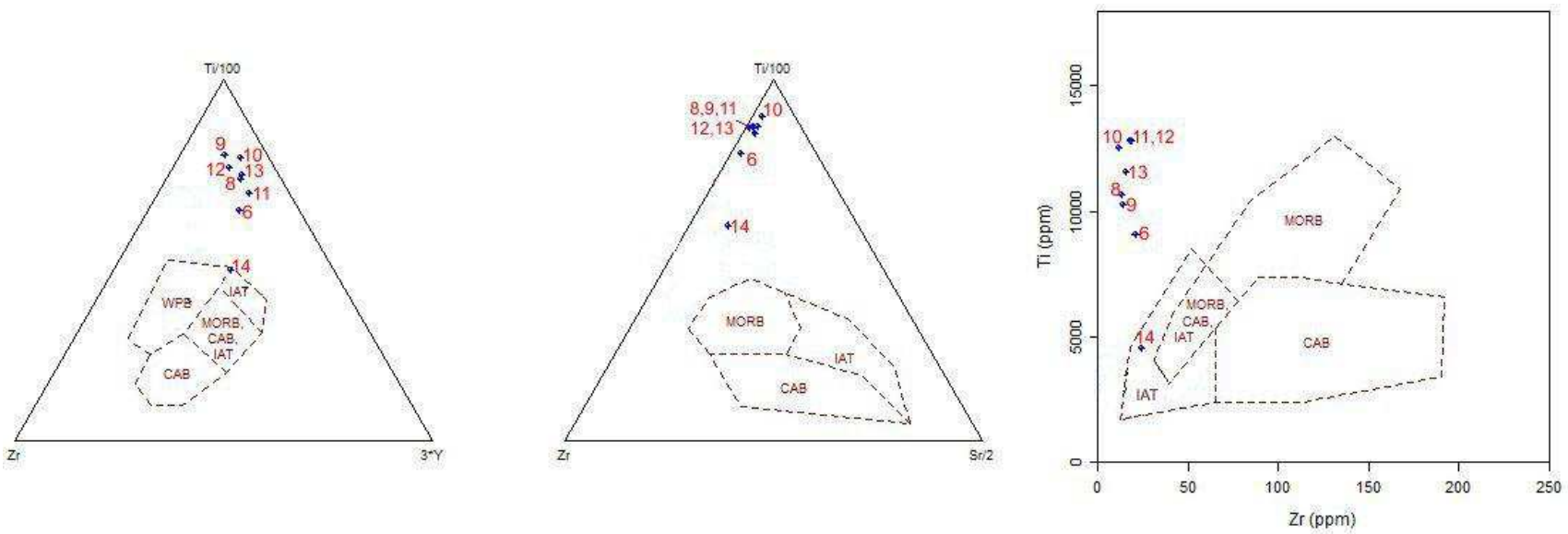

Figure 4.3.5. *Discriminative diagram showing tectonic palaeoenvironment after Pearce and Cann (1973). MORB-mid-ocean ridge basalts; WPB-within-plate basalts; CAB=calc-alkaline basalts; IAB-island-arc tholeiie.*

Sample	Depth	Ag (PPM)	Cu (PPM)	As (PPM)	Bi (PPM)	Sb (PPM)	S (%)	Zn (PPM)	Sn (PPM)	Co (PPM)	Ni (PPM)
NS6	65,49	3,500	0	14,000	1,000	5,500	0,000	150	0,000	0,156	0,035
NS8	74,12	2,800	210	15,000	1,000	1,300	0,020	80	2,400	0,103	0,018
NS9	75,38	5,000	80	19,000	0,000	1,300	0,010	170	6,500	0,164	0,039
NS10	158,37	0,700	50	15,000	0,000	3,400	0,010	100	2,200	0,084	0,021
NS11	81,69	5,000	0	12,000	1,000	7,800	0,210	120	0,000	0,110	0,004
NS12	183,75	4,000	220	13,000	0,000	3,500	0,020	100	1,000	0,134	0,026
NS13	198,00	1,600	0	14,000	0,000	4,000	0,010	210	2,100	0,161	0,073
NS-14	203,38	2,000	30	16,000	1,000	1,300	0,010	40	4,400	0,031	0,003
NS15	206,87	1,200	0	9,000	1,000	5,300	0,090	30	4,800	0,020	0,003
NS16	210,75	9,200	10030	14,000	1,000	3,500	0,310	50	7,000	0,006	0,001
NS-17	214,88	2,500	10	16,000	0,000	6,400	0,000	40	5,900	0,011	0,002
NS-18	219,58	2,300	0	17,000	0,000	4,600	0,000	50	16,100	0,041	0,005
NS-19	221,64	0,000	0	15,000	0,000	4,900	0,000	30	13,200	0,012	0,003
NS-20	225,77	2,400	0	19,000	0,000	7,500	0,080	30	8,600	0,019	0,002
NS-21	227,08	1,700	0	12,000	1,000	4,800	0,000	30	6,000	0,021	0,003
NS-23	231,75	2,300	0	15,000	0,000	3,900	0,000	100	7,300	0,030	0,003
NS-25	234,69	2,700	0	14,000	0,000	4,500	0,020	40	7,700	0,020	0,001

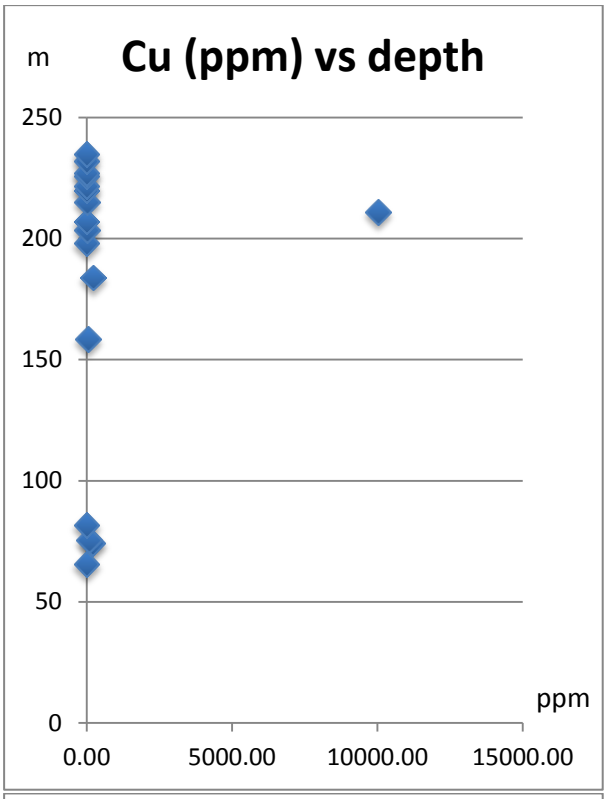
Cu (ppm) vs depth
m
250
200
150
100
50
0
ppm
0.00
5000.00
10000.00
15000.00

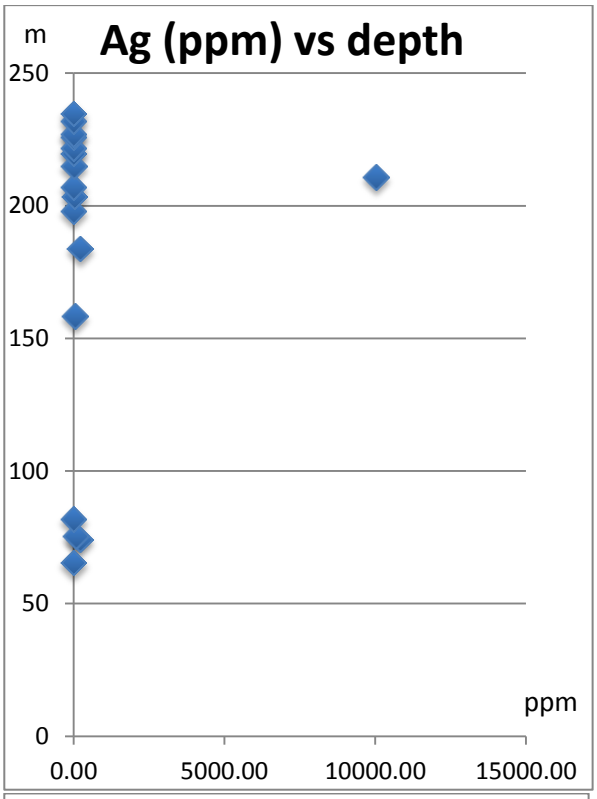
Ag (ppm) vs depth
m
250
200
150
100
50
0
ppm
0.00
5000.00
10000.00
15000.00

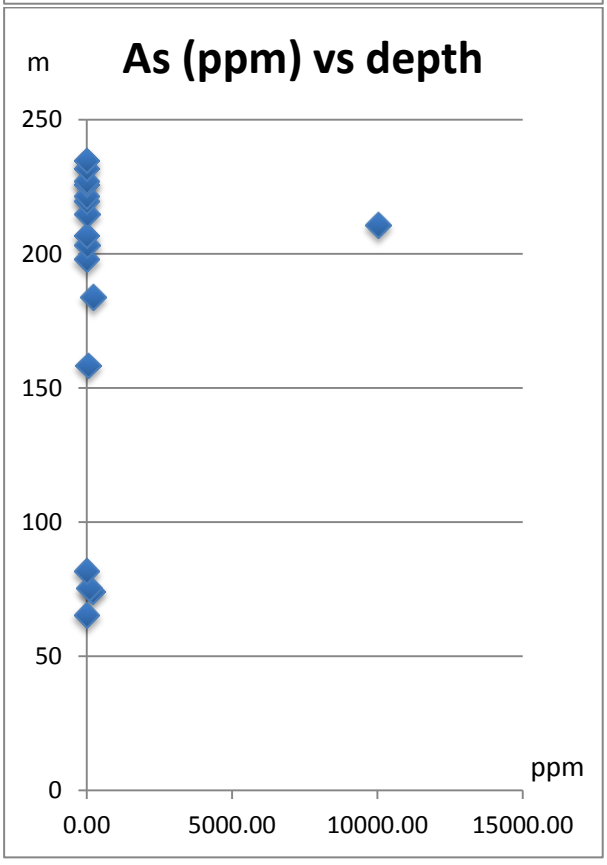
As (ppm) vs depth
m
250
200
150
100
50
0
ppm
0.00
5000.00
10000.00
15000.00

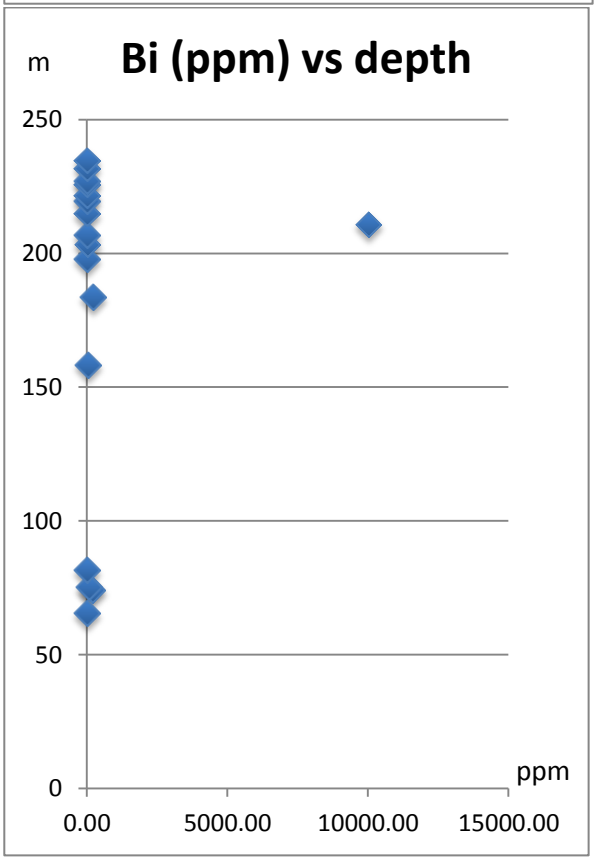
Bi (ppm) vs depth
m
250
200
150
100
50
0
ppm
0.00
5000.00
10000.00
15000.00

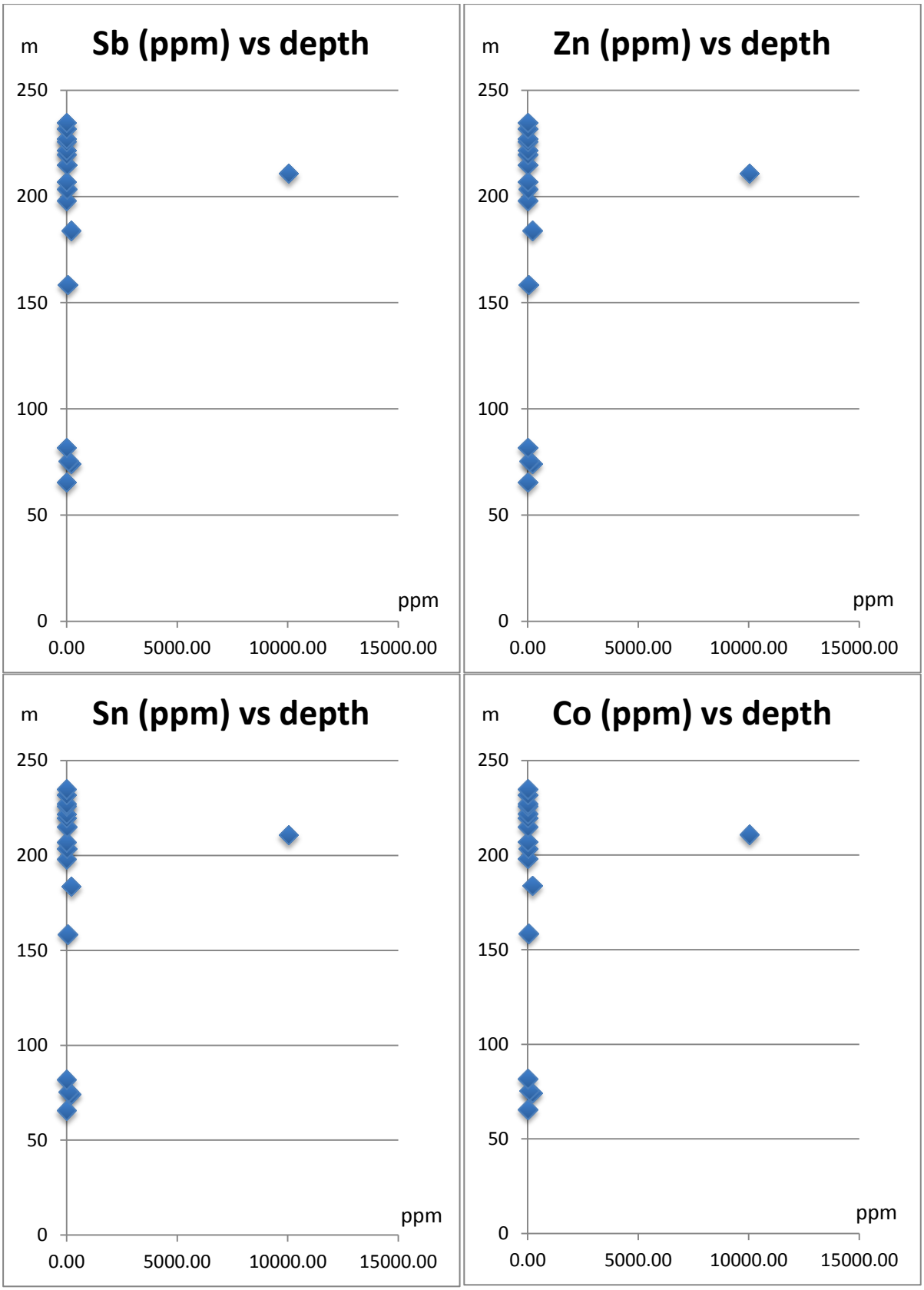

Figure 4.4.1. *Bivariant plots of element vs. depth.*

4.5. ICP-MS analyses

ICP-MS analyses were performed as a test for one sample taken from the BH60 drill core. As it is shown in the Table 4.5.1 copper is present in a very high amount (average 145000 ppm). Besides Ag (600-1000ppm) is found in a considerable amount. An interesting fact is a presence of As (8.20-10.0 ppm), Se (6.40-5.90 ppm); Sb (1.10-1.70ppm); Te (0.98-1.30ppm); Pt (0.01-0.02ppm); Au (0.13-0.15ppm); Bi (20.0-21.0ppm); Pb (320.0-380.0ppm); Th (3.60-5.90ppm). U (0.88-1.50ppm) and Hg (0.085-0.86ppm) are in a minor amount.

A REE spider diagram for REE normalized after Boynton (1984) was constructed and is given in Fig.4.5.1. The spider diagram shows that the light REE dominate upon heavy REE. This observation suggests the idea that parent rock was a tholeitic or calc-alkaline basalt since MORB is enriched in heavy REE.

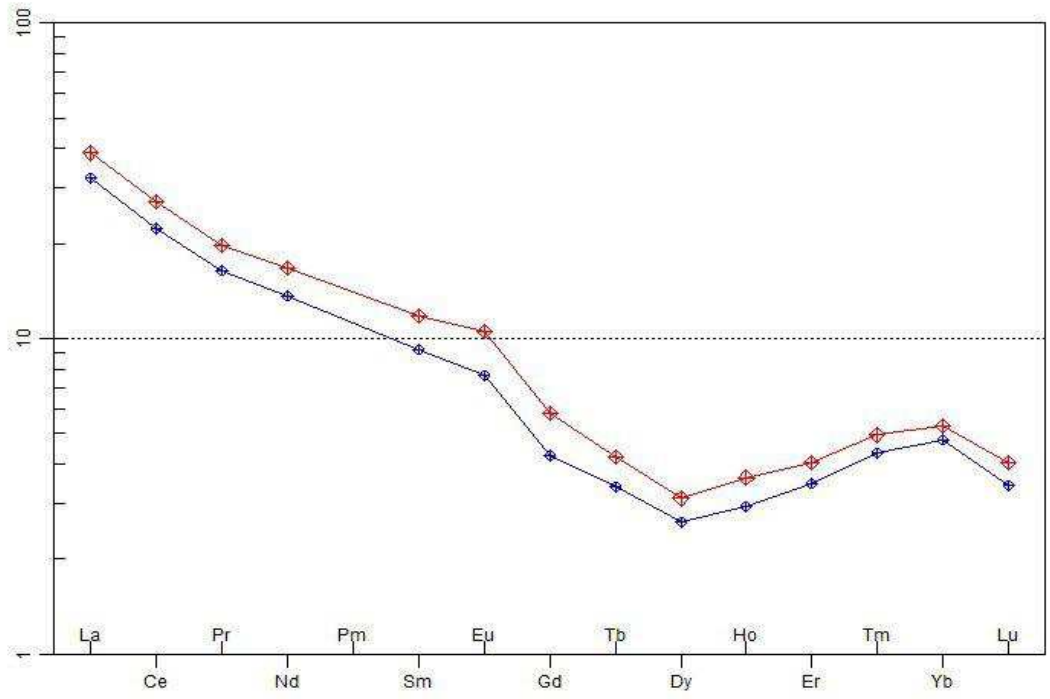

Figure 4.5.1. *Spider plot of REE normalized to chondrite after Boynton (1984). NS-4a is shown with blue, while NS-4b is shown with red colors.*

Sample/Element	Li	Be	Na*	Mg*	Al*	K*	Ca*	Sc*	Ti	V	Cr	Mn*	Fe*	Co	Ni
N-1-4a	7.00	0.41	3,800	12,000	22,000	12,000	53,000	4.10	520.0	78.00	41.00	1,300	100,000	16.00	36.00
N-1-4b	10.00	0.73	5,300	19,000	43,000	23,000	54,000	6.90	1,000	89.00	43.00	1,400	61,000	26.00	34.00
	Cu	**Zn**	**As**	**Se**	**Rb**	**Sr**	**Y**	**Zr**	**Nb**	**Mo**	**Ag**	**Cd**	**Sn**	**Sb**	**Te**
N-1-4a	170,000	34.00	10.00	6.40	33.00	95.00	5.60	21.00	1.20	18.00	1,000	0.96	1.50	1.70	0.98
N-1-4b	120,000	34.00	8.20	5.90	66.00	100.0	6.80	38.00	1.80	39.00	600.0	0.95	1.30	1.10	1.30
	Cs	**Ba**	**La**	**Ce**	**Pr**	**Nd**	**Sm**	**Eu**	**Gd**	**Tb**	**Dy**	**Ho**	**Er**	**Tm**	**Yb**
N-1-4a	0.35	240.0	10.00	18.00	2.00	8.20	1.80	0.56	1.10	0.16	0.84	0.21	0.73	0.14	1.00
N-1-4b	0.59	570.0	12.00	22.00	2.40	10.00	2.30	0.77	1.50	0.20	1.00	0.26	0.85	0.16	1.10
	Lu	**Hf**	**Ta**	**W**	**Re***	**Pt ***	**Au***	**Hg**	**Tl**	**Pb**	**Bi**	**Th**	**U**		
N-1-4a	0.11	0.14	0.14	1.90	0.063	0.01	0.15	0.086	0.036	380.0	21.00	3.60	0.88		
N-1-4b	0.13	0.25	0.20	1.30	0.120	0.020	0.13	0.085	0.062	320.0	20.00	5.90	1.50		

Table 4.5.1. *ICP analysis of NS-4a, NS-4b samples. Concentrations given in ppm. * marks elements of semi-quantitative analysis.*

Chapter 5. Mineral chemistry

5.1. Analytical procedure

Compositions of ore minerals were determined on a Cameca SX 100 electron microprobe at the Department of Geoscienses at the University of Oslo and a Jeol YXA 8800R Superprobe at the Institute on Geology and Geophysics of the Republic of Uzbekistan. Those methods allow determination of samples mineral composition. Besides, elements indicating a presence of mineralization are found using microprobe (usually they are elements that are contained in ppb amounts). Furthermore these methods give an idea about character of element-indicators embedding into the matrix of mineral-concentrator.

Both electron microscopes are equipped with EDS (energy dispersive spectrometer) systems allowing determination of chemical composition of minerals, admixture elements' content, and investigation on the peculiarities of their distribution on the area of the sample. WDS (wavelength dispersive spectrum) allows more detailed analysis of the elements with low concentrations.

The analyses performed with a Cameca SX 100 were carried out at 15 kV accelerating voltage, 15 nA beam current, focused beam and 10 s counting time on peak and 5 s for each side. Standardisation was made on synthetic minerals (As: gallium arsenide), metal (Fe, Co, Cu, Ni, Ag, Au), and on natural minerals (sphalerite, galena). PAP matrix corrections were applied. Mostly optical system was used; backscattered image was obtained for recognition.

The Jeol YXA Superprobe is equipped with Link ISIS 300 (Oxford) electron-dispersive spectrometer. The resolution of EDS is 0.01-0.1%. WDS (wavelength dispersive spectrometer) has a resolution of 0.1-0.001% for light and heavy elements. For the majority of the elements the range of determined concentrations is from 0.01-0.005 up to 100 mass%.

ED spectrometer is used for a quick quantitative, semi-quantitative and qualitative microanalysis of elements from Na to U with a concentration >0.05-0.1 weight %. The spectral sensitivity of EDS is 138eV.

The analyses obtained with Jeol Superprobe were carried out at 20 kV accelerating voltage, under the regime of high and low vacuum with resolution of 90-x10000. High

quality images were taken in SEI (Secondary Electron Images), BEI (backscattered electron images), and characteristic X-ray in the limits of indicated diapason.

5.2. Mineral chemistry

Mineral chemistry of the ore minerals has been studied. The results are given in the appendix 5 in tables 5.2.1-5.2.12.

The minerals names were given after calculation of modal composition.

The results of *chalcopyrite ($CuFeS_2$)* analyses show that the mineral often contains minor amounts of Au (0.11-0.01 wt %), Ag (0.12-0.01 wt %), As (0.08-0.01 wt %), Zn (0.12-0.02 wt %) (Ap.5.2.1). Chalcopyrite is observed in intergrowth with bornite where chalcopyrite appeared as a secondary mineral (Fig. 5.2.2 b,c,e; 5.2.3, c,d). Chalcopyrite was observed in equilibrium contacts with with pyrite (Fig. 5.2.2.,d) and gersdorffite (NiAsS). Chalcopyrite also occurs in veinlets (Fig.5.2.1).

Chalcopyrite occurs along the whole vertical section of the drill hole NS-08/06 (Fig.3.2.1). It is noted however, that in the upper parts chalcopyrite appears as a pure mineral nearly without inclusions. In the lower parts bornite dominates and chalcopyrite appears in a minor amounts, usually as a secondary mineral replacing bornite (Fig.5.2.2,e, 5.2.3,c).

In the intensively hydrothermally altered interval of the drill hole BH60 (See chapter 3) chalcopyrite is found in an assemblage together with silver minerals (Fig.5.2.3,f).

Bornite (Cu_5FeS_4) is a second widely distributed mineral after chalcopyrite. The composition of bornite is given in Appendix 5 (Table 5.2.2). As it is shown in the table, similar to chalcopyrite bornite contains minor amounts of As (0.01-0.08 wt.%). Bornite also contains some Zn, Co, and Ni. Interestingly, some chemical analyses of bornite show Ag concentrations that reaches up to 3.70 wt.% (NS-4). Note that sample NS-4 is from the drill hole BH60, from the interval of 28.75-28.80m, which shows evidence of strong hydrothermal alteration. Bornite also shows trace content of Au (< 0.07 wt.%).

Along the studied section (drill hole NS-08/06, Fig.3.2.1) bornite appears from 198.0m depth and continues to lower depth. It is nearly always altered and partly or wholly replaced by chalcopyrite, chalcocite (Cu_2S), digenite (Cu_9S_5), and covellite (CuS) (Fig.5.2.2,a,b,c,e,f; 5.2.3,a,b,c,d). Inclusions of galena (PbS) have been observed within

bornite (5.2.2,a; 5.2.3, d). Figure 5.2.4. demonstrates BEI (backscattered electron image) of the intergrowth of bornite with stromeyerite (CuAgS), and chalcocite from sample NS-1b.

Digenite (Cu_9S_5) and *chalcocite (Cu_2S)* compositions are presented in tables 5.2.3 and 6.2.4 respectively in Appendix 6. Neither digenite nor chalcocite form separate mineral grains but they are usually observed as a secondary minerals (Fig.5.2.2,b,c,f; 5.2.3,a,c). Chalcocite is distributed as an emulsion in bornite replacing it (Fig.5.2.3,b). Both digenite and chalcocite show minor contents of Au, Ag, As, and Zn. Digenite is confined to the zones of intense carbonatization and silicitization. Thus, in the geological section NS-08/06 digenite is observed on the interval of 74.10-81.68m where dolomite layers are observed and lower along the sequence within 203.35-211m interval. Besides digenite was observed in sample NS-5b (Ap.3) from drill hole BH60.

Chalcocite was identified in the lower part of drill core NS-08/06, at depths below 203m.

Covellite (CuS) is a secondary copper mineral, replacing chalcopyrite, bornite and chalcocite. The covellite investigated here shows up to 1wt.% Ag. Similar to other minerals described above, covellite shows minor contents of As, Zn, Co (Appendix 5, 5.2.5).

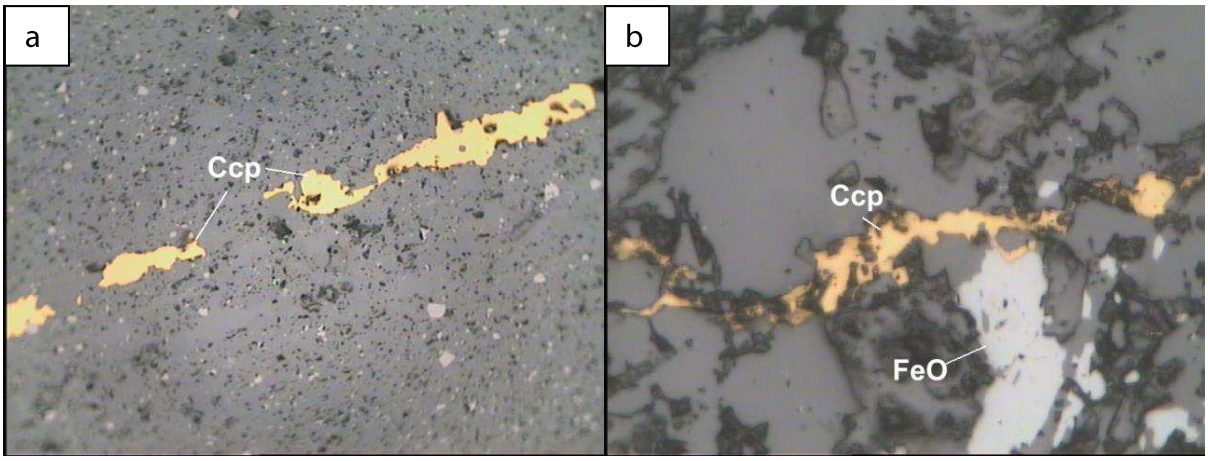

Figure 5.2.1. *Photomicrographs in reflected light: a) chalcopyrite veinlet. NS-12; b) chalcopyrite veinlet located close to hematite. NS-14.*

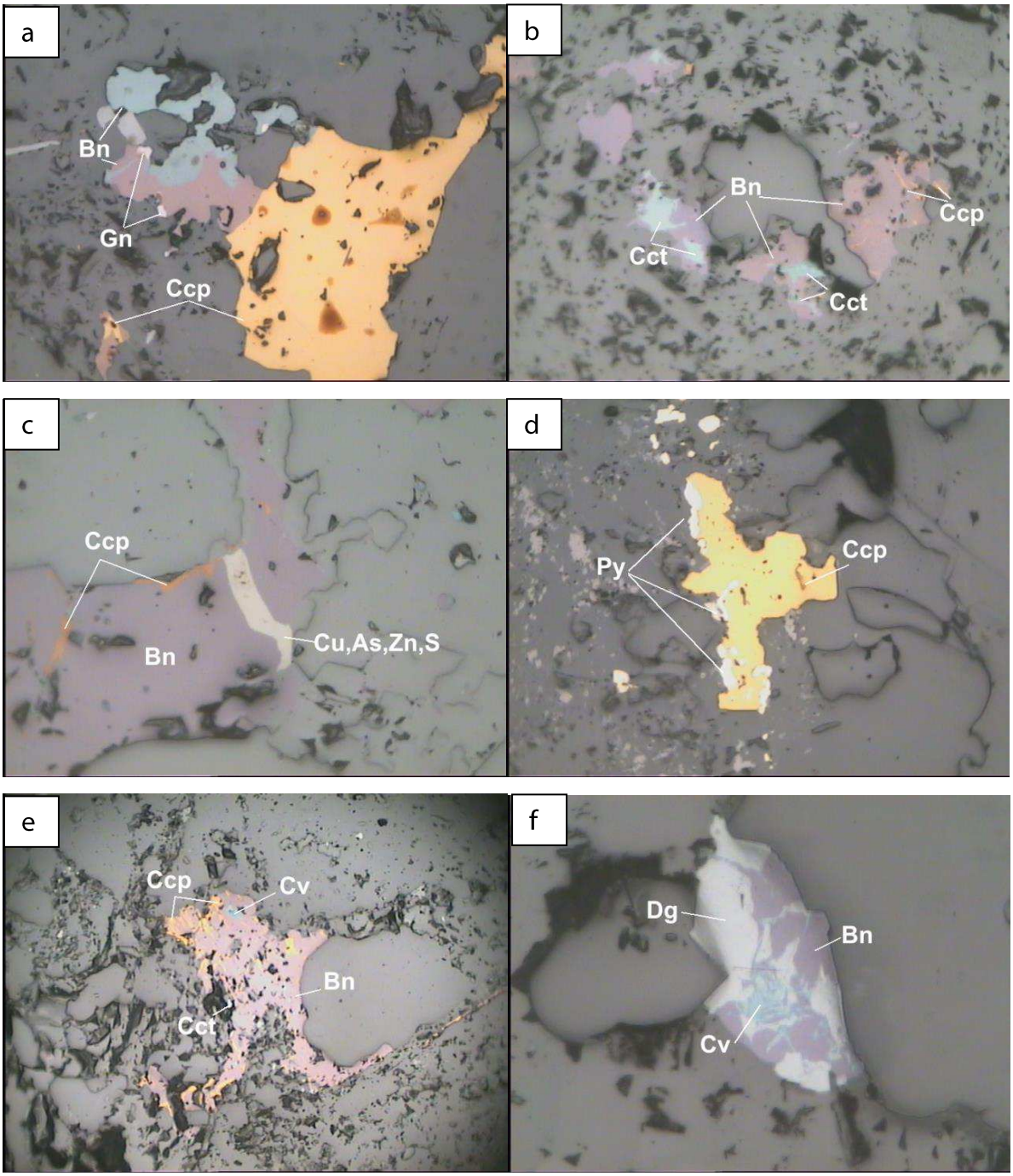

Figure 5.2.2. *Photomicrographs in reflected light showing: a) assemblage of chalcopyrite (Ccp), bornite (Bn) and galena (Gn). NS-5b; b) microinclusions of chalcocite (Cct) and chalcopyrite (Ccp) within bornite (Bn). NS-26; c) chalcopyrite (Ccp) emulsion in bornite (Bn) and an unknown Cu,As,Zn,S bearing mineral occurring as a vein in bornite. NS- 2b; d) intergrowth of chalcopyrite with pyrite. NS-10; e) secondary replacement of bornite (Bn) grain with chalcopyrite (Ccp), chalcocite (Cct) and covellite (Cv). NS-14; f) bornite (Bn) together with digenite (Dg) being replaced by covellite (Cv). NS-16.*

Note: Abbreviations of the mineral names are after *Whitney and Evans (2010).*

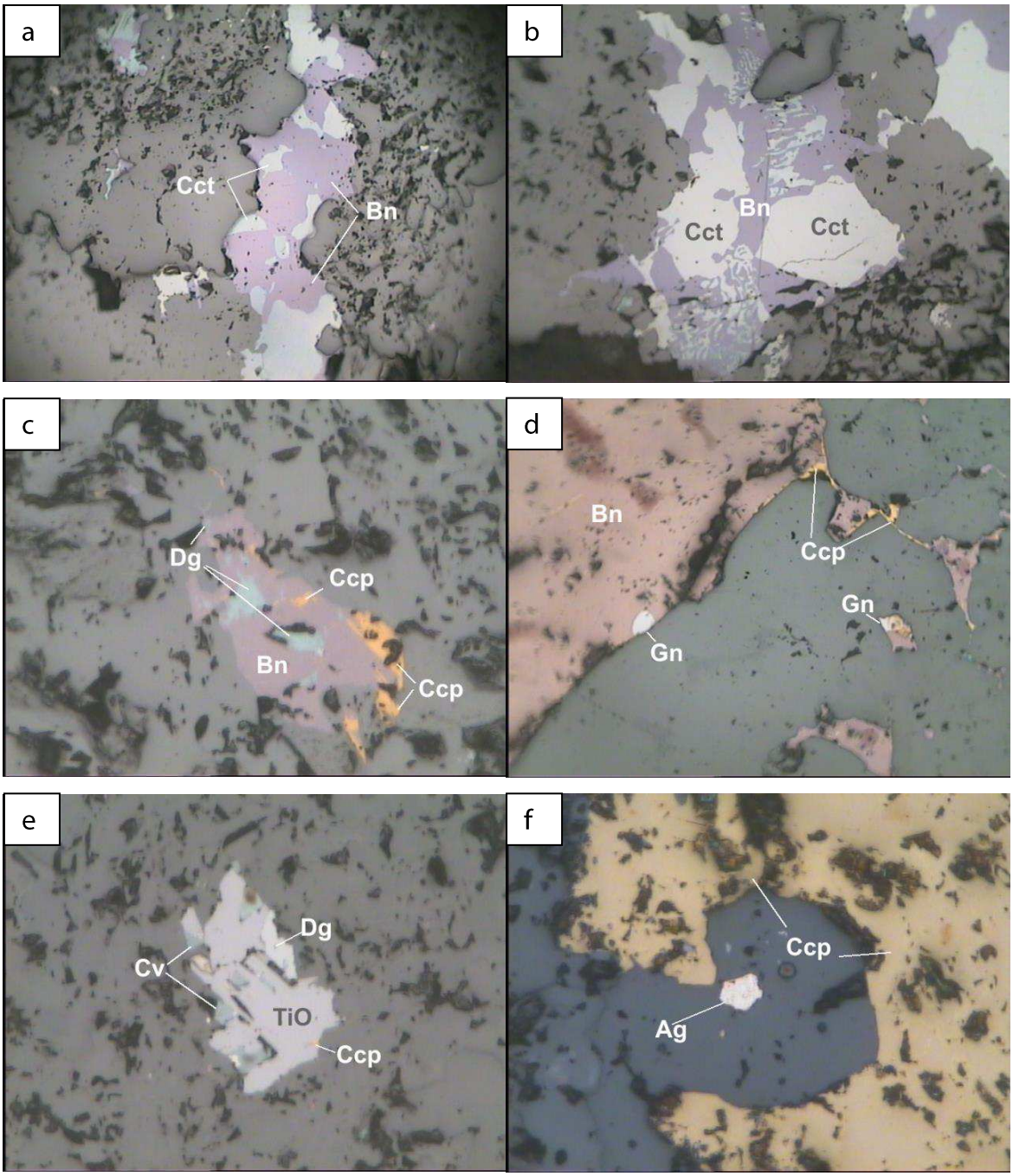

Figure 5.2.3. *Photomicrographs in reflected light. a) Microassemblage of bornite (Bn) with chalcocite (Cct). NS-16; b) Microphotograph of bornite grain partly replaced by chalcocite. NS-16; c) Microphotograph of bornite (Bn) grain replaced by chalcopyrite (Ccp), digenite (Dg). NS-26; d) Inclusion of galena (Gn) in bornite (Bn), formation of chalcopyrite on behalf of bornite (Ccp). NS-4; e) Microassemblage of chalcopyrite (Ccp), covellite (Cv), digenite (Dg) in a grain of rutile (TiO_2). NS-26; f) Microphotograph of native silver grain (Ag) close to chalcopyrite. NS-5b.*
Note: Abbreviations of mineral names are after *Whitney and Evans (2010).*

Pyrite (FeS) is a ubiquitous mineral that has been observed throughout the studied sequence. The mineral is distributed both in the matrix in form of single grains, but also forms intergrowths with chalcopyrite (Fig.5.2.2, d). The composition of the pyrite studied here is given in the Appendix 5 (Table 5.2.6).

Galena (PbS) was found in form of inclusions within bornite in drill hole BH60. However it was also found minor amounts in drill hole NS-08/06 in on the 91.86-198.0m interval. Galena shows trace concentrations of Au, Ag, Cu, Zn, and As (Appendix 5, 5.2.6).

Besides the minerals described above, silver minerals were have also been observed. Ag is occurring in different minerals. It has been observed as a native element that is often oxidized and contains some contaminant of Fe, As, S and Cu; as *argentite (Ag_2S)*; *cerargyrite* (also called chlorargyrite) – *AgCl*; and *stromeyerite (CuAgS).* The inclusions are, as a rule, very small (2-20µm). Only EDS spectrometer allowed obtaining analysis and the observation of intergrowths with bornite and chalcocite (Fig.5.2.4), and assemblage of two silver minerals (Fig.5.2.5). The chemical data obtained for the minerals of silver are given in Appendix 5 (5.2.8).

Other rare minerals that have been observed include *gersdorffite (NiAsS)*, *molybdenite (MoS_2), an* unknown Pb,S,O-bearing mineral, an unknown Cu,Zn,As,Fe,S-bearing mineral, and an unknown As,S-bearing mineral. The chemical compositions of these minerals are given in Appendix 5, tables 5.2.9-5.2.11.

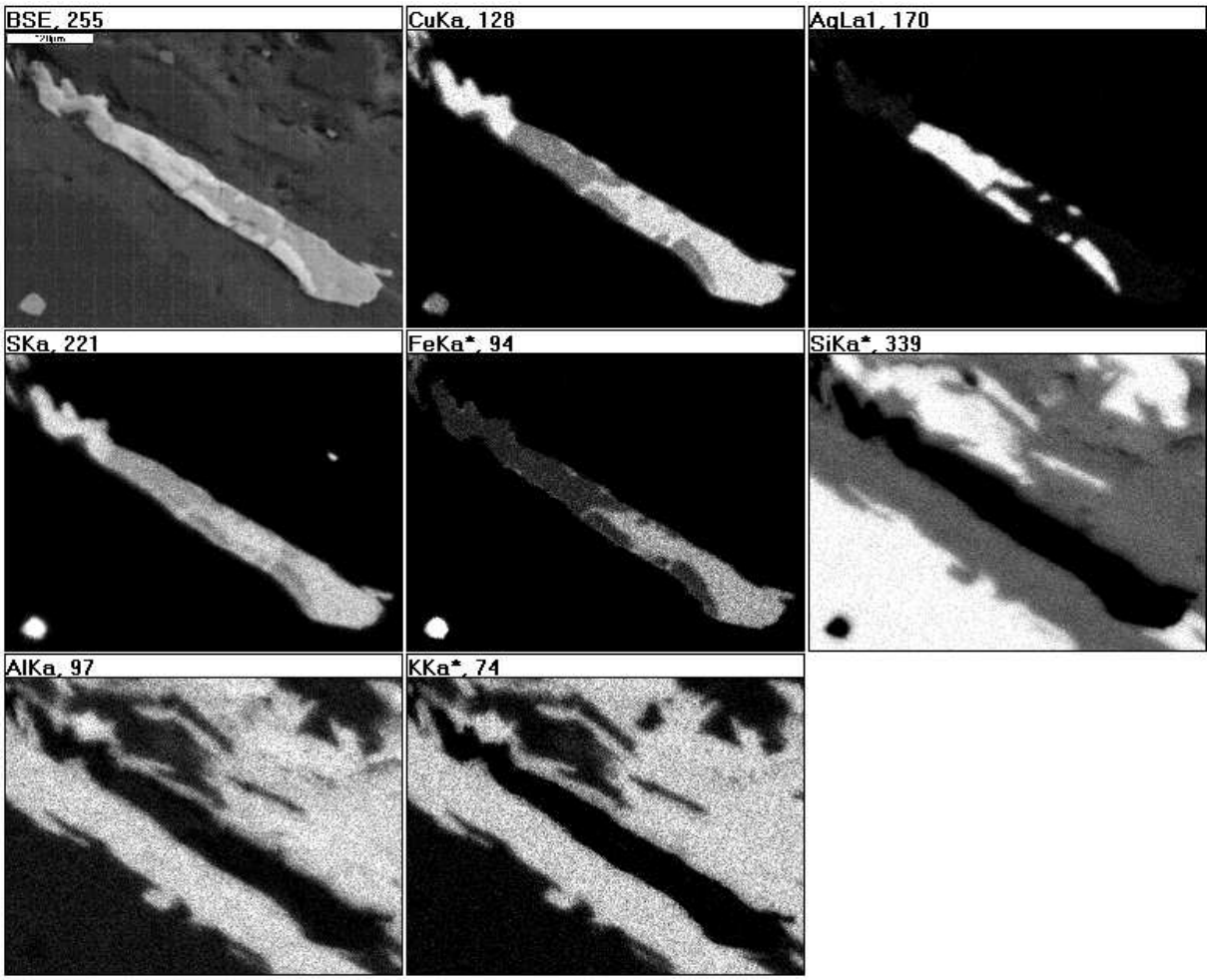

Figure 5.2.4. *Back-scattered electron image showing the elements distribution within a veinlet-like appearance of stromeyerite (CuAgS), bornite (Cu_5FeS_4) and chalcocite (Cu_2S) in biotite. NS-1a.*

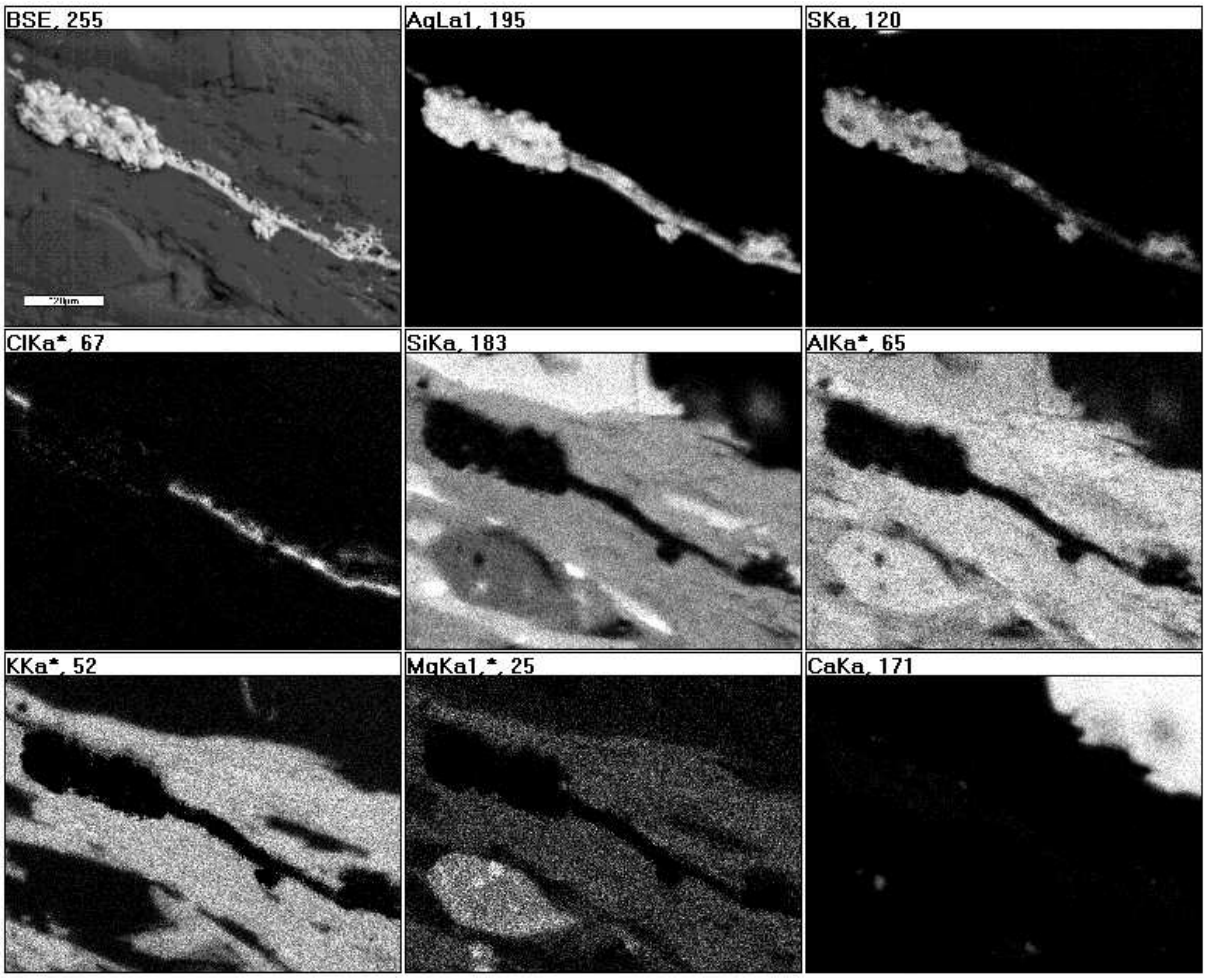

Figure 5.2.5. *Back-scattered electron image demonstrating distribution of elements within intergrowth of argentite (Ag_2S) with cerargyrite (AgCl) in biotite. NS-1a.*

Chapter 6. Discussion

The Nussir deposit of copper is a volcanogenic-sedimentary deposit that has undergone green-schist facies methamorphism and deformation. The mineralization is distributed over different lithologies. However, it can be observed that the mineralization is enriched in dolomite and dolomitic layers. The highest amount of metals is always confined to carbonate, quartz-carbonate and quartz veins. Deformation structures including crenulation cleavage in mica-rich layers, sigmoidal shaped aggregates of quartz and carbonate, as well as elongated grains of quartz in veinlets and recrystallized quartz grains, suggest that the rock was exposed to contractional forces after its formation. Most likely, the alteration of the host rocks resulting in low-grade metamorphism took place during formation of veinlets and subsequent deformation processes. Veins of deformed and undeformed carbonate grains indicate at least two generations of carbonate formation; the last generation of carbonate formed as a result of compressional deformation.

The samples taken from drill hole NS-08/06 from 65.4m to 203.4m depth show characteristics of mafic compositions, therefore these samples were plotted in classification diagrams for basaltic rocks. Looking on the compositional diagrams presented in chapter 4, it is clear that the majority of the samples from the upper intervals (NS-6-NS-14) belong to subalkaline/tholeiite basalts (Fig.4.2.2, 4.2.3. 4.3.3). The variations observed in the TAS diagram might be explained by that Na_2O+K_2O as well as SiO_2 contents have been significantly altered during hydrothermal reworking of the rocks. However, other classification schemes applied to the rocks show different result. The AFM diagram (Fig.4.2.3) demonstrates that samples NS-6-NS-13 plot in the field of tholeiitic series, while NS-14 plot in the field of calc-alkaline series. These two series represent to different tectonic environments; tholeiite is typical for mid-oceanic ridge environments, while calc-alkaline for oceanic islands and continents. However, there are some uncertainties associated with the AFM diagram, since the studied rocks obviously have been metamorphosed, and the alkali group elements might have been modified due to this. The diagram after Mullen, 1983 gave more information and it was determined that NS-12 belongs to ocean-island tholeiite, NS-10 to island-arc tholeiite and NS-13 and NS-11 to mid-oceanic ridge basalt. Comparison with the diagram after Pearce et al (1977) showed that most of the samples belong to the subalkaline-alkaline series, and were formed in an

environment similar to ocean island, continental and spreading center island. Also the diagram after Winchester and Floyd (1977) confirmed alkali composition of samples NS-6 and NS-14. Further work with samples and attempts to plot them on the diagrams proposed by Pearce (1982) and Pearce and Cann (1973) did not give any clear results. However, it should be mentioned that one sample (NS-14) appeared to be in the field of island-arc tholeiite in both diagrams. A spider diagram made on the distribution of REE in sample NS-4 shows that light REE dominate upon heavy REE, excluding that the rock is confined to MORB (mid-ocean ridge) basalts. Nevertheless, it is likely to be inappropriate to use these diagrams, since the studied samples are not strictly basalts. However, attempts were made in order to understand the tectonic position of the rocks and their composition.

The ore mineral content of the studied rocks shows a vertical zonation. Thus, in the upper parts of the section, chalcopyrite dominates. During mineral chemical analysis of the sample from drill hole BH-60 taken from 28.45m, it was discovered native silver, argentite (Ag_2S); cerargyrite (also called chlorargyrite – AgCl); and stromeyerite (CuAgS). In the upper horizons of NS-08/06 drill hole galena was also found. Deeper along the section, chalcopyrite was changed by bornite, digenite, chalcocite and covellite. This is a classical hydrothermal zonation, with silver and lead on top and copper distributes lower along the vertical section. Also copper minerals show enrichment of copper toward depth. The more copper a mineral contains the more difficult it is dissolved, therefore, such minerals as chalcocite and digenite will dominate in the bottom parts (Pirajno, 2009).

The Nussir deposit was earlier compared and described as a sedimentary-stratiform copper deposit like Kupferschifer (Germany, Poland) and Zambian Copper Belt (Central Africa) (Brems et al, 2009, Sillitoe et al, 2010, Dewaele et al, 2006, Desouky et al, 2009, Selley et al., 2005). Besides, other examples exist in the world. Among them Redstone Copperbelt (Canada) (Ripley et al., 1980, Chartrand and Brown, 1985), Udokan deposit in Siberia, Kalahari Copperbelt (Namibia and Botswana), White Pine (Michigan, USA) (Brown, 1971), Donchuan (China) and a number of smaller deposits. Indeed, there are big similarities. As it was mentioned above, the dolomitic layers, as well as those which have been carbonatized and silicized contain the highest amounts of copper and other metals. The same picture is observed on the Zairian Copperbelt where the rock hosting the copper mineralizations is dolomite and dolomitic carbonaceous shale; in the Zambian Copperbelt host rock is sandstone, argillite, dolomite; in Redstone the mineralizations occur in dolomitic

carbonate; and the hosting rock for the Troy (Spar Lake) deposit of Montana is an argillaceous quartzite. Interestingly, the footwall sediments that are associated with the deposits of the Zambian Copperbelt is a sandstone-conglomerate. Note, that in the Nussir area, conglomerate and breccia occur in the lowermost part of the formation. Another feature that allows comparison of Nussir with these deposits is the zonation of ore minerals that was observed from the Zairian portion of Central African Copperbelt. It was noticed and emphasised that iron-rich sulfides were gradually replaced by copper-rich sulfides in the following sequence: (from top to bottom) pyrite→chalcopyrite→bornite→digenite→chalcocite. The similar assemblage of copper sulfides plus covellite was observed also from the Nussir samples.

There are two main ideas of the formation of these deposits. The first one is based on circulating chloride-rich saline fluids containing dissolved metals. Important factors for this type of formation is the presence of an evaporite formation that is capable of producing salts and sulphates that are important for the formation of brines according to Pirajno (2009). Furthermore, the presence of red beds (hematite-containing sediments) is necessary as a source of copper (Brown, 1984, Brown, 1992, Hitzman et al. 2005, Hitzman et al, 2010) and for creating a reduced environment. However, alkaline mafic intrusions could also be a source of metals. Undoubtedly, diagenetic processes also play an important role. (Pirajno, 2009). Sulphur necessary for sulphide formation might have been derived from evaporites or seawater during bacterial reduction according to following formula:

$$CaSO_4+CH_4 \rightarrow CaCO_3+H_2S+H_2O$$

$$MeCl_2+H_2S \rightarrow MeS+2HCl$$

Another way of copper ore formation can be related to hydrothermal processes, as for the White Pine, Central African Copperbelt, Zambian Copperbelt. An example of particular interest is the Klein Aub Cu-Ag deposit from Kalahari Copperbelt (Botswana).

The hydrothermal fluids formed as a result of evolution of the sedimentary basin. This process is described in details in Hanor (1979), Garven and Raffensperger (1997) and a review was done by Pirajno (2009). The key factors for the formation of the fluids are diagenesis and compaction of the basin. During the compaction pore water trapped in the sediments is released and subjected to overpressure because of overloading sediments or due to dehydration reactions, and pressure solution (deformation mechanism that involves dissolution of minerals at grain-to-grain contacts). Afterwards, tectonic

compression and thrusting occurred, followed by crustal extension and normal faulting. According to Sibson et al (1975) seismic pumping mechanism is also involved in the process provoking fluids to move along faults and adjacent cracks and failures. In order to form metalliferous hydrothermal vein deposits, the faults should penetrate volcanic rocks, sediments under the lithification process or metamorphism, or a granitic pluton.

The Klein Aub Cu-Ag deposit is an interesting example since it has some similarities with the Nussir deposit. First of all, the geological structure of the Klein Aub deposit include the following lithologies from the bottom to top: granite and gneiss; acid volcanics; conglomerate, quartzite with basaltic horizons; quartzite, argillite, limestone containing mineralization, overlain by a breccia zone and fine-grained quartzite. The leaching of copper and other metals was, according to Borg and Maiden (1987) from underlying basaltic lavas. The reserves of copper were 7.5Mt with 2 wt % Cu, while silver contained 5.5Mt with 50 ppm Ag. The initial sulphur isotopic value was $\delta^{34}S$ - 0‰. The data reported by Nilsen (2006) on the Nussir deposit showed varying sulphur isotopes $\delta^{34}S$ from -10.5‰ (in pure bornite) to +0.5‰ (chalcopyrite with some bornite) that likely corresponds to marine sulphate followed by bacterial reduction.

Another example resembling the Nussir deposit was described by Sillitoe et al (2010). On the Central African Copperbelt they established a connection between copper and quartz-carbonate veins and veinlets. The mineralization here is hosted by siliciclastic, argillaceous, and dolomitic lithologies. Similar to the Nussir deposit, the mineralization is found in two types: fine-grained disseminated and coarser grained confined to quartz-carbonate veinlets and veins. In all places, the ore minerals are the same both in host rock and in the corresponding vein. This gave a base for stating the simultaneous formation of the disseminated mineralization and the accompanying vein-like mineralization. Besides, these veins contain K-feldspar, chlorite, sericite, biotite, albite and tremolite.

Conclusion

The Nussir copper deposit is a sedimentary-hosted deposit formed under hydrothermal alteration of the host rock. It has undergone green-schist facies metamorphism during contractional deformation. Evidences for this include ubiquitous chlorite, sigmoidal shaped quartz aggregates, and widespread quartz recrystallization.

The mineralization is represented by chalcopyrite, bornite, chalcocite, digenite and covellite.

The mineralization is observed both in disseminated form and confined to veins and veinlets. The enhanced copper content that have been observed in dolomitic layers indicate that that dolomite has played a role as chemical traps during the hydrothermal processes. Copper minerals dominate upon silver minerals (argentite, stromeyerite, cerargirite, and native silver), and galena.

It is observed a vertical zonation of ore minerals, from top to bottom: pyrite, galena, silver minerals, chalcopyrite–bornite–chalcocite, digenite, and covellite. This sequence is typical for hydrothermal processes, when lower temperature minerals (galena and silver minerals) are deposited in the uppermost levels of the mineralized formation.

References

1. Bingen B., Nordgulen, Ø., Viola G., 2008. A four-phase model for the Sveconorwegian orogeny, SW Scandinavia. *Norwegian Journal of Geology*. Vol. 88, pp. 43-72. Trondheim.
2. Borg G., Maiden K.J., 1987. Alteration of late Middle Proterozoic volcanics and its relation to stratabound copper-silver-gold mineralization along the margin of the Kalahari Craton in SWA/Namibia and Botswana. *Geol. Soc. Spec.Publ.* 33, pp. 347-354.
3. Boynton W.V., 1984. Geochemistry of the rare earth elements: meteoric studies. In: Henderson P. (edn). *Rare earth element geochemistry*. Elsevier, pp. 63-114.
4. Brems D., Muchez Ph., Sikazwe O., Mukumba W., 2009. Metallogenesis of the Nkana copper-cobalt South orebody, Zambia. *Journal of African Earth Sciences*, vol. 55, pp. 185-196.
5. Brown A.C., 1971. Zoning in the White Pine copper deposit, Ontogon Country, Michigan. *Economic Geology*, vol. 66, pp. 543-573.
6. Brown A.C., 1984. Alternative sources of metals for stratiform copper deposits. *Precambrian Research*, 25. Elsevier Science Publishers B.V., Amsterdam, pp. 61-74
7. Brown A.C., 1992. Sediment-hosted stratiform copper deposits. *Ore Deposits Models*, vol. II. Geoscience Canada Reprint Series 6, pp. 99-115.
8. Bugge A. U., 1982. Norway. In: Bowie S.H.U., Kvalheim A. and Haslam, H.W (eds.). *Mineral Deposits of Europe*. Vol. 1. Northwest Europe. Moscow, pp. 330-408.
9. Chartrand F.M., Brown A.C., 1985. The diagenetic origin of stratiform copper mineralization, Coates Lake, Redstone Copperbelt, N.W.T., Canada. *Economic Geology*, vol. 80, pp. 325-343.
10. Desouky H.A.El, Muchez Ph., Cailteux J., 2009. Two Cu-Co sulfide phases and contrasting fluid systems in the Katanga Copperbelt, Democratic Republic of Congo. *Ore Geology Reviews*, vol. 36, p. 315-332.
11. Dewaele S., Muchez Ph., Vets J., Fernandez-Alonso M., Tack L., 2006. Multiphase origin of the Cu-Co ore deposits in the western part of the Lufilian fold-and-thrust belt, Katanga (Democratic Republic of Congo). *Journal of African Earth Sciences*, vol. 46, p. 455-469.
12. Ehlers C., Lindroos A., Selonen O., 1993. The late Svecofennian granite-migmatite zone of southern Finland – a belt of transpressive deformation and granite emplacement. *Precambrian Research,* 64, pp. 295-309.
13. Gaàl, G., Gorbatchev, R., 1987. An outline of the Precambrian evolution of the Baltic Shield. *Precambrian Research*, 35, 15-52.
14. Garven G., Raffensperger J.P., 1997. Hydrology and geochemistry of ore genesis in sedimentary basins. In: Barnes H.L. (ed) *Geochemistry of ore deposits*, 3rd edn. John Wiley & Sons, New York, pp. 125-189.
15. Gee D.G., Fossen H., Henriksen N., Higgins A.K., 2008. From the earlty Paleozoic platform of Baltica and Laurentia to the Caledonide orogen of Scandinavia and Greenland. *Episodes,* vol. 31, No.1, pp. 44-51.

16. Griffin W.L., Taylor P.N., Hakkinen J.W., Heier K.S., Iden I.K., Krogh E.J., Malm O., Olsen K.I., Ormaasen D.E., Tveten E., 1978. Archaean and Proterozoic crustal evolution in Lofoten-Vesterålen, N Norway. *J. geol Soc. Lond.,* vol. 135, pp. 629-647.
17. Gorbatschev R., Bogdanova S., 1993. Frontiers in the Baltic Shield. *Precambrian Research*, 64, Elsevier Science Publishers B.V., pp. 3-21
18. Hitzman M., Kirkham R., Broughton D., Thorson J., Selley D., 2005. The sediment-hosted stratiform copper ore system. Society of Economic Geologists, Inc. *Economic Geology 100th Anniversary Volume*, pp. 609-642.
19. Hitzman M.W., Selley D., Bull S., 2010. Formation of sedimentary rock-hosted stratiform copper deposits through Earth history. *Economic Geology*, vol. 105, Society of Economic Geologists. Inc. pp. 627-639.
20. Hanor J. S. 1979. The sedimentary genesis of hydrothermal fluids. In. Barnes H.L. (ed) *Geochemistry of hydrothermal ore deposits*, 2nd edn. John Wiley & Sons, New York, pp 137-172.
21. Irvine, T.N., and Baragar, W.R.A., 1971. A guide to the chemical classification of the common volcanic rocks. *Canadian Journal of Earth Sciences,* vol. 8, pp. 523-548.
22. Jensen P.A., 1996. The Altenes and Repparfjord tectonic windows, Finnmark, northern Norway: Remnants of a Palaeoproterozoic Andean-type plate margin at the rim of the Baltic Shield. Unpubl. Dr.Thesis, Univ. of Tromsø.
23. Johansson, L., Lindh, A., Möller, C., 1991. Late Sveconorwegian (Grenville) high-pressure granulite facies metamorphism in south-west Sweden. *Journal of Metamorphic Geology*, 9, pp. 283-292.
24. Kerr, P.F., 1977: Optical mineralogy, pp. 492.
25. Koistinen, T., Stephens, M.B., Bogatchev, V., Nordgulen, Ø., Wennerström, M., Korhonen, J., 2001. Geological map of the Fennoscandian Shield, scale 1:2 000 000. Geological Survey of Finland, Norway and Sweden and the North-Wes Department of Natural Resources of Russia.
26. Krawczyk C.M., McCann T., Cocks L.R.M., England R.W., McBride J.H., Wybraniec S., 2008. Caledonian tectonics. In: *The Geology of Central Europe*, vol. 1: Precambrian and Palaeozoic. McCann T. (edn). The Geological Society of London, pp. 303-381
27. Lebas, M.J., Lemaitre, R.W., Streckeisen, A. and Zanettin, B., 1986. A Chemical Classification of Volcanic-Rocks Based on the Total Alkali Silica Diagram. *Journal of Petrology*, 27(3), pp. 745-750.
28. Lundberg, B., 1980. Aspects of the geology of the Skellefte field, northern Sweden. *Geol. Fören. Stockholm Förh.*, 102, pp. 156-166
29. McKerrow W.S., Mac Niocaill C., Dewey J.F., 2000. The Caledonian Orogeny redefined. *J. Geol. Soc. Lond.,* vol. 157, pp. 1149-1154.
30. Mertanen S., Pesonen L.J., 2005. Drift History of the Shield. In: Lehtinen M., Nurmi P.A., O.T. Rämö *(eds) Precambrian Geology of Finland: key to the evolution of the Fennoscandian Shield*. Elsevier.

31. Mullen, E.D., 1983. $MnO/TiO_2/P_2O_5$. A minor element discriminant for basaltic rocks of oceanic environments and its implications for petrogenesis. *Earth and Planetary Science Letters*, vol. 62, pp. 53-62.
32. Mun Y.S., 2011. Mineralogical and petrologic study of the Nussir deposit of copper. Northern Norway. Geological Project-3222, pp. 38.
33. Nilsen K.S., 2006. Kjerneboringer i Nussir 2006 evaluering av kobbermalm. Rapport N2006. p. 5.
34. Nordgulen, Ø., Andresen, A., 2008. The Precambrian. In: Ramberg, I. B., Bryhni, I., Nøttvedt, A. and Rangnes, K. (eds.) 2008, *The Making of a Land – Geology of Norway*. Trondheim. Norsk Geologisk Forening, p. 624.
35. Peace J.A., Cann J.R., 1973. Tectonic setting of basic volcanic rocks determined using trace element analyses. *Earth and Planetary Science Letters*, vol.19, pp. 290-300.
36. Pearce T.H., Gorman B.E., Birkett T.C., 1977. The relationship between major element chemistry and tectonic environment of basic and intermediate volcanic rocks. *Earth and Planetary Science Letters*, vol. 36. Elsevier Scientific Publishing Company, Amsterdam. pp. 121-132.
37. Pearce J.A., 1982. Trace element characteristics of lavas from destructive plate boundaries. Thorpe R.S (edn). Andesites. Eiley, Chichester. pp. 525-548.
38. Pharaoh T.C., Macintyre R.M., Ramsay D.M., 1982. K-Ar determination on the Raipas suite in the Komagfjord Window, northern Norway. In: Juve G. (edn). *Norsk Geologisk Tidsskrift,* vol. 62. Universitetsforlaget, Oslo, pp. 51-58.
39. Pharaoh T.C., Ramsay D.M., Jansen Ø., 1983. Stratigraphy and structure of the northern part of the Repparfjord-Komagfjord window. Finnmark, Northern Norway. *Nor. Geol. Unders.,* 377, pp. 1-45.
40. Pharaoh T., 1985. Volcanic and geochemical stratigraphy of the Nussir Group of Arctic Norway – an early Proterozoic greenstone suite. *J. geol. Soc. London.,* vol. 142, pp. 259-278.
41. Pharaoh T.C., Brewer T.S., 1990. Spatial and temporal diversity of early Proterozoic volcanic sequence – comparison between the Baltic and Laurentian shields. *Precambrian Research,* vol. 47, Elsevier Science Publishers B.V., pp. 169-189.
42. Pirajno F., 2009. Metalliferous Sediments and sedimentary rock-hosted stratiform and/or stratabound hydrothermal mineral systems. In: *Hydrothermal processes and mineral systems.* Springer Science + Business Media B.V. pp. 727-883.
43. Priyatkina, N., 2013. Petogenesis and tectonic setting of the mafic-ultramafic rock association from NW Senja, West Troms Basement Complex. Unpubl. Master thesis in Geology. p. 77.
44. Qian X.L., 1997. Tectonic Correlation of the Precambrian Evolution of the North China Craton with the Baltic Shield. *Proceedings of the 30th International Geological Congress,* vol. 17. Part 1, pp. 43-58.
45. Ramdor, P., 1962: Ore minerals and their intergrowths, p. 1142.

46. Reitan P.H., 1963. The geology of the Komagfjord tectonic window of the Raipas suite. Finnmak, Norway. *Norges Geologiske Undersøkelse*, 221. Universitetsforlaget. p. 71.
47. Ripley E.M., Lambert M.W., Berendsen P., 1980. Mineralogy and paragenesis of Red-Beds copper mineralization in the lower Permian of South Central Kansas. *Economic Geology,* vol. 75, pp. 722-729.
48. Rollinson H.R., 1994. Using geochemical data: evaluation, presentation, interpretation. Essex: London Group UK Ltd., p. 352.
49. Sandstad, J.S., 2010. Microscopic and SEM (scanning electron microscope) investigations of thin sections from the Nussir copper deposit. NGU report 2010.025., p. 55.
50. Selley D., Broughton D., Scott R., Hitzman M., Bull S., Large R., McGoldrick P., Croaker M., Pollington N., Barra F., 2005. A new look at the geology of the Zambian Copperbelt. *Economic Geology 100th Anniversary Volume*, Society of Economic Geologists, Inc. pp. 965-1000.
51. Sibson R.H., Moore J.Mc.M, Rankin A.H., 1975. Seismic pumping- a hydrothermal fluid transport mechanism. *J Geol Soc London,* 131, pp. 653-659.
52. Sillitoe R.H., Perelló J., García A., 2010. Sulfide-bearing veinlets throughout the stratiform mineralization of the Central African Copperbelt: temporal and genetic implications. *Economic Geology*, vol. 105, pp. 1361-1368.
53. Slabunov A.I., Lobach-Zhuchenko S.B., Bibikova E.V., Balagansky V.V., Sorjonen-Ward P., Volodichev O.I., Shchipansky A.A., Svetov S.A., Chekulaev V.P., Arestova N.A., Stepanov V.S., 2006. The Archean of the Baltic Shield: geology, geochronology, and geodynamic settings. *Geotectonics,* vol. 40 (6), Pleiades Publishing, pp. 409-433..
54. Viola, G., Sandstad, J.S., Nillson, L.P. & Heincke B. Structural and ore geological studies in the northwestern part of the Repparfjord Window, Kvalsund, Finnmark, Norway. NGU report 2008.029, p. 93.
55. Whitney D.L., Evans B.W., 2010. Abbreviations for names of rock-forming minerals. *American Mineralogist*, vol. 95, pp. 185-187.
56. Winchester J.A., Floyd P.A., 1977. Geochemical magma type discrimination; application to altered and metamorphosed basic igneous rocks. *Earth Planet. Sci. Lett.*, vol. 28, pp. 325-343.
57. www.nussir.no
58. http://geo.ngu.no/kart/arealisNGU/
59. http://www.ngu.no/kart/mineralressurser/

APPENDIXES

Contents

Appendix to chapter 3 3
3.1. Drill hole NS-08/06 3
NS-6 (NS-08/06 - 65,46-65,51m) 3
NS-8 (NS-08/06-74.10-74.14m) 4
NS-9 (NS-08/06-75.35-75.40m) 4
NS-10 (NS-08/06-79.11-79.26m) 5
NS-11 (NS-08/06-81.68-81.70m) 6
NS-12 (NS-08/06-91.86-91.89m) 7
NS-13 (NS-08/06-198.0m) 8
NS-14 (NS-08/06-203.35-203.40m) 9
NS-15 (NS-08/06-206.84-206.9m) 9
NS-16 (NS-08/06-210.70-210.80m) 10
NS-17 (NS-08/06-214.85-214.9m) 11
NS-18 (NS-08/06-219.53-219.63m) 12
NS-19 (NS-08/06-221.62-221.66m) 13
NS-20 (NS-08/06-225.74-225.79m) 14
NS-21 (NS-08/06-227.05-227.10m) 15
NS-23 (NS-08/06-231.74-231.76m) 16
NS-24 (NS-08/06-231.90-231.92m) 17
NS-25 (NS-08/06-234.69m) 17
NS-26 (NS-08/10-132.8-133.0m) 18
3.2. Drill hole BH60 19
NS-1a (28.45-28.50m) 19
NS-1b (28.45-28.50m) 23
NS-2a (28.52-28.56m) 27
NS-2b (28.52-28.56m) 31
NS-3a (28.60-28.65m) 34
NS-3b (28.60-28.65m) 38
NS-4 (28.75-28.80m) 40
NS-5a (28.80-28.92m) 44
NS-5b (28.80-28.92m) 46
Appendix 2. To chapter 5.2 49

Appendix to chapter 3

3.1. Drill hole NS-08/06

NS-6 (NS-08/06 - 65,46-65,51m) (Fig.3.1.1,a)

The rock is a volcanite (Fig. 3.1.1,b), which is composed by fine-crystalized mass with fragments of quartz and plagioclase. The matrix is crosscut by quartz-carbonate veinlets, which also contain grains of biotite and Mg-Al rich chlorite (Fig. 3.1.1,c).

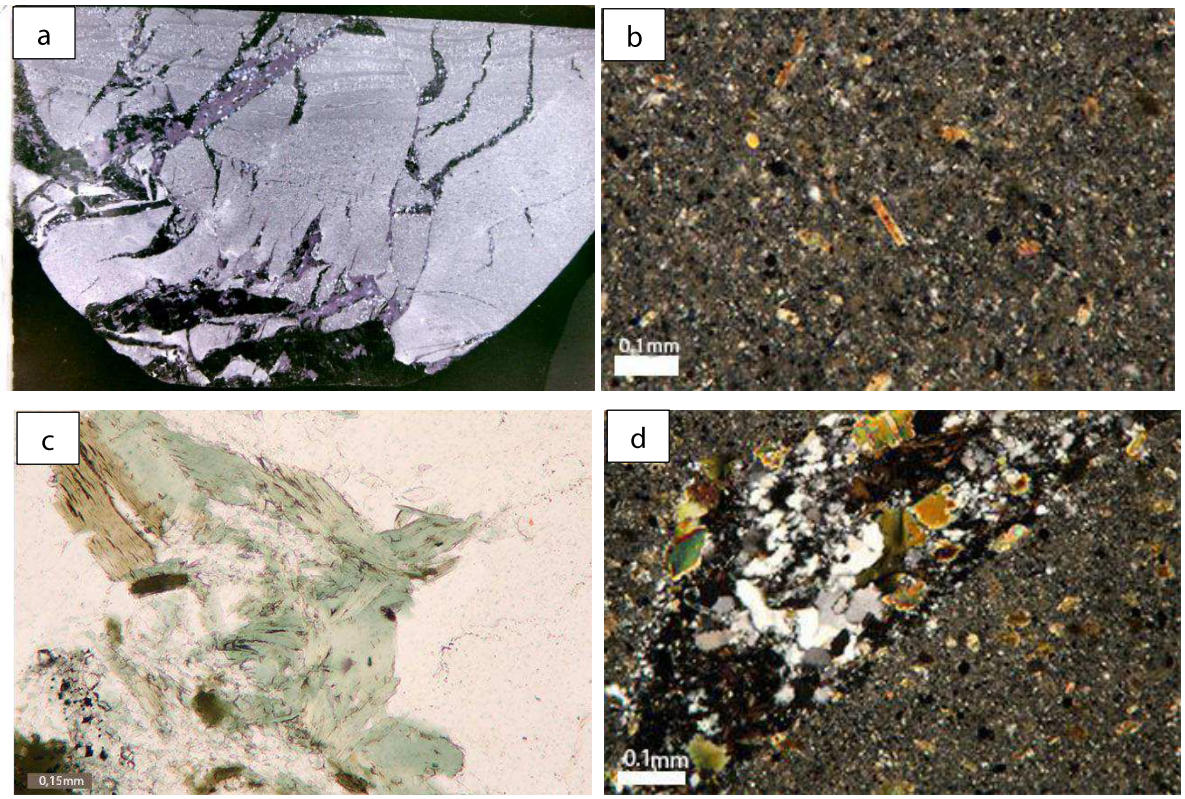

Figure. 3.1.1. *a) Photo of polished thin-section. b) Microphotograph of the volcanite in crossed polarizers (XPL); c) Chlorite and biotite in a quartz vein in plane-polarized light (PPL); d) Quartz-carbonate vein in volcanite (XPL).*

The grain size of quartz in the veinlets varies from 0.02 mm to 0.1 mm in diameter. Carbonate is represented by dolomite (rhomboidal crystals showing zonation and twins). The grain size of dolomite varies from 0.1 to 0.2mm. (Fig. 3.1.1,d).

Ore minerals are maily found in the matrix. The veinlets show low contents of ore minerals. The ore minerals include pyrite and copper minerals that are evenly distributed both in the matrix and in the veins.

NS-8 (NS-08/06-74.10-74.14m) (3.1.2,a)

The sample was collected from the contact zone between volcanite and dolomite. Both rocks are crosscut by quartz-carbonate veins, in which carbonate dominates. The veinlets also contain flakes of Mg-Al-rich chlorite (Fig. 3.1.2,b).

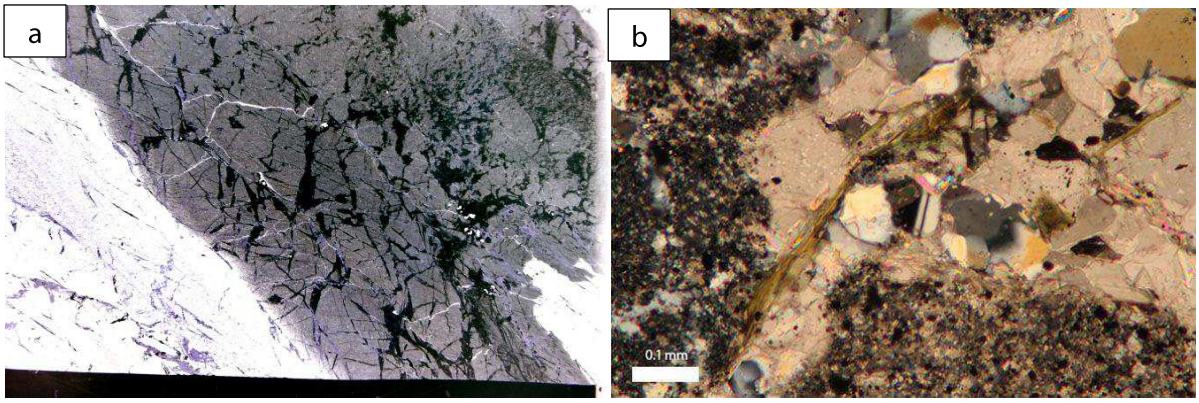

Figure 3.1.2. *a) Photo of the polished thin-section; b) Microphotograph of quartz-carbonate vein intruded into volcanite (XPL).*

Ore minerals are dispersed within the volcanite, as well as in the veins. The ore minerals include chalcopyrite that is predominantly found in the carbonate veins. Crystals of pyrite and iron oxides are also observed. Some chalcopyrite grains are partly replaced by digenite (Fig. 3.1.2, a,b).

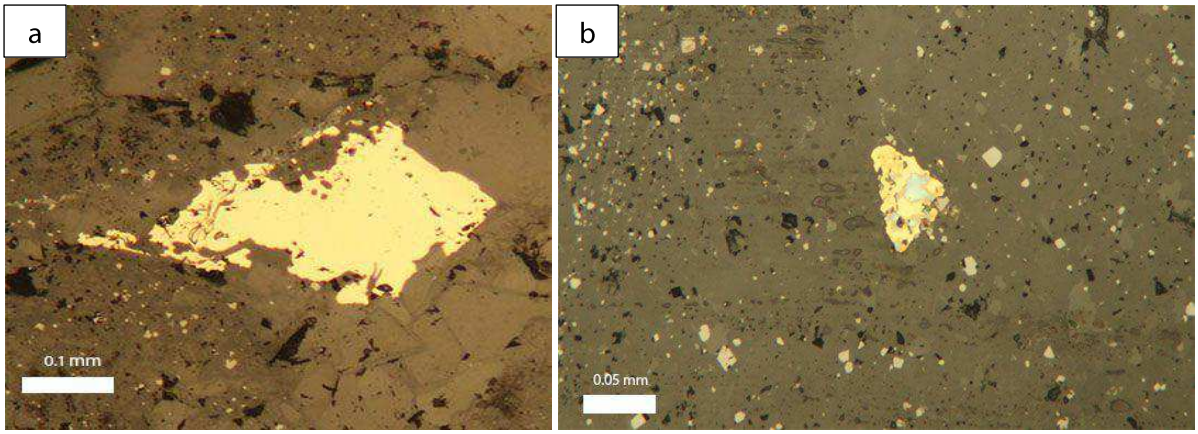

Figure 3.1.2 *a) microphotograph of chalcopyrite grain (Reflected light); b) Digenite (blue) replacing chalcopyrite (yellow); dispersed iron oxides within the matrix (Reflected light)*

NS-9 (NS-08/06-75.35-75.40m) (Fig.3.1.3,a)

The rock is a strongly chloritized volcanite, with cracks that are filled with quartz and dolomite.. In addition, flakes of muscovite are observed within the veinlets. Chlorite is Mg-Al rich (higher order interference colors different from those typical for pure chlorite).

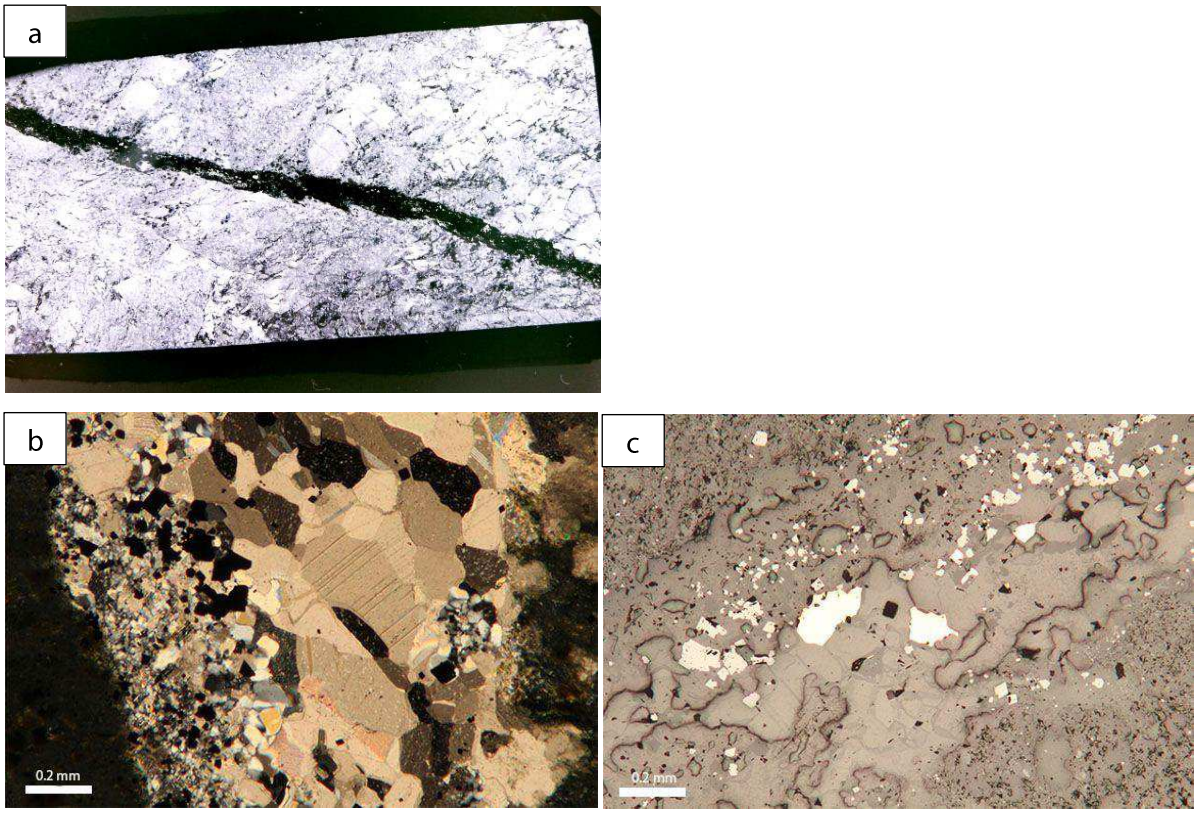

Figure 3.1.3. *a) Photograph of polished thin-section; b) Fragment of quartz-dolomite vein (XPL); c) Chalcopyrite and pyrite grains in vein (Reflected light)*

Veins have different lengths (from 0.1mm), and some of them are quite long (up to about 3mm) and crosscut whole thin section. Quartz grain size is much smaller than of carbonate and it is becoming smaller approaching the host rock (Fig. 3.1.3, b). Quartz-plagioclase veinlets are also observed. The dominating ore mineral is chalcopyrite, which can be observed both in the matrix and in the veins. Pyrite is also present. The grain size of the ore minerals varies; the largest grains are found in the veins. (Fig. 3.1.3,c).

NS-10 (NS-08/06-79.11-79.26m) (Fig.3.1.4,a)

The host rock is an intensively altered (chloritized) volcanite (Fig. 3.1.4,b). The thin section is crosscut by predominately carbonate veinlets. In the volcanite, flakes of muscovite are observed as well as seritized feldspar. The volcanite is also carbonatized.

Ore minerals include pyrite, digenite and chalcopyrite (Fig. 3.1.4,c), partly replaced by covellite.

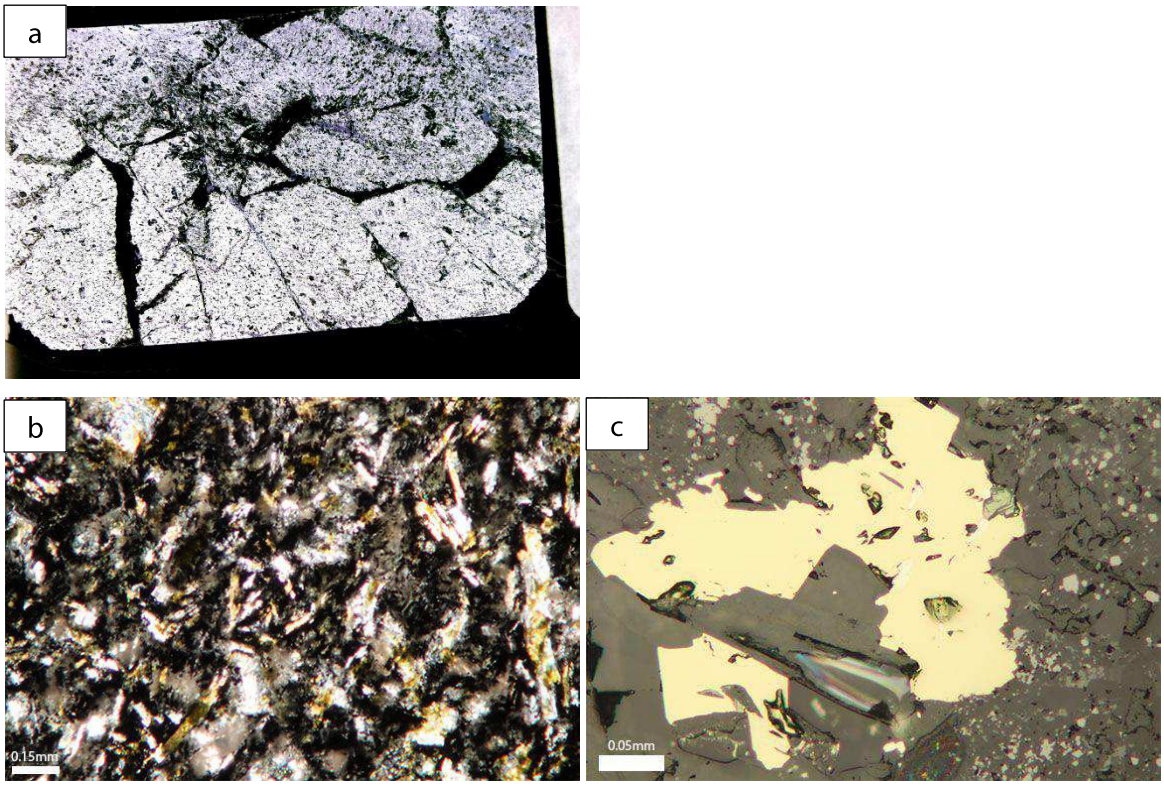

Figure 3.1.4. *a) Photograph of polished thin-section NS-10; b) Microphotograph of volcanite (XPL); c) Chalcopyrite grain with inclusions of pyrite (white)(Reflected light).*

NS-11 (NS-08/06-81.68-81.70m) (Fig.3.1.5,a)

The rock is a strongly chloritized tuffite crosscut by carbonate veins. Some domains and remnants of tuffite could be found. The degree of chloritization is increasing from the carbonate veinlet towards the tuffite. A chlorite-rich zone,also containing biotite is observed (Fig. 3.1.5, b,c). It goes through the entire sample.

Ore minerals occur as evenly dispersed small grains of chalcopyrite and pyrite. No ore minerals were observed in the carbonate veinlets.

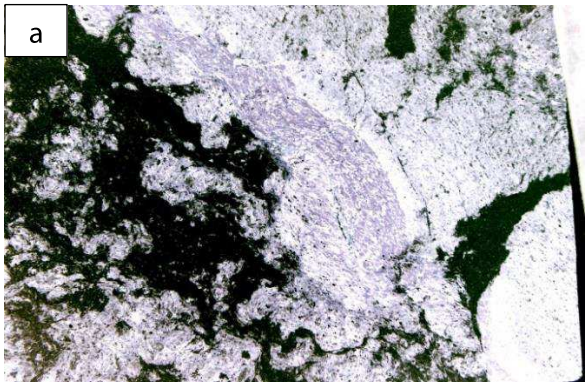

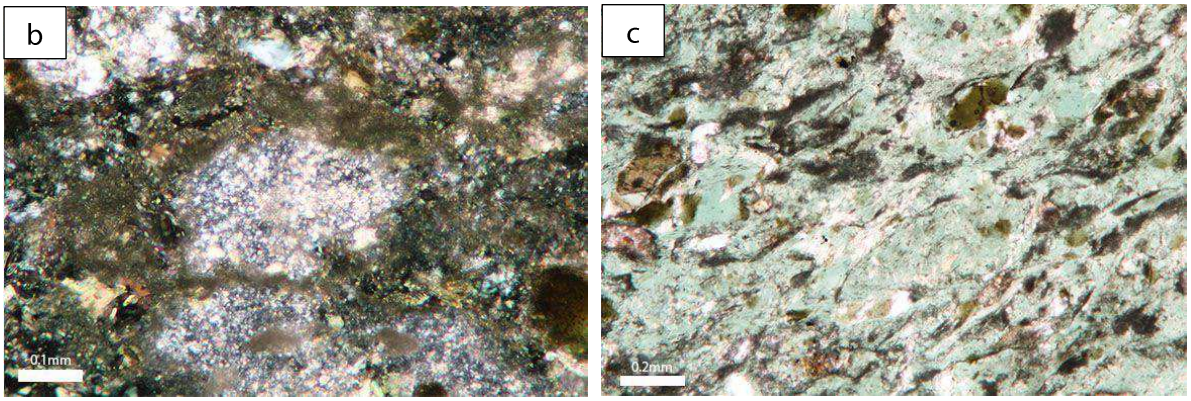

Figure 3.1.5. *a) Photograph of polished thin-section NS-11; b) remnants of tuffite surrounded by chlorite. (XPL); c) completely altered zone, composed of chlorite (XPL).*

NS-12 (NS-08/06-91.86-91.89m) (Fig.3.1.6,a)

The rock is layered (Fig. 3.1.6,b). Chlorite-rich layers contain fragments of plagioclase. Among ore minerals, chalcopyrite is distinguished and it is concentrated in zones in the tuffite (Fig. 3.1.7,a). In chlorite veins (Fig.3.1.7,b), single grains of galena are observed.

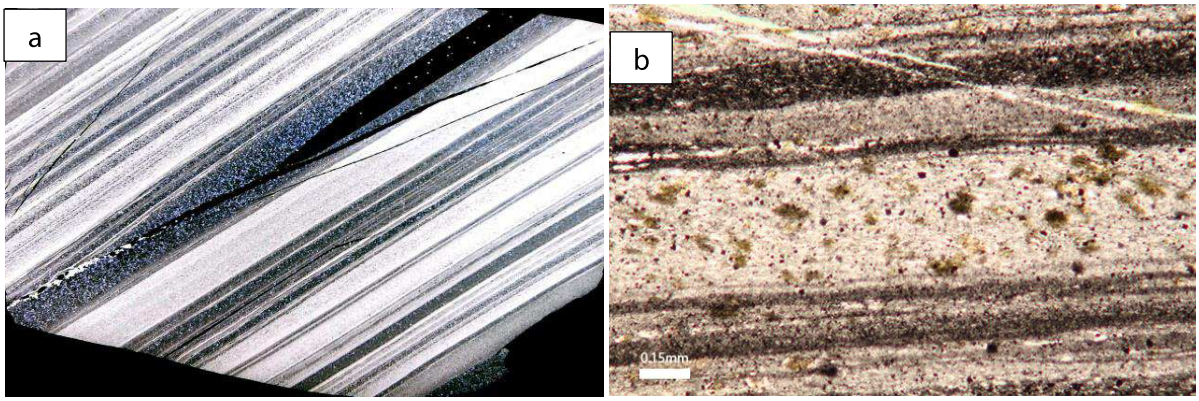

Figure 3.1.6. *a) Photograph of polished thin-section NS-12; b) Microphotograph showing layering of the rock (PPL).*

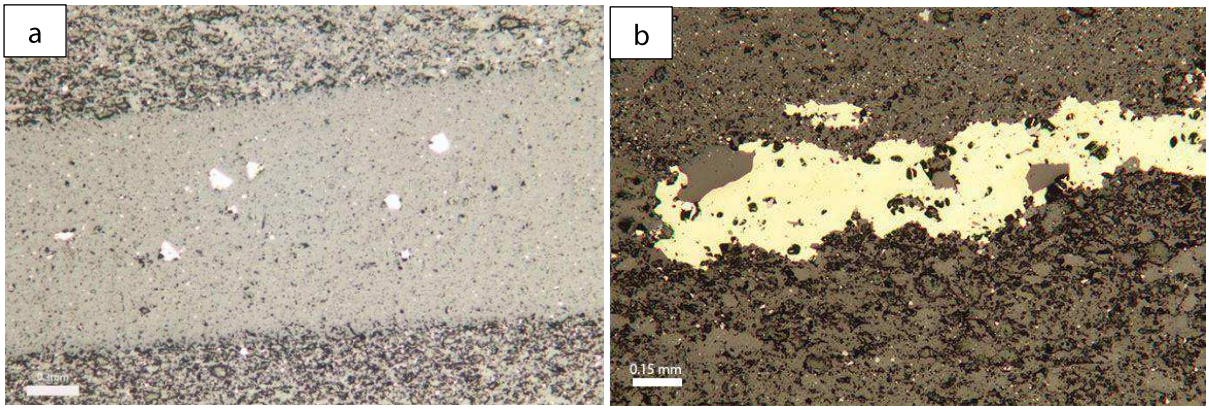

Figure 3.1.7. *a) Microphotographs of zonally distributed chalcopyrite in tuffite (PPL); b) Chalcopyrite grain formed within chlorite vein (XPL).*

NS-13 (NS-08/06-198.0m) (Fig.3.1.8)

Chloritized carbonatized tuffite containing: biotite, quartz, carbonate and sericitized feldspar (Fig. 3.1.9, a, b). Zones enriched in quartz are observed.

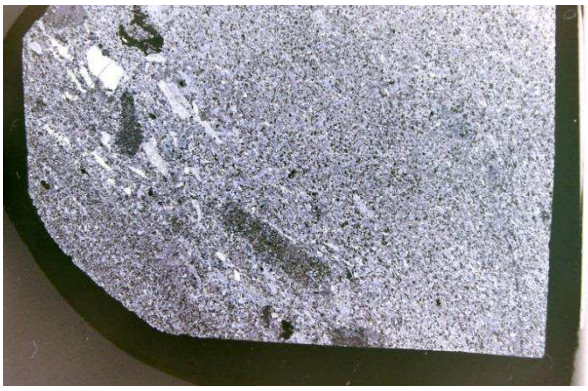

Figure 3.1.8. *Photograph of polished thin-section NS-13.*

The ore minerals include small grains of pyrite replaced by hetite and hydrohetite. It is often observed that chalcopyrite is replaced by bornite (Fig.3.1.10.). Copper minerals occurs in the matrix, but it is absent in the quartz-veins.

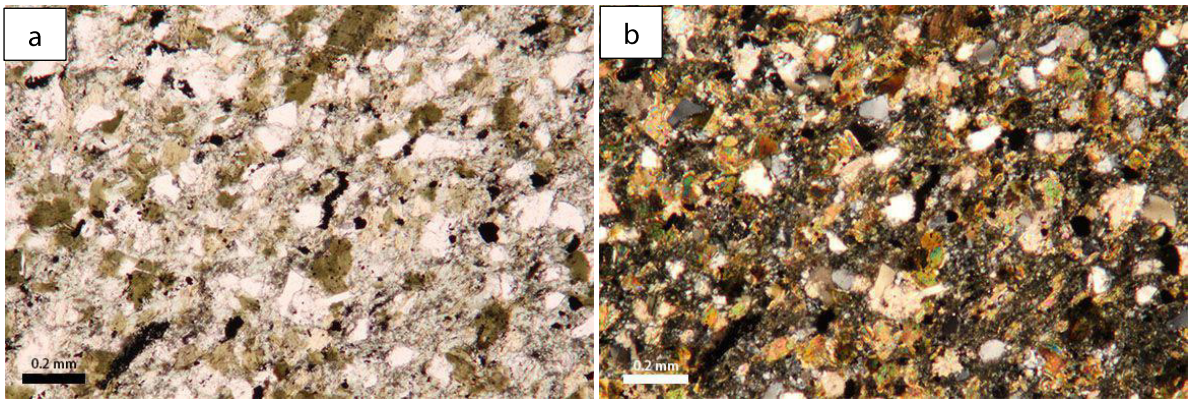

Figure 3.1.9. Microphotographs of *tuffite made in plane-polarized light (a) and in crossed nicols (b)*

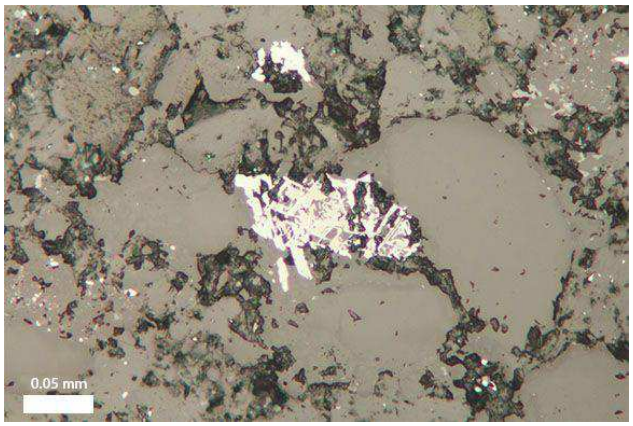

Figure 3.1.10. *Microphotograph of chalcopyrite replaced by bornite (PPL).*

NS-14 (NS-08/06-203.35-203.40m) (Fig.3.11,a)

The rock of this interval is a strongly chloritized carbonatized volcanite (Fig. 3.1.11,b.). Ore minerals are localized in the chloritized remnants of the host rock. The grain size is quite small but it increases towards the carbonate veins.

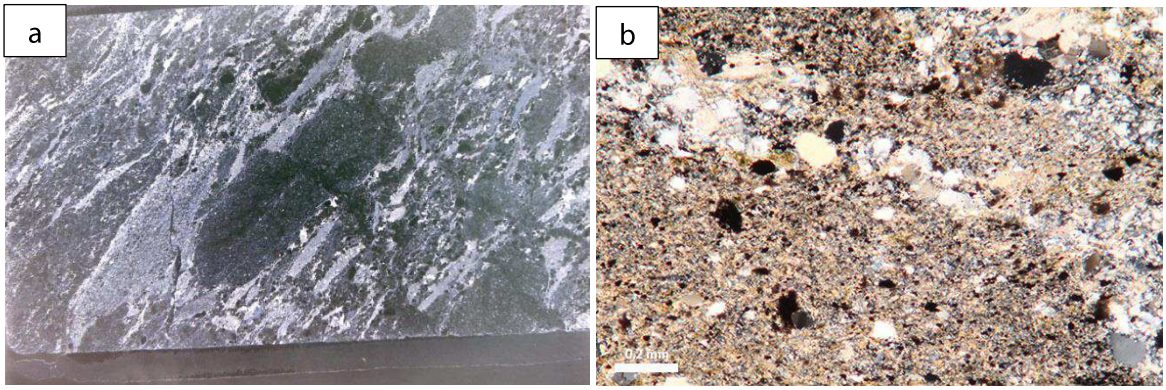

Figure 3.1.11. *a) Photograph of polished thin-section. NS-14; b) Microphotograph of chloritized remnants of volcanite crosscut by quartz vein (XPL).*

Ore minerals observed in this polished thin section include pyrhotite, bornite and chalcopyrite. Chalcopyrite, together with covellite and digenite, replace bornite (Fig.3.1.12,a).

Chalcopyrite is a secondary mineral forming on bornite. It propagates along the grain edges, and filling the cracks. Digenite and covellite are observed within bornite and in intergrowths with it (Fig. 3.1.12,a,b). Covellite and digenite are the last in a bornite-chalcopyrite-digenite-covellite row.

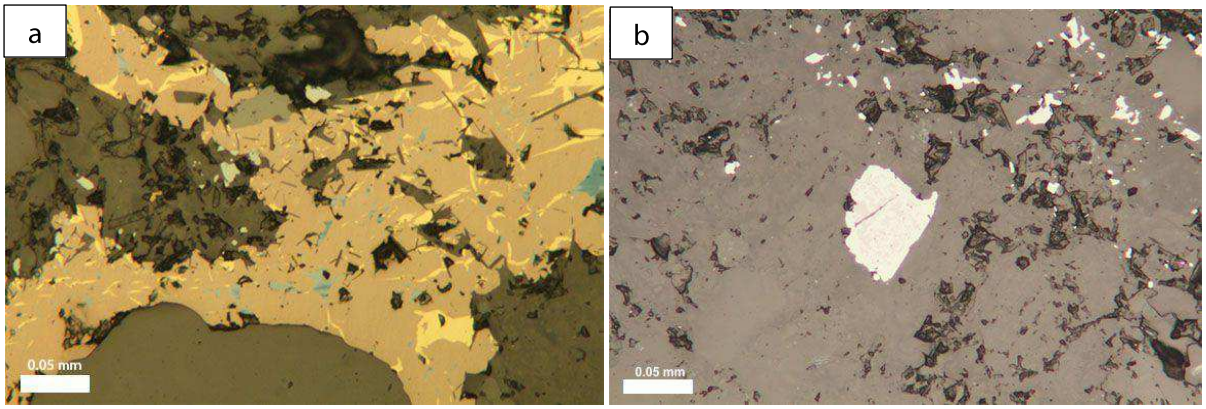

Figure 3.1.12. *a) Microphotograph demonstrating chalcopyrite (yellow), digenite (light blue) and covellite (blue) replacing bornite (pink) Ref.light); b) Digenite grain (very light blue nearly white) with emulsion of bornite (light pink within the digenite grain) (Ref.light).*

NS-15 (NS-08/06-206.84-206.9m) (Fig.3.1.13)

The rock is intensively chloritized and seritized and intruded by quartz and carbonate veins (Fig. 3.1.14, a, b). Biotite is locally observed and it is confined to quartz-carbonate

veins. The biotite shows flakes of different sizes (0.1-0.5mm). Plagioclase and K-feldspar are also observed within the veinlets.

Figure 3.1.13. *Photograph of thin-polished section. NS-15*

Based on the observation that carbonate veins crosscut quartz veins, it is concluded that the carbonate veinlets were intruded after the quartz veins (Fig.3.1.14). Carbonate is represented by dolomite (twins and zonation of grains are observed).

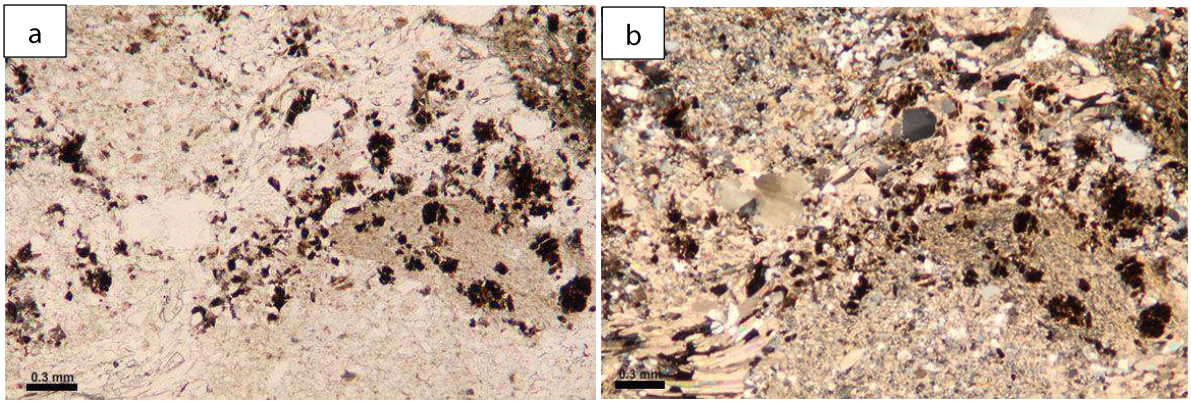

Figure 3.1.14. *Microphotographs of host rock intruded by quartz-carbonate veinlet taken in plane-polarized light (a), and in crossed polarizers (b).*

The rock shows low contents of ore minerals. The ore minerals occur as aggregates predominantly in the biotite-rich zones. Small chalcopyrite grains and various iron oxides are found in the matrix.

NS-16 (NS-08/06-210.70-210.80m) (Fig.3.1.15,a)

The matrix is a strongly chloritized layered sedimentary rock consisting of carbonate-rich rock and layered semipelite crosscut by quartz-carbonate veins (Fig. 3.1.15,b,c). The carbonate is represented by dolomite. Veins contain single grains of plagioclase and sericitized feldspars. Zircon and rutile are observed.

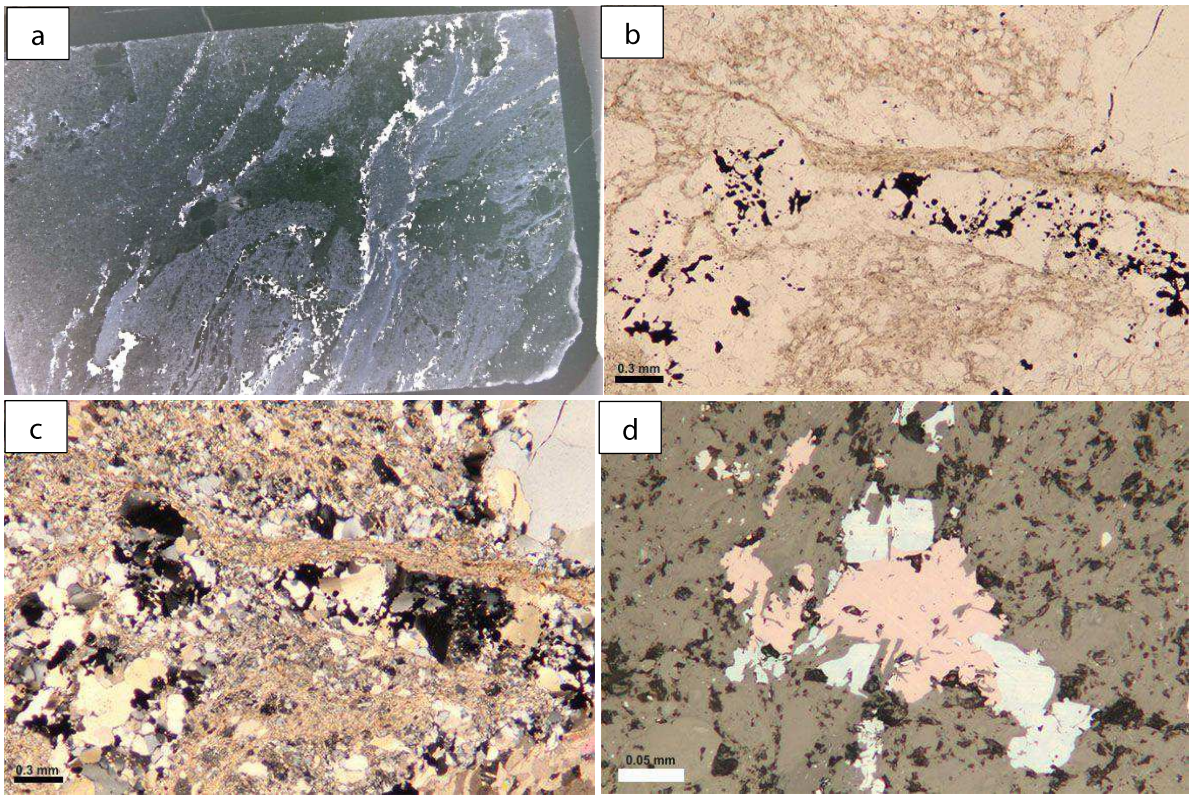

Figure 3.1.15. *a) A photograph of polished thin-section NS-16; (b) and (c) microphotographs of strongly chloritized rock with ore minerals (black), taken in PPL (b), and XPL (c); d) microphotograph taken in XPL showing bornite grain (pink) intergrown with chalcocite (blue); single grains of chalcopyrite (light yellow) in the matrix.*

Ore minerals include by bornite, digenite, and chalcocite.

Copper minerals, up to 0.15 mm in diameter, are widely distributed. Chalcocite and digenite appear replacing and intergrown with bornite. In turn covellite propogates on behalf of chalcocite, digenite and bornite. Rare chalcopyrite grains are also found (Fig. 3.1.15,d).

NS-17 (NS-08/06-214.85-214.9m) (Fig.3.1.16,a)

The rock is a chloritized schist containing quartz, chlorite, and fragments of sericitized alkali feldspars.

Quartz grains are elongated and oriented parallel to the foliation. The foliation is determined by chlorite, which is evenly distributed forming bands. The grain size of quartz varies from 2mm up to 15 mm in diameter. Potassium feldspar shows similar variations in size (Fig.3.1.16,b). Carbonate-rich zones are also found.

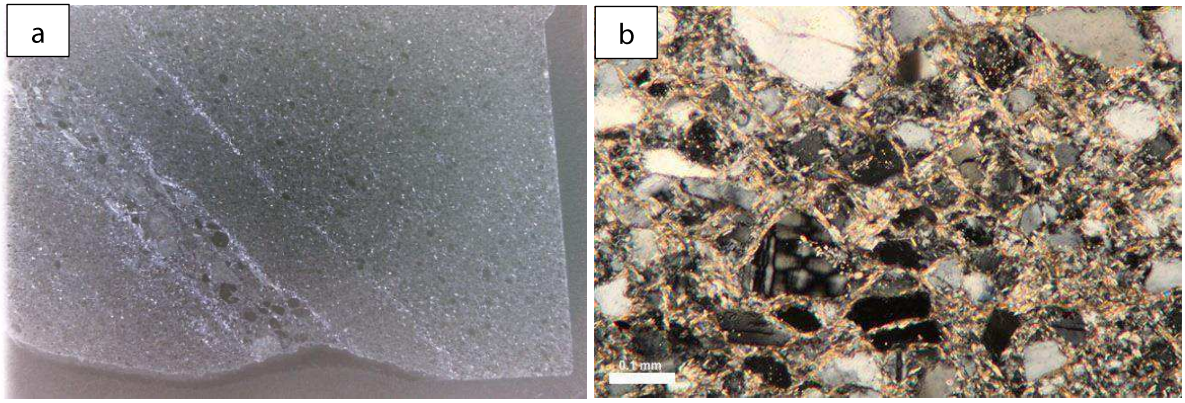

Figure. 3.1.16. *a) A photograph of polished thin-section NS-17; b) Microphotograph showing a fragment of the host rock containing quartz, feldspar, chlorite (XPL).*

The rock shows low contents of evenly distributed ore minerals. The ore minerals include pyrite and iron oxides formed as a result of oxidation and decomposition of pyrite (Fig.3.1.17). Some chalcopyrite grains are also observed.

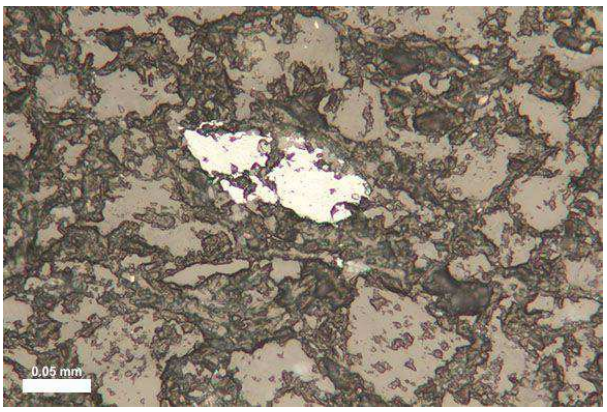

Figure 3.1.17. *Microphotograph taken in plane-polarized light demonstrating oxidized pyrite.*

NS-18 (NS-08/06-219.53-219.63m) (Fig.3.1.18)

The rock shows interlayering of pelitic schist with a quartz-carbonate zone (dolomite) (Fig. 3.1.18,b). The quartz-carbonate zone contains also quite big grains of plagioclase and potassium feldspar. K-feldspar is often seriticized.

A chlorite-rich zone divides the pelitic schist and the quartz-carbonate zone (Fig. 3.1.18,c).

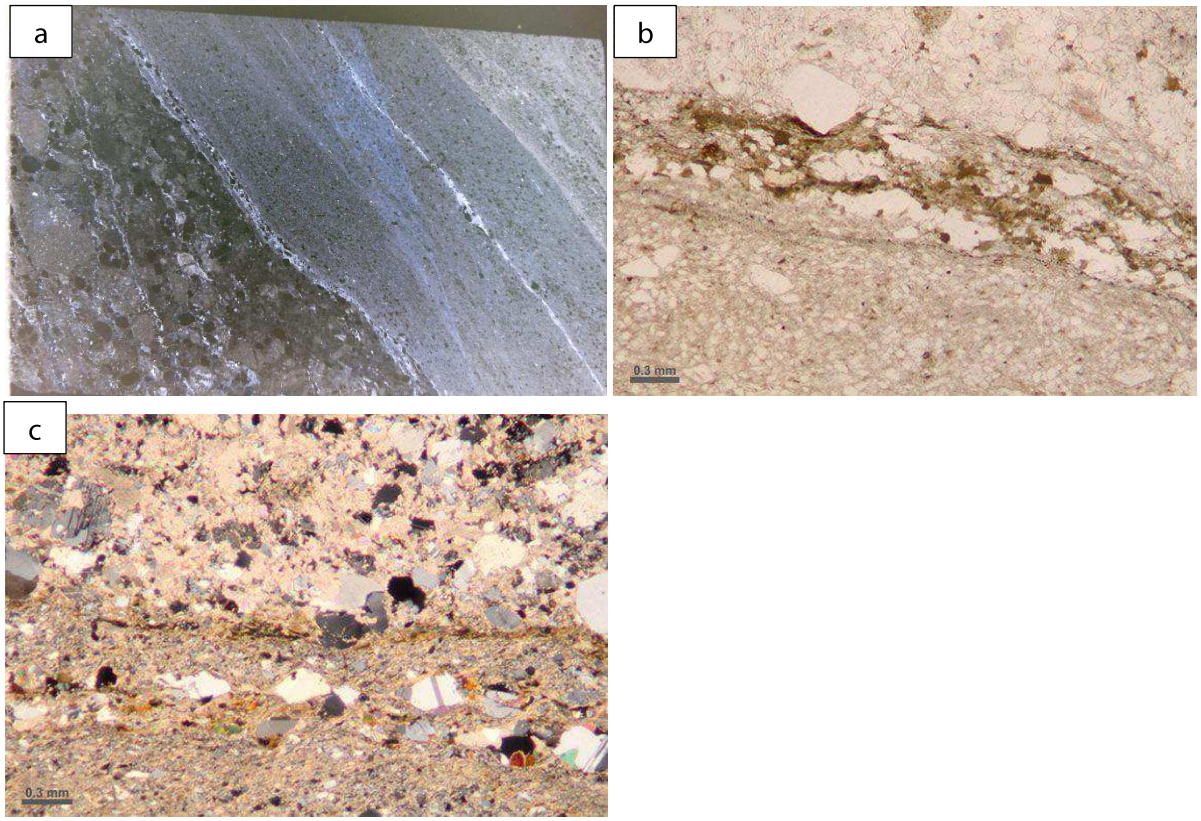

Figure 3.1.18. *a) Photograph showing polished thin-section NS-18; b) Microphotograph taken in XPL showing the contact zone between dolomite and pelitic schist; c) Microphotograph in PPL demostrating chlorite-rich zone on the contact between pelitic schist and dolomite.*

The rock shows minor amounts of ore minerals, which are disseminated both in the schist and the dolomite. The ore minerals include small grains of chalcocite, chalcopyrite, and pyrite.

NS-19 (NS-08/06-221.62-221.66m) (Fig.3.1.19,a)

The rock is a quartzitic semischist (Fig.3.1.19,b). Remnants of sandstone, mainly composed of quartz, K-feldspar, and plagioclase, are preserved in a schistose matrix dominated by chlorite. Carbonate-enriched zones which have elongated shape and look like veins were observed.

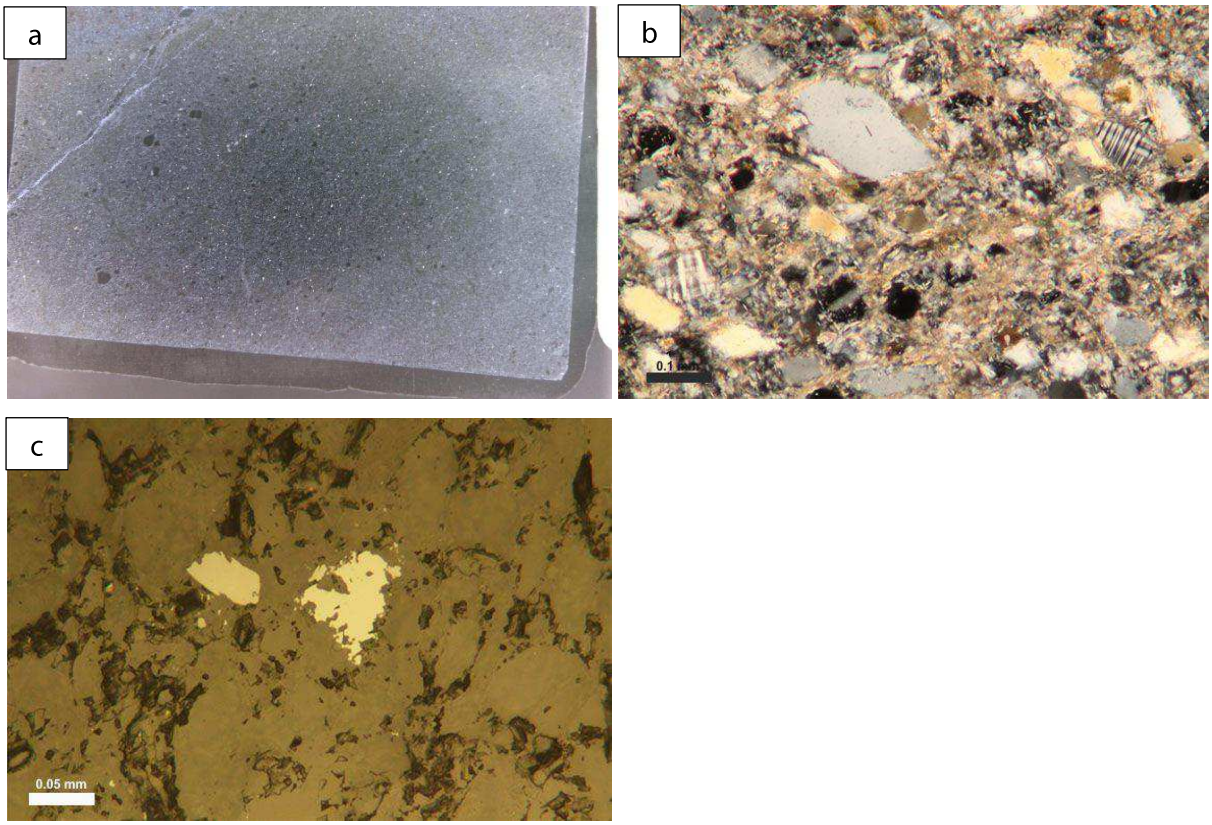

Figure 3.1.19. *a) Photograph demonstrating a polished thin-section NS-19; b) Microphotorgraph taken in XPL and demonstrating a quartzitic semischist with fragments of K-feldspar, quartz, plagioclase. The matrix is chloritized; c) Microphotograph of pyrite (light yellow) and pyrrhotite (light brown, creamy) (XPL).*

Ore minerals include chalcocite, single and rare grains of chalcopyrite, pyrrhotite, and pyrite (Fig. 3.1.19,c). The content of ore minerals is low and fine-interspersed.

NS-20 (NS-08/06-225.74-225.79m) (Fig.3.1.20)

The rock is a breccia composed of quartz, seriticized K-feldspar, and plagioclase (Fig. 3.1.21,a). The fragments are cemented by chlorite-muscovite cement. Quartz-carbonate veins intruding to a fine-crystallized mass were found (3.1.21,b). The ore minerals are fine-grained and disseminated. Among the ore minerals chalcocite and chalcopyrite are observed in small amounts.

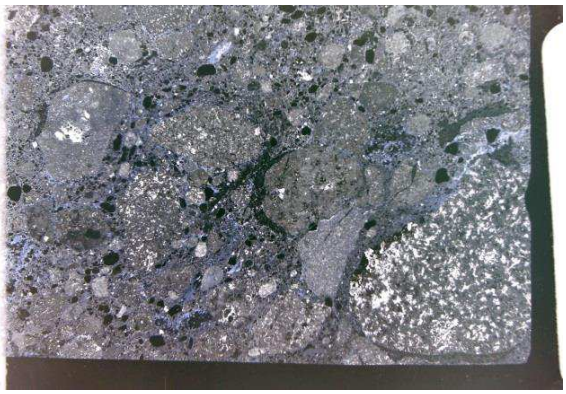

Figure 3.1.20. *A photograph of polished thin-section NS-20*

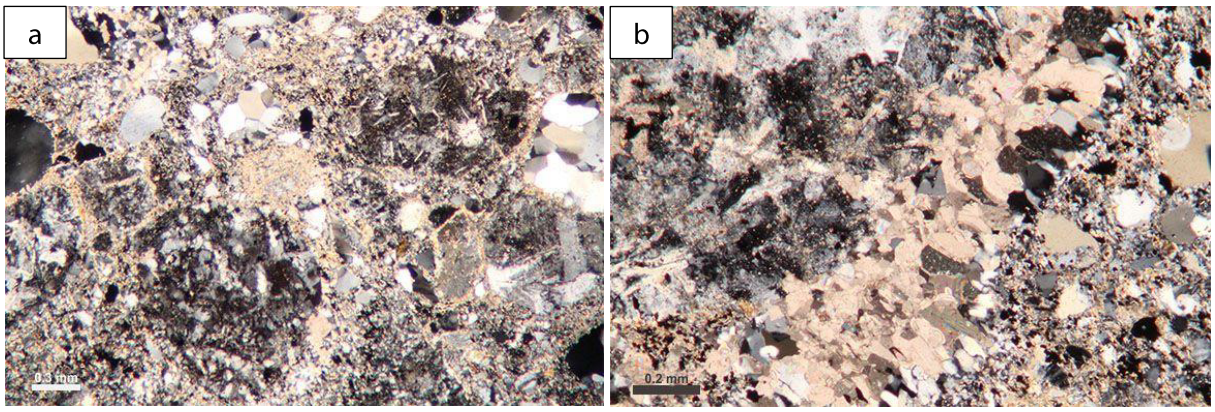

Figure 3.1.21. *a) Microphotograph of breccia texture. The photo is taken in XPL; b) Microphotograph of a quartz-carbonate veinlet crosscutting the hosting rock (XPL).*

NS-21 (NS-08/06-227.05-227.10m) (Fig.3.1.22)

The rock is composed of pelitic schist interlayered with siltstone. From one part to another (on Fig.3.1.22 the direction is shown by red arrow) the grain size is increasing and the rock turns to coarser grained and carbonate-rich. Carbonate veins are intruded in the host rock. Furthermore, quartz, relics of plagioclase and alkali feldspars are observed. Ore minerals are disseminated within the host rock and are mainly represented by iron oxides and pyrite.

Figure. 3.1.22. *Photo of NS-21 polished thin-section. A red arrow shows the direction of increasing grain size.*

NS-23 (NS-08/06-231.74-231.76m) (Fig. 3.1.23)

The rock is a hydrothermally altered sandstone with relics of quartz and alkali feldspars. The feldspar is sericitized.

Figure 3.1.23. *Photograph showing polished thin-section NS-23.*

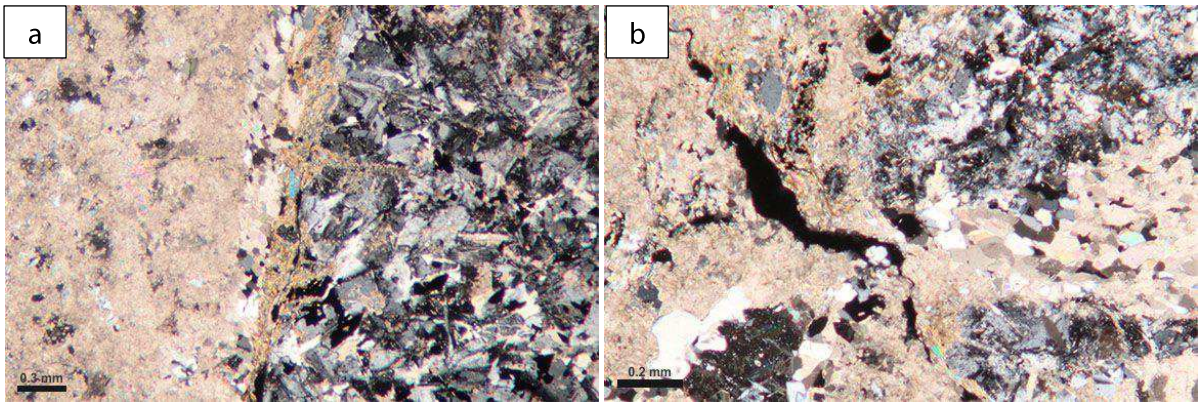

Figure 3.1.24. *Microphotographs, taken in XPL showing (a) a transition zone between intensively seriticized K-feldspar and limestone; and (b) a carbonate veinlet (right side) intruding to the limestone and sandstone. To the right a grain of sericitized K-feldspar is observed. Along the contact between limestone and parent sandstone a biotite-rich contour can be observed.*

Figure 3.1.24, (a) shows the transition from an intensively seritized K-feldspar grain containing biotite flakes to a coarse-carbonate biotite-rich zone and afterwards to a carbonate-rich rock. The carbonate-rich rockcontains fragments of K-feldspar, plagioclase, quartz, and zircon. The rock contains large amounts of carbonate. At the same time, the presence of relics of quartz and plagioclase could be an evidence for that the carbonate-rich rock was formed as a result of hydrothermal reworking of the sandstone.

Among ore minerals, chalcocite and covellite are found. The content of ore mineral, nevertheless, is low. The ore minerals are mostly fine-grained and dispersed, and mainly confined to the relics of sandstone.

NS-24 (NS-08/06-231.90-231.92m) (Fig.3.1.25)

The rock examined in thin section NS-24 is a dolomite interlayered with breccia. A quartz vein is found between dolomite and breccia (Fig. 3.1.26). Ore minerals include pyrite and chalcopyrite.

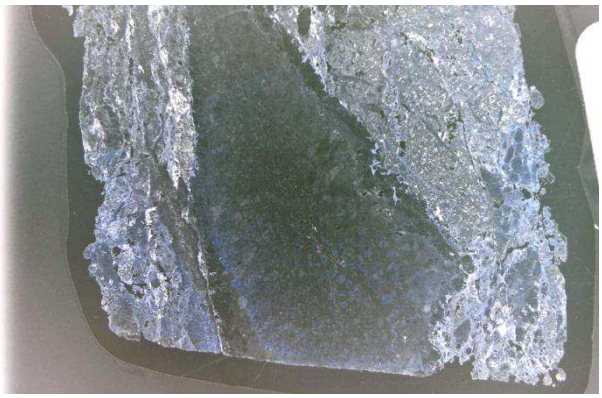

Figure 3.1.25. *Photograph showing polished thin-section NS-24.*

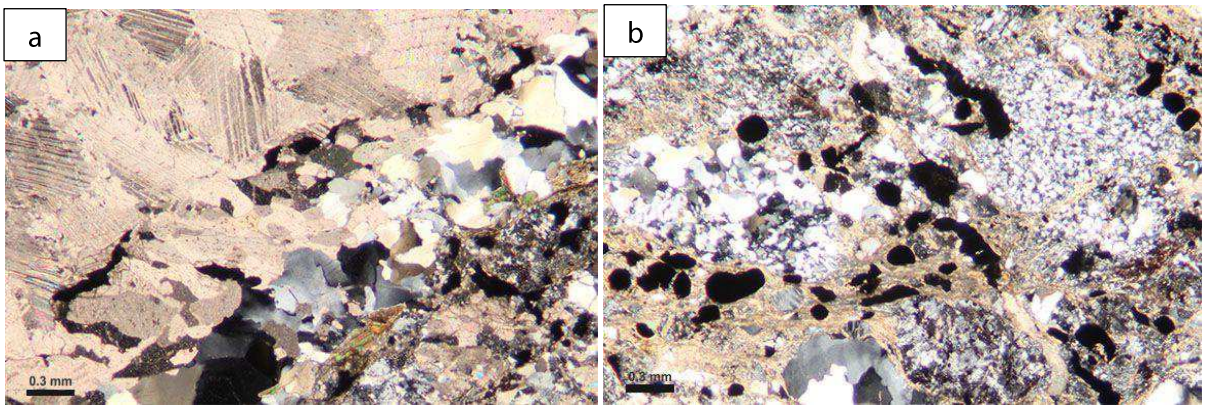

Figure 3.1.26. *Microphotographs taken in XPL showing (a) a contact zone between dolomite and breccia; and (b) ore minerals (black spots) in breccia. The breccia is cemented by biotite-carbonate cement.*

NS-25 (NS-08/06-234.69m) (Fig.3.1.27)

A host rock is brecciated and crosscut by a quartz-carbonate veinlet. Quartz, K-feldspar, muscovite, and fine-grained aggregates compose the fragments of the breccia. (Fig. 3.1.28,a).

In one part of the thin section, siltstone, enriched in muscovite, is observed (Fig. 3.1.28,b). The siltstone is similar to one described in NS-21.

Ore minerals include fine-grained to coarse-grained pyrite that is widely distributed. Bigger grains are confined to the veinlets.

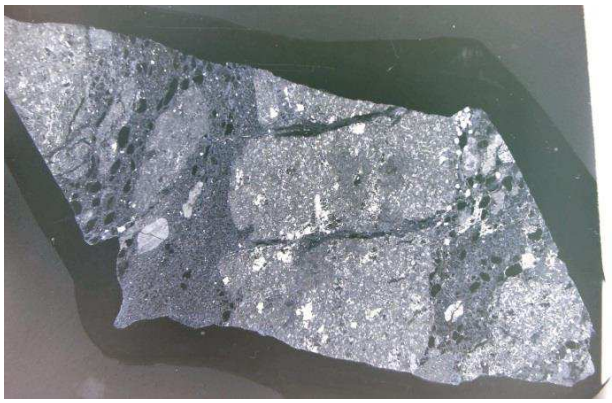

Figure 3.1.27. *Photograph of polished thin-section NS-25.*

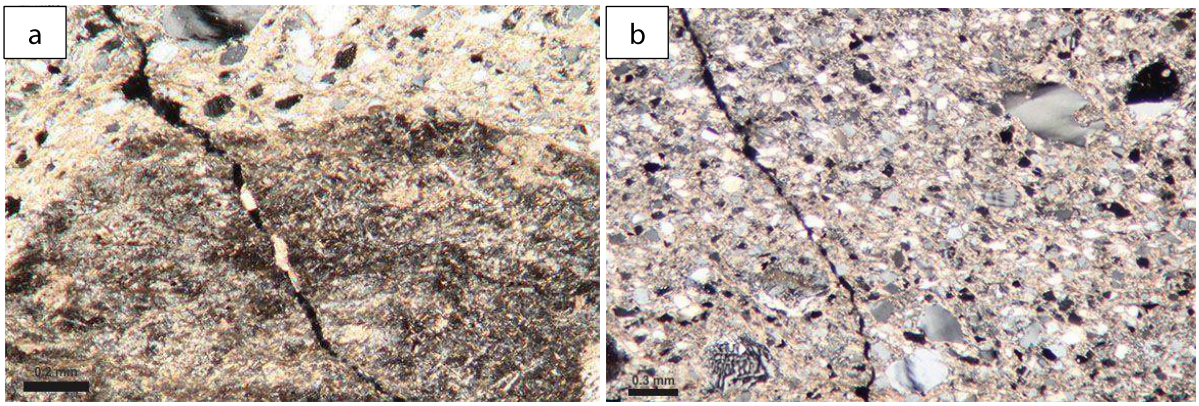

Figure 3.1.28 *Microphotographs demonstrating the rock which is represented by (a) a breccia and (b) a siltstone. The images were obtained in XPL.*

NS-26 (NS-08/10-132.8-133.0m) (Fig.3.1.29)

The rock is a limestone-dolostone containing needles of chlorite. The rock is intruded by quartz veins.

The ore minerals include chalcopyrite, bornite, and chalcocite (Fig. 3.1.30). The ore minerals are observed in the limestone, and they are confined to zones that are located close to the quartz-carbonate veins.

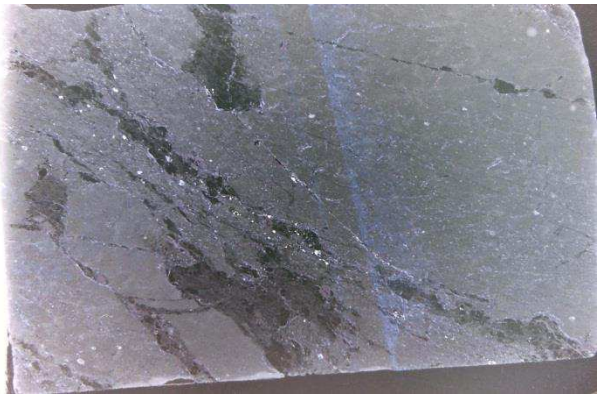

Figure 3.1.29. *Picture of NS-26 polished thin-section.*

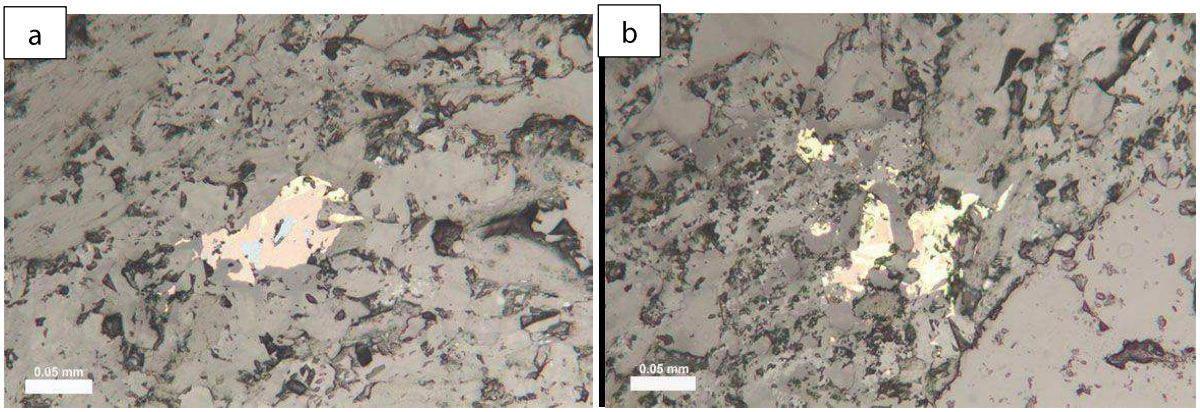

Figure 3.1.30. *Microphotographs taken in reflected light showing replacement of bornite (pink) by (a) chalcopyrite (yellow) and chalcocite (blue), and (b) by chalcopyrite (yellow).*

3.2. Drill hole BH60

NS-1a (28.45-28.50m) (Fig.3.2.1)

The rock is a pelitic siltstone crosscut by a quartz-carbonate veinlet. The siltstone has a nematoblastic structure and layered texture. It is weakly metamorphosed due to intrusion of veinlets.

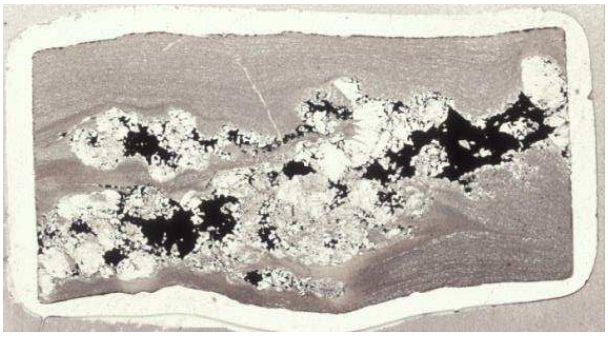

Figure 3.2.1. *Photograph of NS-1a polished thin-section.*

The material of the matrix is rich in mica and more fine-grained than the veinlet. Mica is mainly represented by muscovite. Muscovite forms lepidoblastic texture. The mineral is evenly distributed bordering quartz and carbonate grains (Fig.3.2.2,a). Locally the muscovite is distributed more intensively and forming bands. Locally, foliation cleavage is observed (Fig. 3.2.2,b).

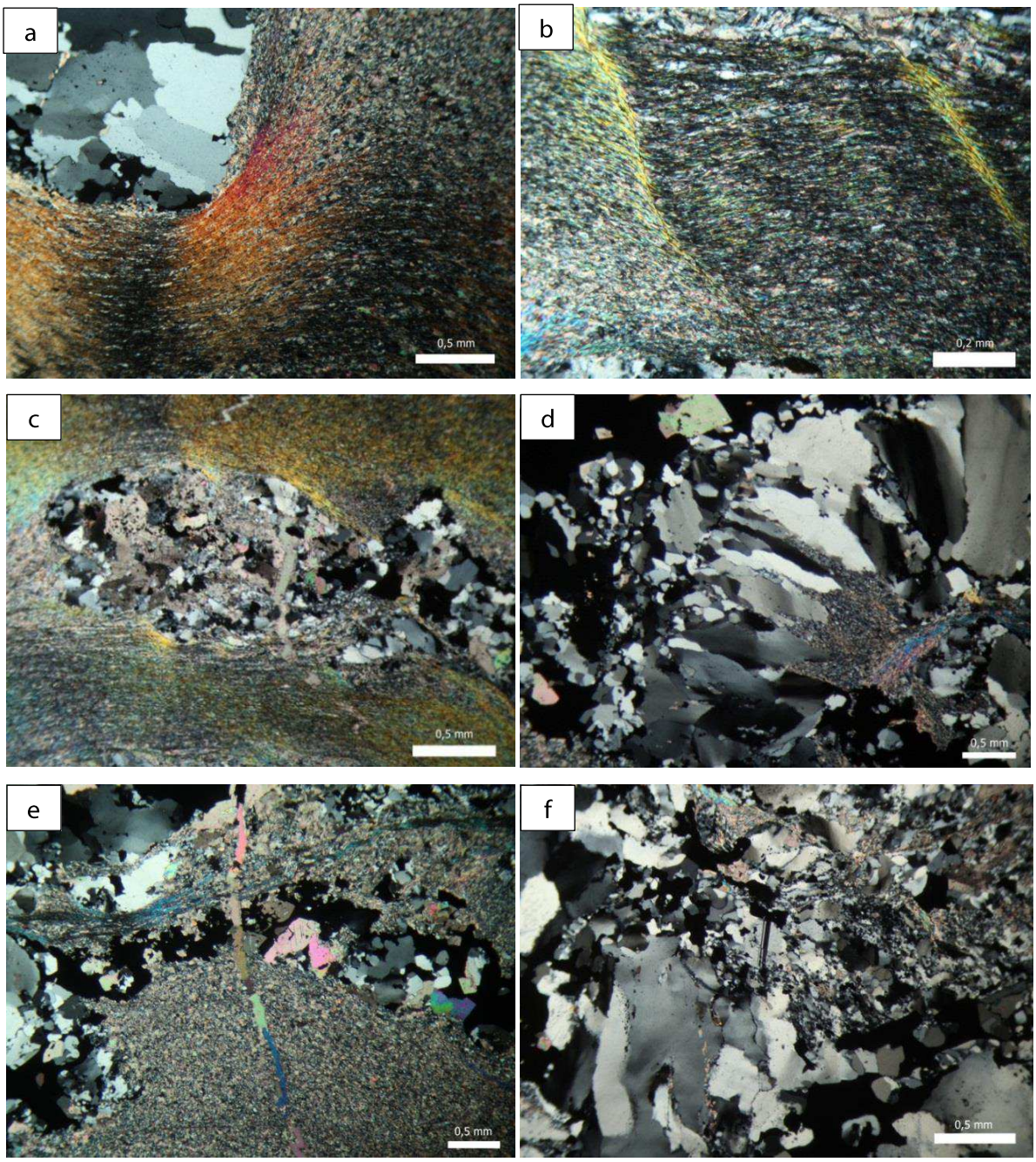

Figure 3.2.2. *Microphotographs taken in XPL and representing: a) contact between mica-rich pelite and a veinlet. The amount of mica increases towards the veinlet; b) crenulation cleavage and shear bands in mica-rich pelite; c) sigmoidal shaped quartz-carbonate accumulation in pelite; d) deformed quartz grains in the veinlet, and recrystallization of the matrix due to intrusion of quartz-carbonate veinlet; e) carbonate veinlet crosscutting quartz-carbonate vein and pelite; f) plagioclase grain in the veinlet.*

Carbonate is represented by calcite and dolomite. The grains have different shapes that vary from rhombs to anhedral grains. The size varies from 0.11 mm to 0.3 mm.

Chlorite was formed as a result of a metasomatic process; it is unevenly distributed within the matrix. The amount of chlorite increases towards the veinlets.

Quartz is evenly distributed throughout the rock. The grains are 0.1-0.2 mm in size. The shape of the grains is mainly elongated, the grains are oriented parallel to muscovite. Locally sigmoidal shape accumulations of quartz, carbonate and copper minerals are observed (Fig. 3.2.2,c).

Two types of veinlets are observed: monomiralic carbonate and quartz-carbonate. Carbonate veinlets crosscut quartz-carbonate veinlets. Mineral content: quartz, carbonate, single grains of plagioclase.

The quartz grains have different sizes and shapes. The biggest grains reaches 2.5 mm in size and the smallest are less than 0.1 mm. Small quartz grains form nest-like aggregates. It is possibly an evidence of redistribution of substance during intrusion of the veinlet when the matrix was recrystallized. In the polished thin-section, there are places where contact relationship between matrix and veinlet are distinctly observed (Fig. 3.2.2,a). Big grains of quartz have distinct elongated shape and preferred orientation (Fig. 3.2.2,d).

Carbonate in the veinlet is represented likely by dolomite (regular rhomboidal crystals, polysynthetic twins). In comparison with carbonate in the matrix, the crystals of carbonate in the veinlet are big – 0.5-1.5 mm. The crystals in the monomiralic carbonate veinlet are represented by calcite. Grains are long, prismatic, and elongated; the ratio of length to width is approximately 1.1:0.1mm. The veinlet crosscuts both matrix and quartz-carbonate veinlet (Fig. 3.2.2,e).

Plagioclase is represented by single grains of labradorite (determined by extinction angle 27 ½°-38°, gained during microscopic study) (Kerr, 1977) having tabular shape. The size is about 0.4 mm (Fig. 3.2.2,f).

Copper mineralization is associated woth the quartz-carbonate veinlet. In the groundmass, copper minerals are nearly not observed.

Ore minerals are represented by bornite, chalcopyrite, chalcocite, sphalerite, and covellite.

Bornite forms intergrowths with chalcopyrite. The mineral is mainly confined to the quartz-carbonate veinlet though single grains are observed also in the matrix. Possibly,

chalcopyrite has replaced bornite. There are also zones where bornite is replaced by (neo)digenite (prefix (neo-) is after Ramdor, 1962) and chalcocite. Bornite grains have irregular shape and are represented by both quite big (> 1.5 mm) and small grains (0.1 mm and less). In addition, bornite is observed as a vein-forming mineral. Along the cracks and edges of bornite grains, chalcopyrite has developed. Chalcopyrite is further replaced by covellite, chalcocite or digenite (Fig. 3.2.3, a, b). In intergrowths with bornite, sphalerite is observed.

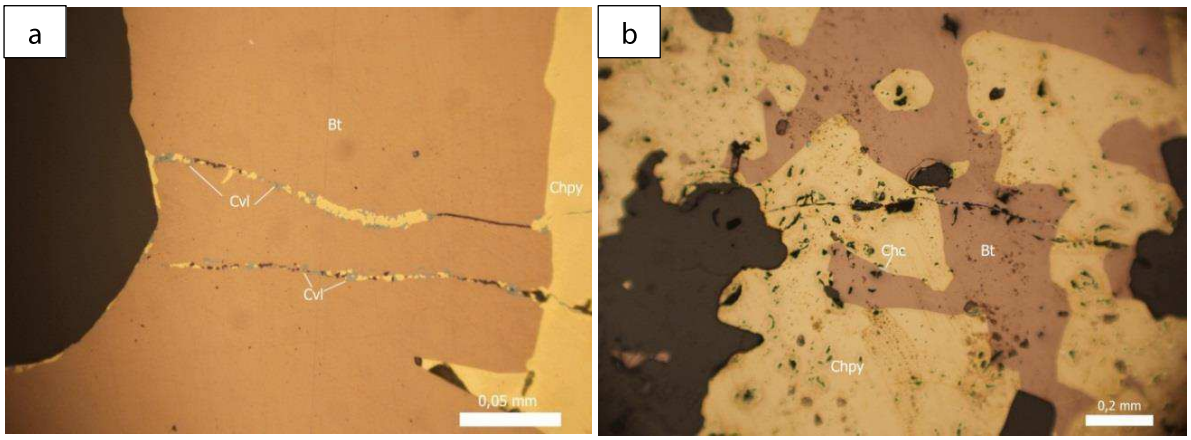

Figure 3.2.3. *Microthographs obtained during inverstigation under reflected light with XPL. a) Intergrowth of bornite (Bt) and chalcopyrite (Chpy). Formation of chalcopyrite along the cracks in bornite and its replacement by covellite; b) Intergrowth of bornite, chalcopyrite; appearing of chalcocite (Chc) in the contact zone between bornite and chalcopyrite.*

Sphalerite is represented by single grains of various sizes. The shape is predominantly rounded or irregular. Twinning is distinct. Chalcopyrite occurs as widely dispersed inclusions in sphalerite, but also as plates parallel to the edges of twins. Chalcopyrite is likely to be a product of decay of solid solution. One observation supporting this is that chalcopyrite is mainly in the central part of the sphalerite grain and not along its edges. Deformation that had place could play considerable role at the beginning of the decay.

Chalcopyrite forms intergrowths with bornite as well as separate grains. It is locally replaced by chalcocite and digenite. Chalcopyrite is confined to the quartz-carbonate veinlets, but also the host rock comprises chalcopyrite grains. The size is various and there are both big and small grains. The shape is mainly irregular.

Covellite is represented by small grains that likely were formed during replacement of bornite and chalcopyrite. The shape of the grains is mainly irregular (Fig. 3.2.3).

Chalcocite is a product of replacement of chalcopyrite. Chalcopyrite is disseminated within chalcocite grains as well as locally grid-like texture is observed. Here chalcopyrite occurs as bands in chalcocite. The shape of chalcocite grains is mainly rounded. The mineral is observed both in the matrix and in the veins (Fig. 3.2.5).

Galena forms single grains that have tabular shape (Fig. 3.2.4).

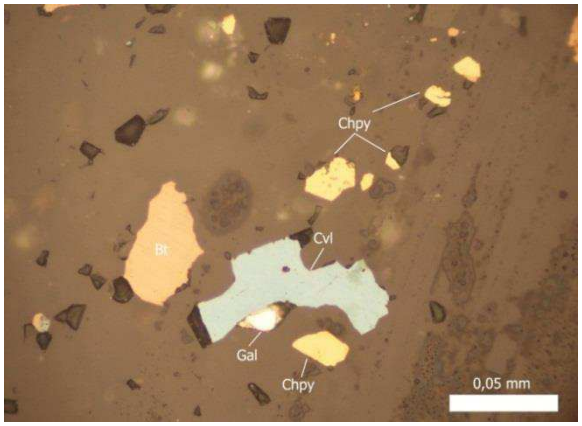

Figure 3.2.4. *Microphotograph in XPL showing replacement of chalcopyrite by covellite. Galenite (Ga) (?) is in intergrowth with covellite. Dispersed mineralization in the matrix.*

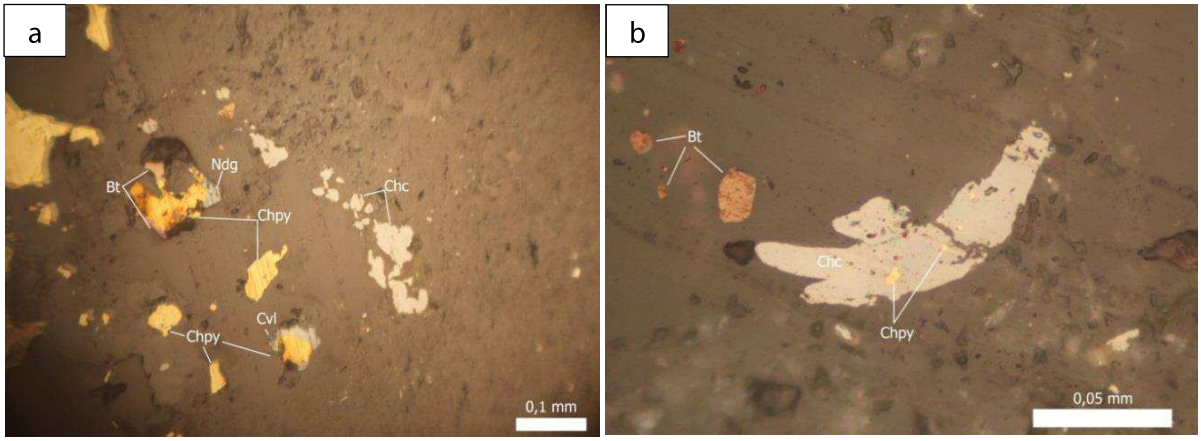

Figure 3.2.5. *Microphotographs taken in XPL showing (a) dispersed copper mineralization in the matrix (Bt-bornite, Ndg-(neo)digenite, Chc-chalcocite, Cvl-covellite, Chpy-chalcopyrite); and (b) inclusions of chalcopyrite in a grain of chalcocite.*

NS-1b (28.45-28.50m) (Fig.3.2.6,a)

The rock is a siltstone having a nematoblastic structure, and layered and locally massive texture. It is crosscut by a quartz-carbonate veinlet. In spite of the fact that polished thin sections NS-1a and NS-1b are made from one sample, copper mineralization is observed also in the matrix in NS-1b.

The sample is nearly identical to NS-1a however quartz in the matrix has bigger size – approximately 0.2 mm. The grain shape is mainly rounded (Fig. 3.2.6 b). Similar to NS-1a,

the matrix in NS-1b is comprised by carbonate of different shapes and sizes. The space between grains is filled by muscovite. In the matrix, monomineralic zones of quartz are observed (Fig. 3.2.6, c). The amount of carbonate increases towards the veinlet.

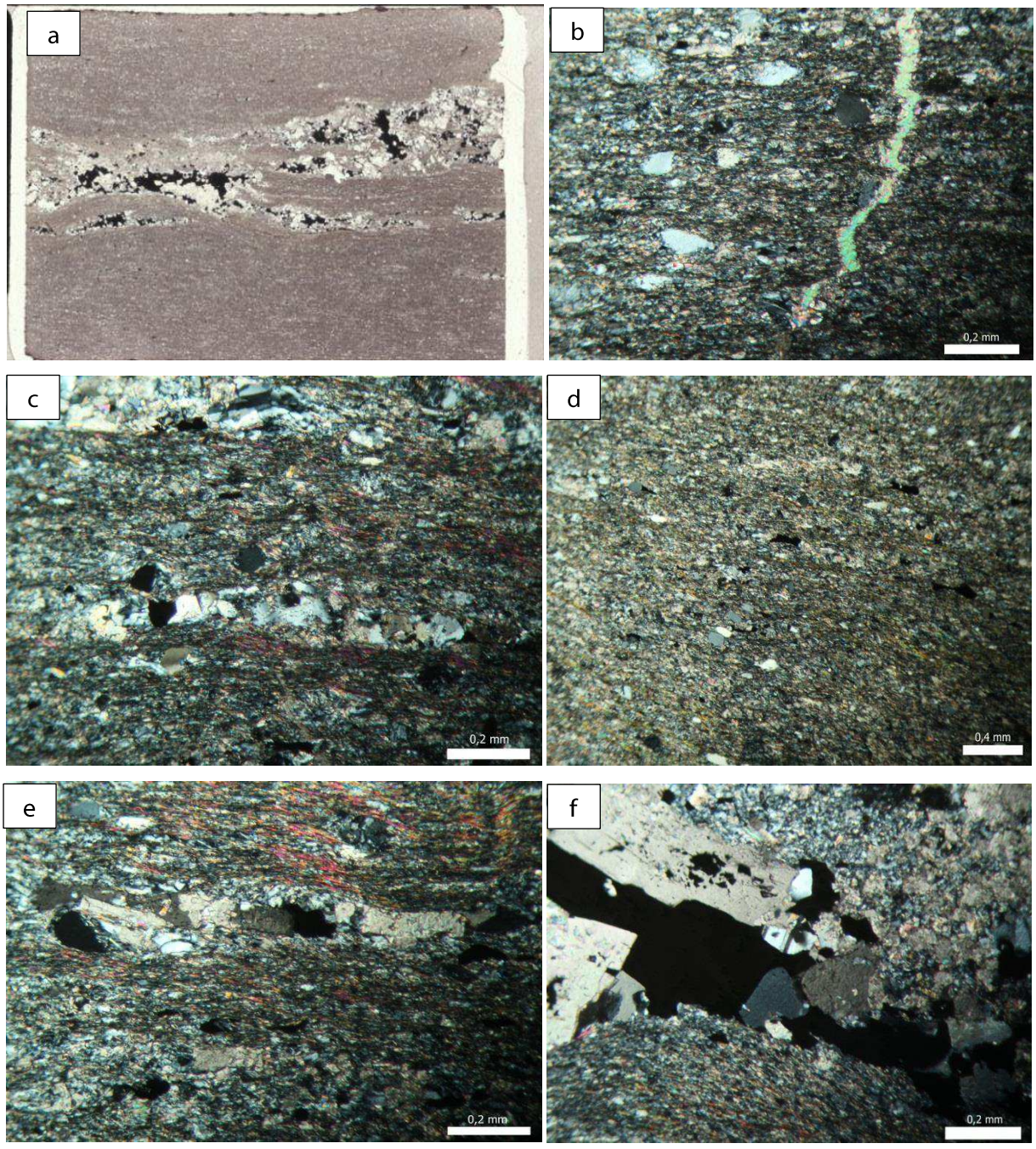

Figure 3.2.6. *a) Photograph of polished thin section NS-1b; b) microphotograph of carbonate veinlet crosscutting siltstone matrix enriched with big quartz grains (XPL); c) quartz clast in the matrix. The matrix shows crenulation cleavage and shear bands (XPL); d) mica-rich siltstone with big rounded grains of quartz (XPL); e) quartz-carbonate accumulation within mica-rich siltstone. In the central upper part sigmoidal shape quartz accumulation is shown; f) Plagioclase grain in the veinlet (XPL).*

In the matrix of siltstone there are single grains of plagioclase. It is euhedral, the size is approximately 0.2 mm.

Shear bands and crenulation cleavage are observed in the matrix as well as aggregates of quartz and carbonate enclosed in mica-rich layers (Fig. 3.2.6,d,e).

The mineral content of the veinlet is nearly identical to that described in thin section NS-1a, however there are slight differences:

The quartz grains have smaller size and more rounded shape. However there are grains having tabular shape. In comparison with NS-1a, the grains of quartz are more randomnly oriented.

Carbonate – calcite and dolomite – occurs as anhedral grains. The size varies from 0.1 to 1.5 mm. There are monomineralic zones of carbonate (Fig. 3.2.6, b).

Plagioclase is more abundant than in NS-1a though the size of grains does not exceed 0.2 mm (Fig. 3.2.6, f).

Ore minerals are represented by chalcopyrite, bornite, chalcocite, covellite, and galena (Fig. 3.2.7).

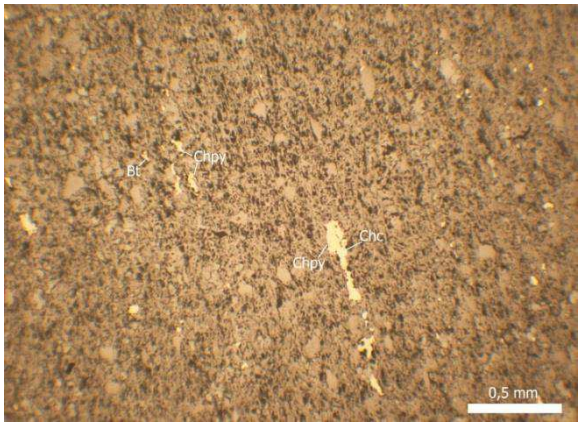

Figure 3.2.7. *Microphotograph, taken in XPL, of disseminated copper minerals in the matrix of the siltstone.*

Chalcopyrite is the dominating sulfide. It is mainly confined to veins, however, disseminated grains are also observed in the rock. Chalcopyrite occurs as intergrowths with bornite and fills cracks in the latter mineral. The shape of the grains is mainly irregular. The size of the chalcopyrite in the veinlets varies from 0.1 mm to more than 3 mm. In the matrix of the siltstone, the size of grains does not exceed 0.1 mm.

Similar to chalcopyrite, bornite is confined predominantly to the veins, but it is also present in the host rock. Along cracks and edges of grains chalcopyrite and chalcocite occur. There are zones of intergrowths of bornite with galena and (neo)digenite. Bornite is

represented by big vein grains with size locally exceeding 2 mm, and small disseminated inclusions in the matrix (0.03 mm – 0.05 mm). Within the siltstone the grains have elongated or tabular shape. Often, bornite occurs in intergrowth with chalcopyrite both in the matrix and in the veinlets (Fig. 3.2.8).

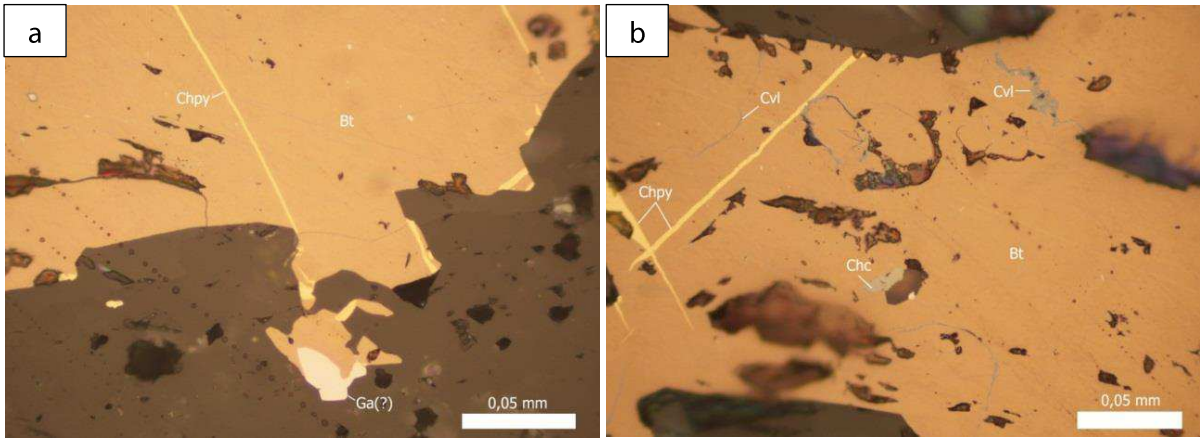

Figure 3.2.8 *Microphotographs taken in XPL showing: a) intergrowth of bornite with galena. Chalcopyrite occurs within bornite and along its edges; b) cracks in bornite filled by chalcopyrite that further is replaced by covellite.*

Galena forms single small grains of rounded shape, occurring in contact with bornite (Fig. 3.2.8, a). Galena also occurs in the matrix of the host rock. The grains are rather small and its detailed study is complicated. Galena is also observed in the intergrowth with digenite.

Covellite is a secondary mineral that has been growing on bornite and chalcopyrite typically filling microfractures. Big grains are not observed.

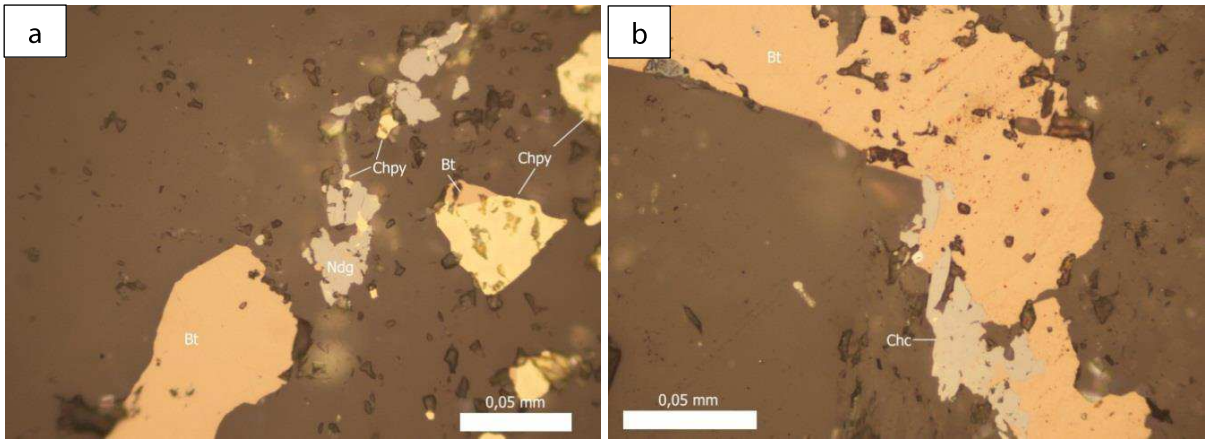

Figure 3.2.9. *a) Association of (neo)digenite (Ndg), chalcopyrite (Chpy) and bornite (Bt); b) replacement of bornite by chalcocite.*

(Neo)digenite and chalcocite are rather widely spread minerals. It is likely that they are products of decay of solid solutions of bornite and chalcopyrite. Replacement textures are observed (Fig. 3.2.9).

NS-2a (28.52-28.56m) (Fig.3.2.10)

The rock is a sericitic siltstone with a quartz-carbonate veinlet. The siltstone has a lepidoblastic structure and layered texture. The matrix is represented by the clasts of quartz, plagioclase, and carbonate in mica-rich siltstone. Locally the siltstone is chloritized. Crenulation foliation is observed. The clasts are oriented parallel to the mica (Fig. 3.2.11).

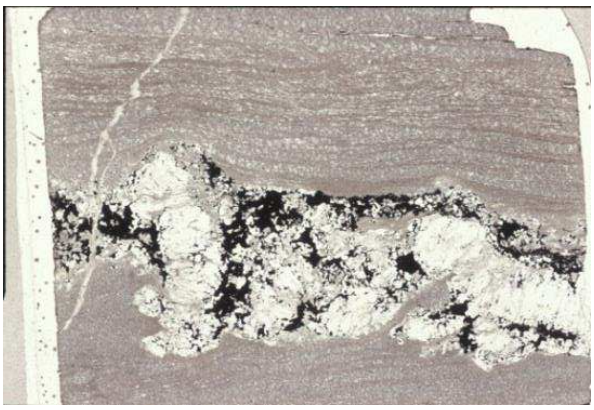

Figure 3.2.10. *Photograph of NS-2a polished thin section.*

Carbonate occurs as andedral grains of different size, commonly smaller than 0.5 mm in diameter. The total modal amount of carbonate is about 10 %. Quartz is represented by small grains of different sizes and shapes. Approximately 80% of all quartz grains are oriented parallel to the foliation. Towards the veinlet the minerals of the matrix become more fine-grained and the degree of chloritization increases. The matrix is crosscut by a carbonate veinlet. The veinlet contains both calcite and dolomite; the grains show mainly a tabular shape, with sizes of about 0.3 mm width and about 1.2 mm length. It is notable that the grains are undeformed (Fig. 3.2.11,c,d).

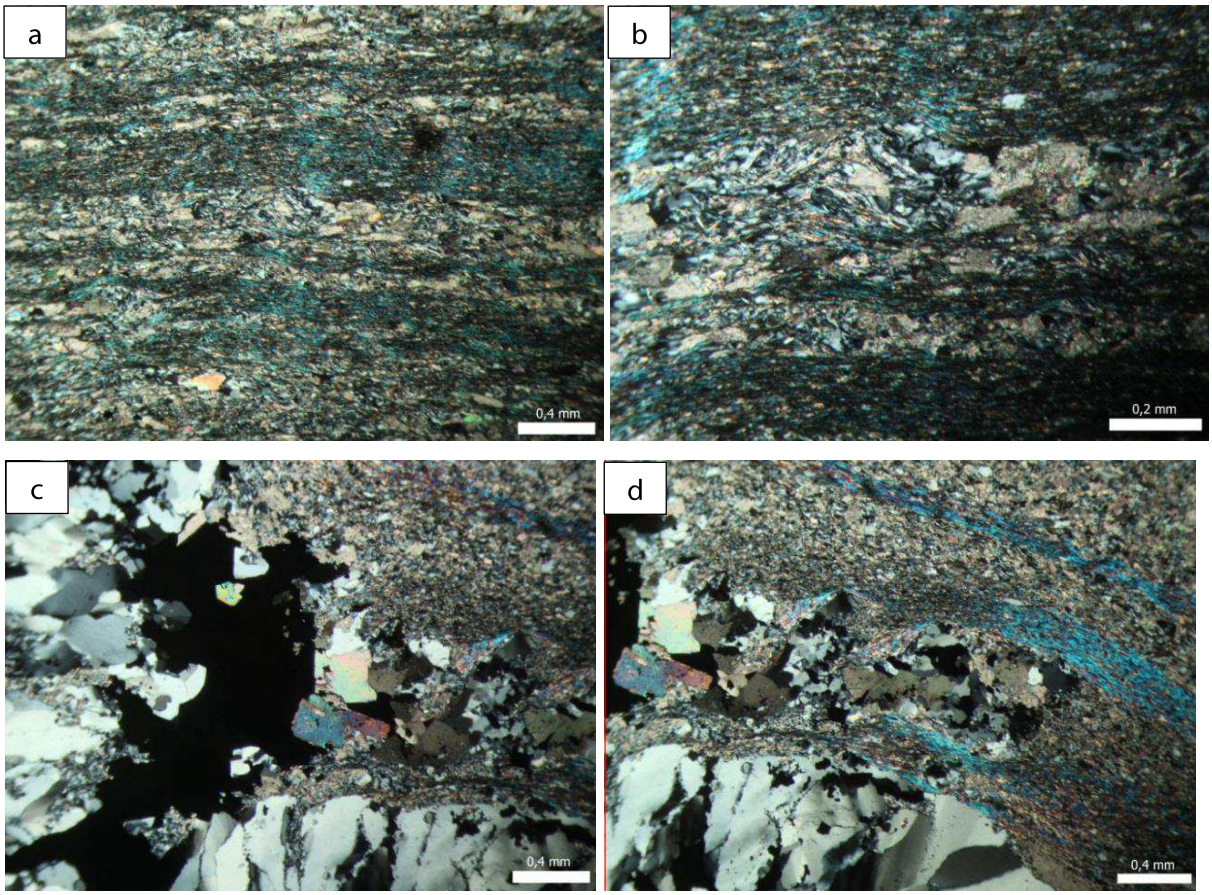

Figure 3.2.11. *Microphotographs of a host rock taken in XPL. a) mica-rich siltstone with crenulation cleavage and accumulations of quartz grains; b) scaled-up image of accumulation of quartz in the matrix; c),d) textural relationship between quartz veinlet containing copper minerals with host rock.*

The veinlet is composed of quartz and carbonate. Quartz occurs in grains of different sizes and shapes. The largest aggregates have a preferred orientation, which might be an evidence of late compressional processes (Fig. 3.2.12, a). The grains are up to 2.5 mm in diameter. They are cemented by more fine-grained materials dominated by rounded grains of quartz, <0.1 mm in diameter (Fig. 3.2.12, b), but also containing some grains of carbonate. Possibly, the fine-grained cement was formed as a result of recrystallization and interaction between fluids and the host rock during formation of veins.

Carbonate is distributed rather locally. The shape of grains varies from tabular to anhedral. The size of grains reaches 1 mm (Fig. 3.2.12, c,d).

Ore minerals are represented by chalcopyrite, bornite, digenite, covellite and galena (Fig. 3.2.13).

Chalcopyrite is represented by rare dispersed grains in the matrix and big and small crystals in the veinlet. It often occurs intergrown with bornite (Fig. 3.2.13, b,c). Chalcopyrite

forms sinter-like shapes; the size of grains is rather diverse and varies from 0.1 mm up to 2 mm and more (Fig. 3.2.13,b).

Similar to chalcopyrite, bornite is widely spread, but a dominant part is confined to the veinlet. Here, the grains are big and do not have a distinct shape. Bornite is also observed as inclusions in chalcopyrite (Fig. 3.2.13, c), while chalcopyrite locally occurs along with covellite and chalcocite as filling of fractures within bornite (Fig. 3.2.13, d). In the matrix, bornite is present as an accessory phase as small grains (up to 2 mm in diameter). The inclusions might be djurleite ($Cu_{49}S_{25}$) or weissite (Cu_2Te), but it is necessary to check using microprobe analysis.

Chalcocite, (neo)digenite are mainly developed on bornite and chalcopyrite repeating the shape of these minerals (Fig. 3.2.13,f).

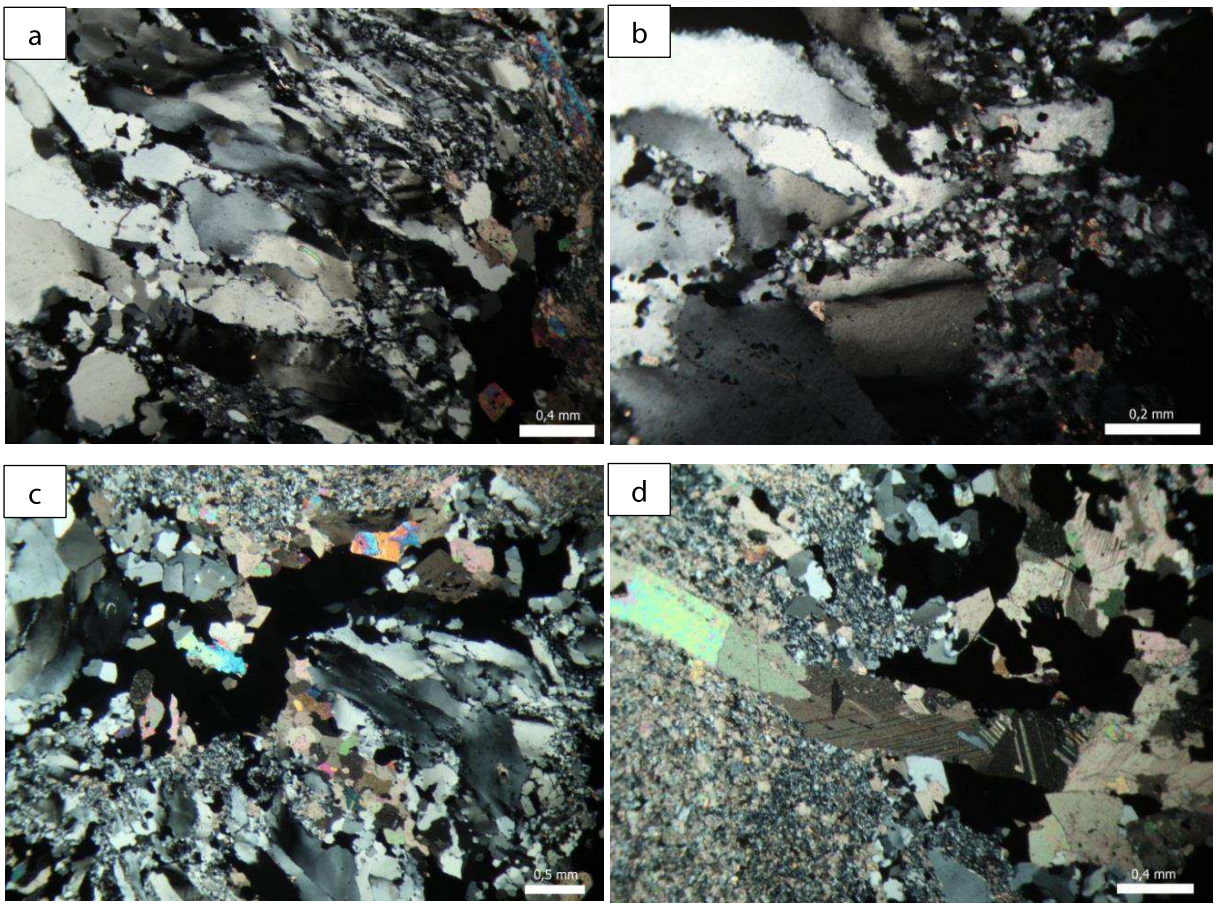

Figure 3.2.12. *Microphotographs of quartz, carbonate, and quartz-carbonate veinlets taken in XPL: a) elongated oriented grains of quartz; b) quartz aggregates and recrystallized quartzitic mass; c) quartz and carbonate bearing veinlet with copper minerals; d) carbonate veinlet crosscutting the host siltstone and quartz veinlet containing copper minerals.*

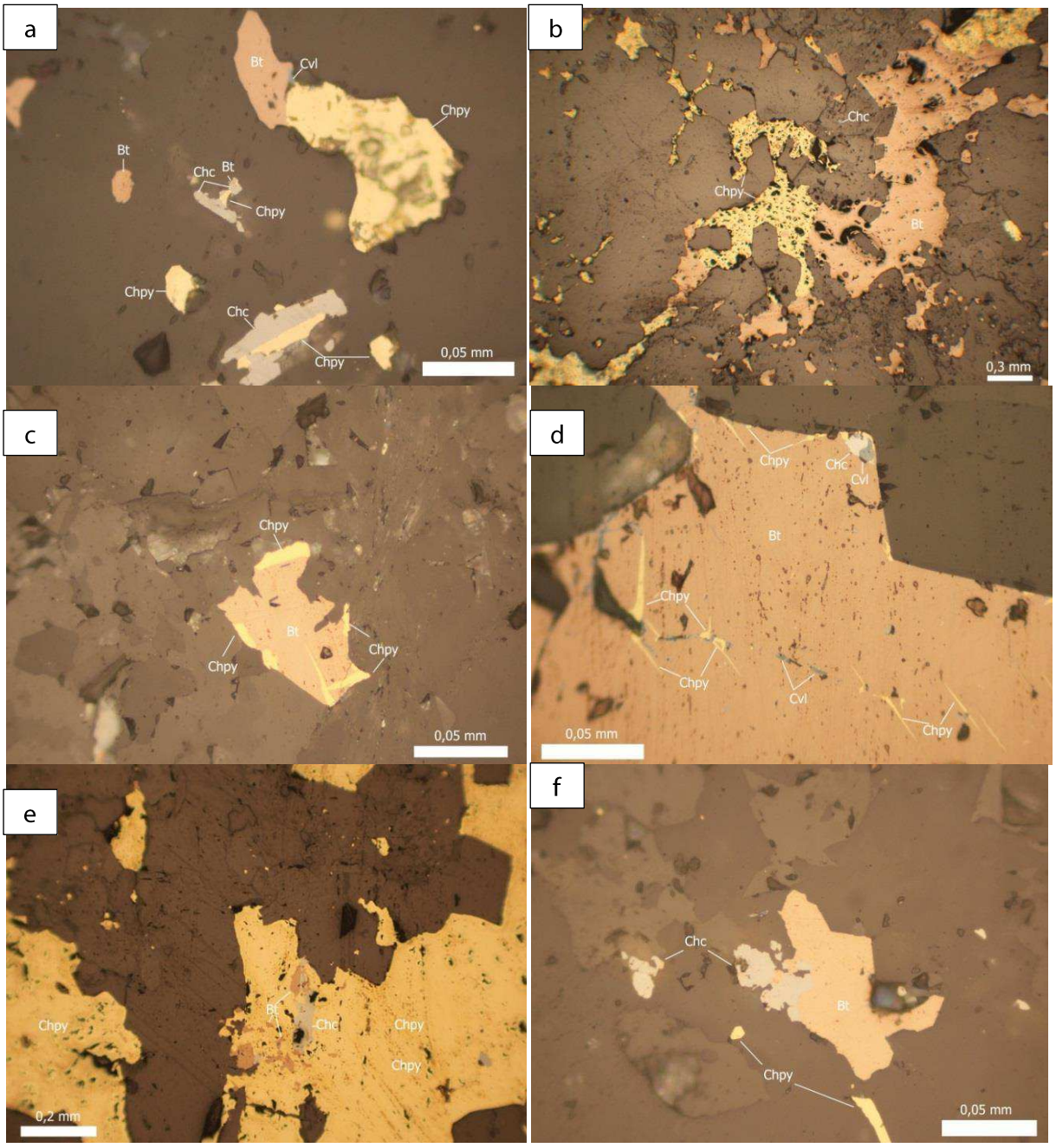

Figure 3.2.13. *Microphotographs in XPL:* a) *association of copper minerals: bornite (Bt), chalcopyrite (Chpy), covellite (Cvl), chalcocite (Chc); b) Intergrowth of bornite with chalcopyrite; c) chalcopyrite occurs along the margins of bornite grain; d) microfractures in bornite filled by chalcopyrite and covellite. Replacement of bornite by chalcocite and covellite (upper right grain in the corner of bornite grain); e) inclusions of bornite and chalcocite in chalcopyrite; f) replacement of chalcopyrite by bornite and chalcocite.*

Covellite fills microfractures in bornite. The thickness of these cracks does not exceed 0.1 mm. Covellite is also observed as single grains that have fragment shape. They are located in association with chalcopyrite. Single grains show rounded shapes with sizes of about 0.2 mm.

Galena is observed as single grains showing rounded shape and small size. Galena is confined to quartz-carbonate veinlet.

NS-2b (28.52-28.56m) (Fig. 3.2.14)

Locally chloritized siltstone has a lepidoblastic, fine-grained structure and massive texture. It is crosscut by quartz-carbonate veins.

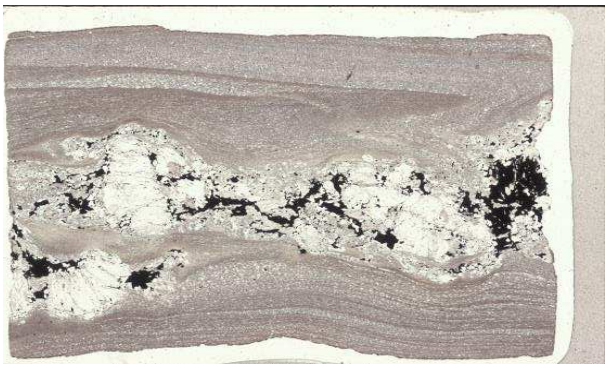

Figure 3.2.14. *Photograph of NS-2b polished thin section.*

The siltstone contains quartz, plagioclase, and carbonate (Fig**.**3.2.15,a). The rock is locally micaceous. Cleavage is observed (Fig. 3.2.15,b). Quartz occurs as anhedral grains of various sizes and shapes. The grain size varies from 0.1 to 0.5 mm in diameter. Carbonate occurs mainly in grains of tabular shape with the size of about 0.1 mm – 0.2mm.

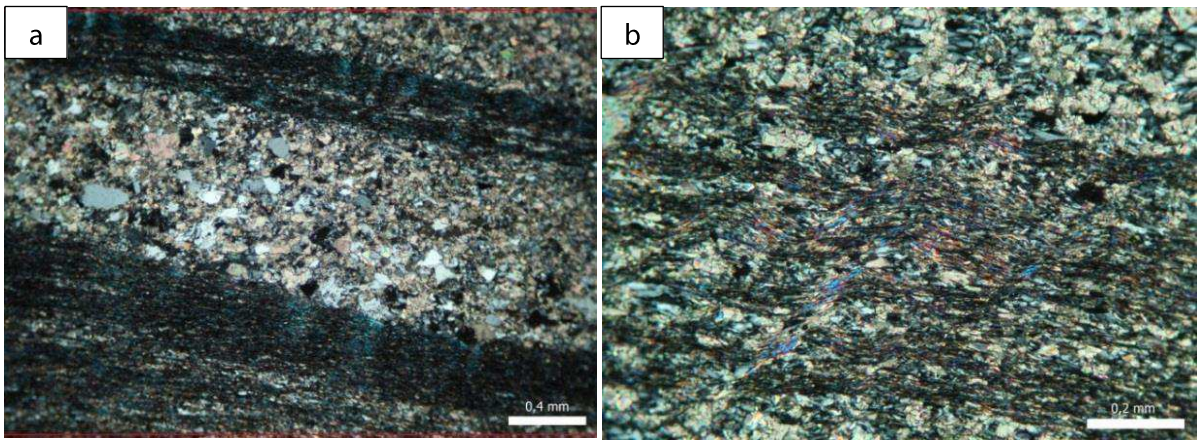

Figure 3.2.15. *Microphographs of the rock textures. Photographs are made in XPL:* a) *siltstone with mica-rich layers; b) foliation cleavage in mica-rich siltstone.*

The veinlet consists of quartz and carbonate. Quartz is represented by two types: elongated grains that have preferred orientation and anhedral crystals that are smaller in size (Fig. 3.2.16, a). Big elongated crystals have 0.5 mm – 2 mm size. Towards the host rock, the grain size becomes smaller while forming a mosaic texture. The size of the grains varies from less than 0.1 mm to 0.5 mm.

Carbonate shows three textural types: 1) big anhedral crystals with signs of deformation. Grains form elongated nest-like accumulations (Fig. 3.2.16, b). The size changes from 0.5 mm to 2 mm; 2) undeformed crystals having rhomboidal shape with size about 0.5 mm in diameter; and 3) crystals in the fine-grained quartz-rich groundmass as well as in the space between big quartz crystals; the size of these carbonate grains does not exceed 0.2mm. Generally carbonate is represented by calcite and dolomite.

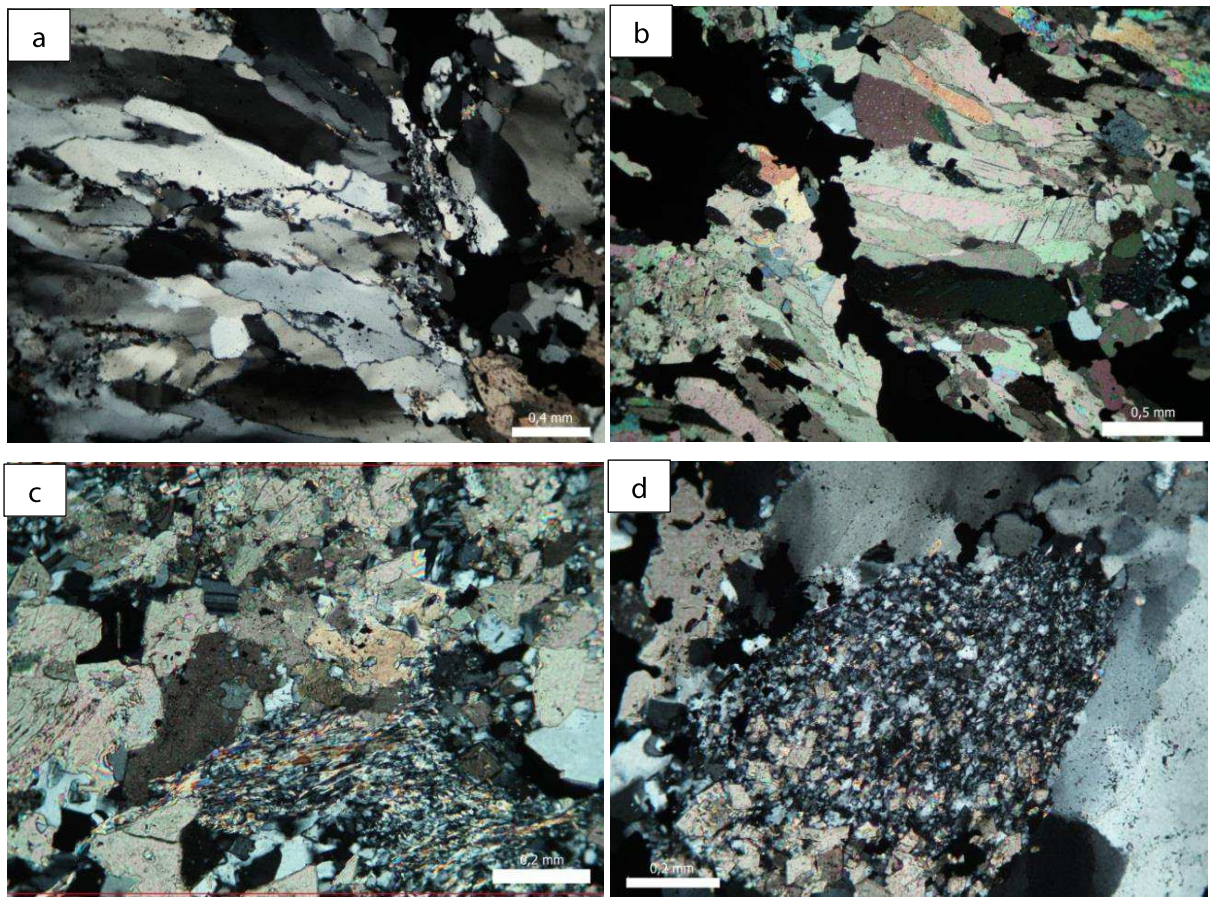

Figure 3.2.16. *Microphotographs taken in XPL. a) Deformed quartz grains in the veinlet; b) deformed carbonate crystals; c) Veinlet of quartz-carbonate composition in the siltstone; d) fine-grained aggregate of quartz and carbonate.*

Most likely, subsequent to formation of the quartz veins, the rock underwent slight deformation in connection with formation of the mica-rich zones in the siltstone. These zones show signs of deformation (foliation cleavage). Two generations of carbonate can be identified; one generation is distinctly deformed (elongated grains not typical for carbonate) and another generation is undeformed, although the carbonate is less stable mineral than quartz.

Chlorite locally formed, while recrystallization of quartz to fine-grained quartz aggregates took place (Fig. 3.2.16, c,d).

Ore minerals are represented by chalcopyrite, bornite, galena, chalcocite and covellite.

The ore minerals are mainly confined to the veinlet, but the host rock also comprises some dispersed ore minerals.

In the veinlet, chalcopyrite forms intergrowths with bornite and fills the cracks in it. Chalcopyrite is also observed along the edges of bornite. Big grains (> 2 mm) have an irregular shape while smaller grains (< 2 mm) show a rounded shape. Chalcocite has to some extent replaced chalcopyrite.

Domains enriched in chalcopyrite alternate with bornite-rich zones (Fig. 3.2.17, a). Bornite grains also have various shapes and sizes. Small grains are relatively rounded while larger grains do not have a distinct shape. Fracturing is observed in the larger grains and the cracks are filled with chalcopyrite and covellite. Covellite is likely to be the youngest mineral (Fig. 3.2.17, b).

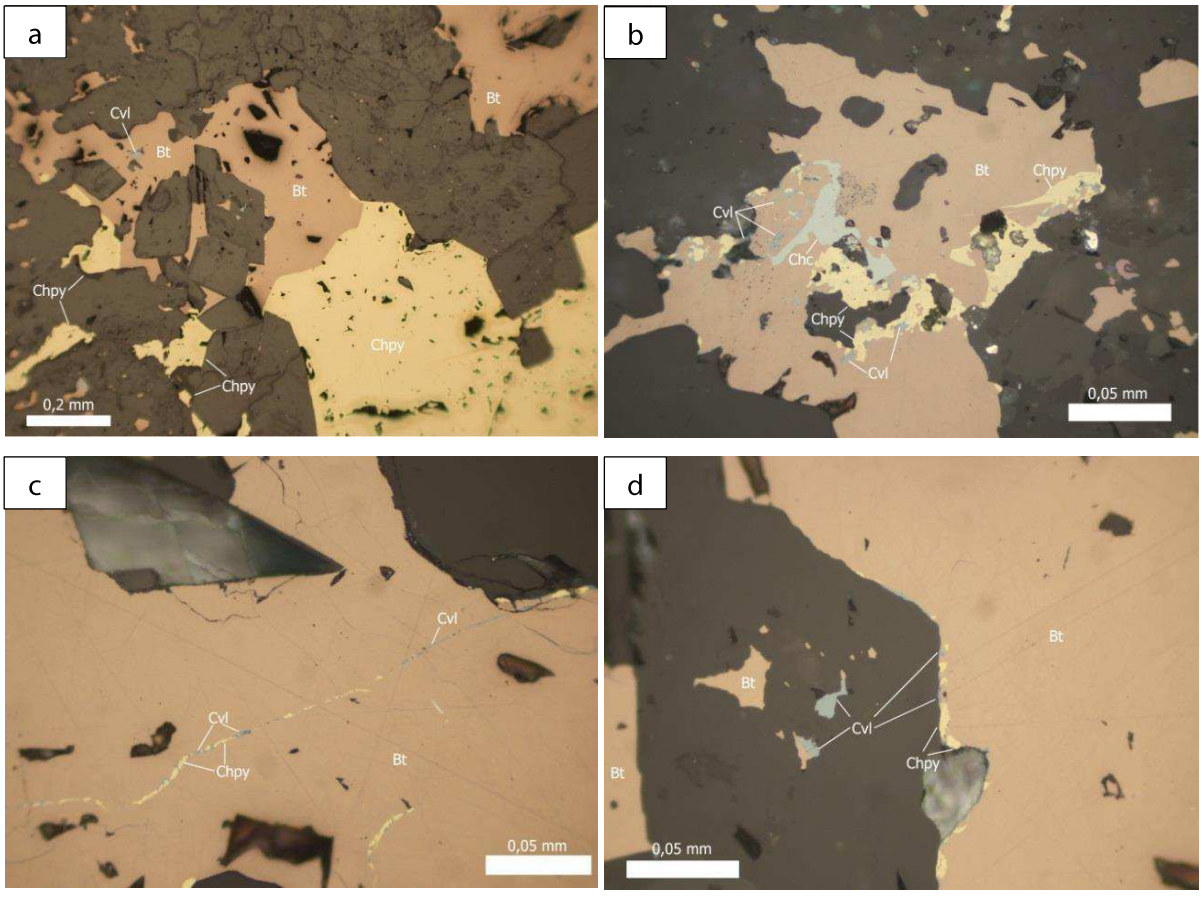

Figure 3.2.17. *Microphototgraphs. a) Microfractures in bornite filled by covellite and chalcopyrite; b) formation of covellite and chalcopyrite on the margin of bornite grain; c) Intergrowth of chalcopyrite (Chpy) with bornite (Bt), appearing of covellite (Cvl) as an inclusion in bornite; d) replacement of bornite by chalcocite, covellite and chalcopyrite.*

Chalcopyrite and bornite are also found as small grains (< 0.2 mm in diameter) dispersed in the matrix. Chalcopyrite and bornite often form intergrowths in the matrix.

Covellite, as it was mentioned before, is found filling the microfractures as well as along the margins of bornite grains (Fig. 3.2.17,c,d). In some cases covellite is also observed within chalcopyrite. In addition, grains showing inclusions of disseminated chalcopyrite are found. This may indicate replacement of chalcopyrite.

Galena forms single rounded grains up to 0.3 mm in diameter. Galena is observed in intergrowths with bornite, and as inclusions in bornite.

Chalcocite and (neo)digenite occur intergrown with chalcopyrite and bornite (Fig.3.2.18), commonly as grains of 0.2 mm – 0.4 mm in diameter. In some grains, inclusions and microveinlets of chalcopyrite are observed. However, there are also larger grains of chalcocite that occur within bornite as microveinlets.

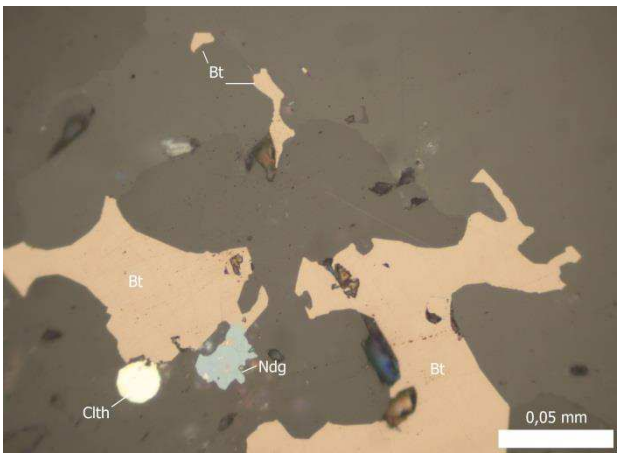

Figure 3.2.18. *Development of (neo)digenite (Ndg) in contact with bornite. One grain of clausthalite (PbSe) (?) is observed in contact with bornite.*

NS-3a (28.60-28.65m) (Fig.3.2.19,a)

The rock is a siltstone with veinlets of quartz. The siltstone has a granoblastic (coarse-grained siltstone) and pelitic (fine-grained siltstone) structure, and holocrystalline (coarse-grained siltstone), and layered (fine-grained siltstone) texture. Two types of siltstone are present: fine-grained mica-rich siltstone (mica – muscovite) and coarse-grained mica-free siltstone (Fig. 3.2.19, b,c).

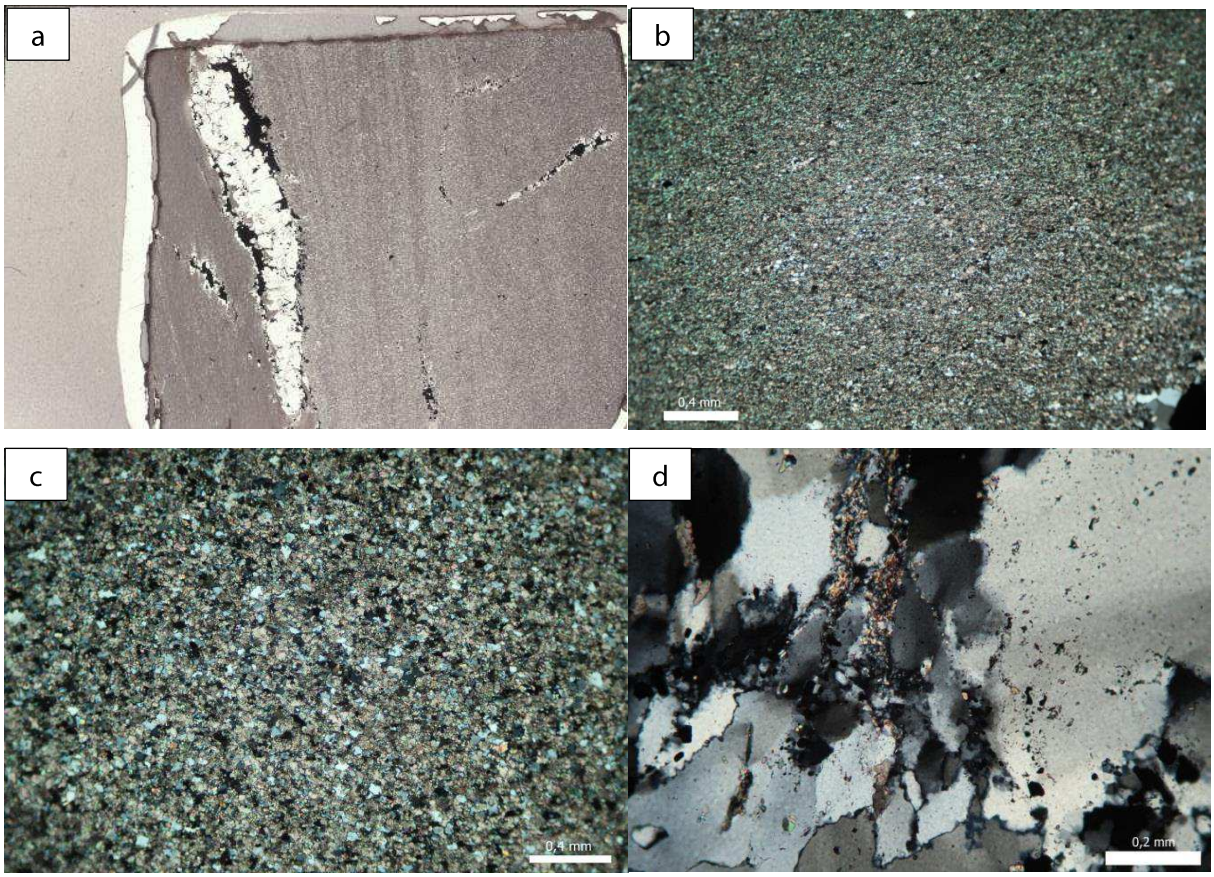

Figure 3.2.19. *a) Photograph of polished thin section NS-3a; microphotographs in XPL of: (b) mica-rich fine-grained siltstone; c) mica-free coarse-grained siltstone; d) Mixture of hydrothermal quartz and the host rock.*

The mica-rich siltstone has a layered texture. The amount of muscovite increases towards the veinlet. The rock also contains quartz as small grains (< 0.15 mm in diameter). Nest-like mica-free aggregates of quartz are observed. Carbonate is present as small tabular shaped single grains. The mica-rich siltstone is crosscut by a quartz veinlet containing copper sulfides. The coarse-grained siltstone contains evenly distributed subhedral and andedral crystals of quartz that are 0.1 mm – 0.3 mm in diameter. Plagioclase is present; the total content of plagioclase in the host rock is about 3%. The grains show prismatic shape and are up to 0.2 mm in length. Carbonate occurs as single anhedral grains with size less than 0.1 mm. Carbonate occurs in the space between quartz grains. Quartz appears as anhedral grains, up to 1 mm in diameter. The grain size of quartz shows a general increase towards the "main veinlet". Within the veinlet, elongated quartz grains (up to 2.5 mm long) show preferred orientation. Some fine-grained quartz-micaceous aggregates within the veinlet (Fig. 3.2.19,d) are inferred to represent a mixture between the hydrothermal vein and the host rock.

Copper minerals are mainly concentrated in the veinlet, but there are also some copper minerals disseminated in the host rock (Fig. 3.2.20,a). The veinlet mainly comprises chalcopyrite with subordinate amount of bornite and inclusions of chalcocite. Observed ore minerals include bornite, chalcopyrite, chalcocite, digenite, and covellite.

Chalcopyrite occurs as big anhedral grains (Fig. 3.2.20,b). Chalcopyrite is intergrown with bornite. It is likely that chalcopyrite has replaced bornite because the mineral occurs mainly along the edges of grains of bornite, and in fracture fillings in bornite. In addition, small crystals of chalcopyrite are observed in the matrix.

Locally chalcopyrite contains inclusions of digenite (Fig. 3.2.20,c). Most commonly chalcopyrite is confined to the border of quartz veins, and only minor amounts of chalcopyrite with bornite are present along quartz grains within the internal parts of the vein.

Zones of bornite being replaced by chalcopyrite, chalcocite as well as covellite are observed (Fig.3.2.20,e). Bornite is present both in the veinlet and in the host rock. The grain size of bornite in the veinlet is rather big (> 2mm in diameter) and bornite grains show intergrowth with chalcopyrite. Chalcopyrite along with covellite also occurs along microfractures in bornite. Inclusions of chalcocite are also found in bornite. Digenite is found throughout the sample as a secondary mineral. It is confined to grains of bornite or chalcopyrite (Fig. 3.2.20,b,c). The size of the grains does not exceed 0.5 mm. Digenite is observed both in the veinlet and the host rock. Chalcocite is less common than digenite, but it is also observed both in the vein and within the matrix. The shape of grains is shortly prismatic; the size is less than 0.1 mm in length. Covellite occurs mainly along microfractures in bornite, however single grains are also found (around 0.1 mm in diameter) (Fig. 3.2.20,f).

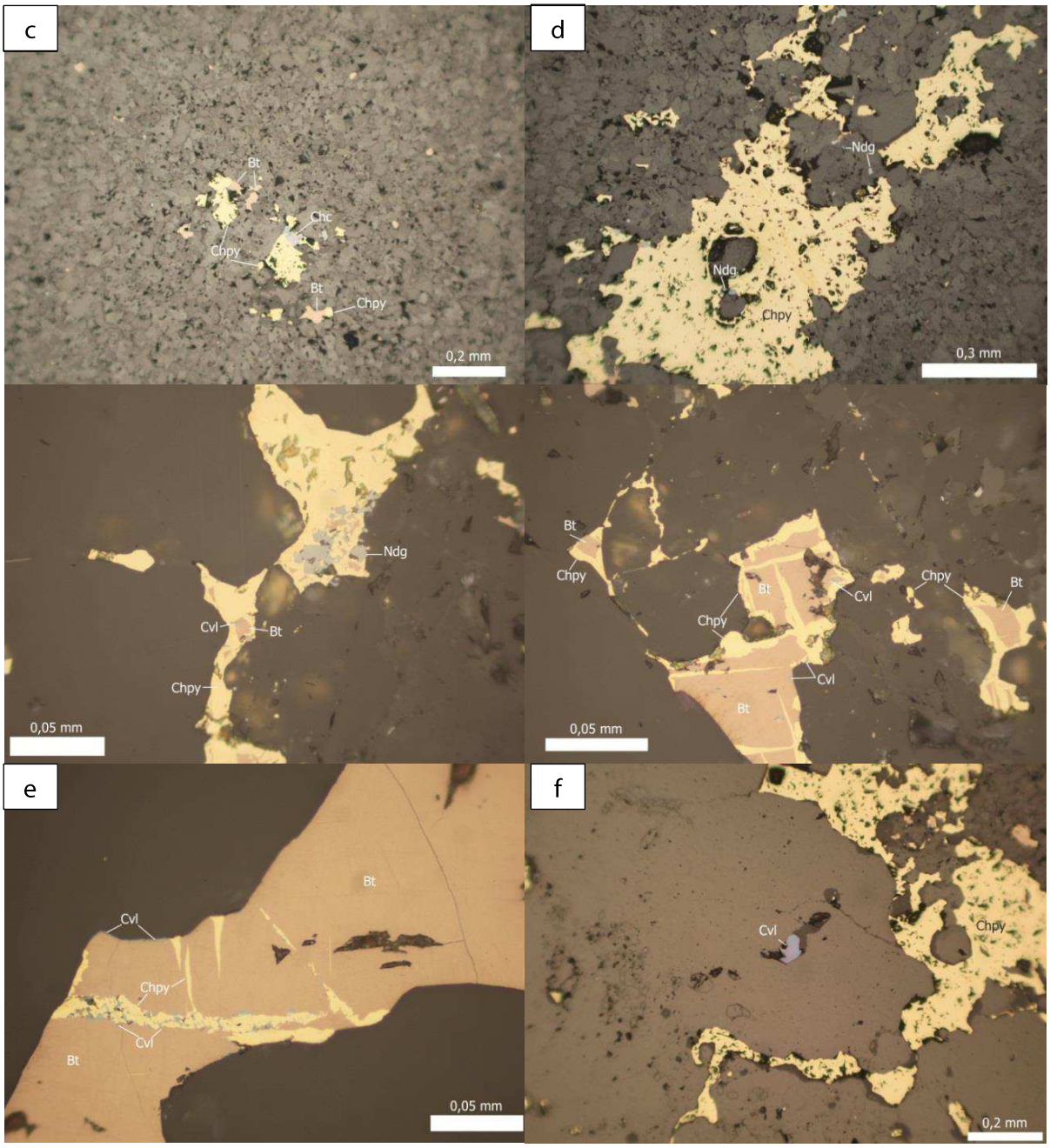

Figure 3.2.20. *Microphotographs in XPL: a) bornite, chalcopyrite and chalcocite in the coarse-grained siltstone; b) chalcopyrite with inclusions of digenite; c) inclusions of bornite in chalcopyrite, development of (neo)digenite in a grain of chalcopyrite; d) replacement of bornite by chalcopyrite and covellite; e) development of chalcopyrite and covellite along cracks in bornite; f) covellite (Cvl) grain in quartz veinlet in the association with chalcopyrite.*

NS-3b (28.60-28.65m) (Fig.3.2.21)

The rock is a coarse-grained siltstone with mica-rich layers crosscut by quartz-carbonate Cu-bearing veinlets. The siltstone has a granoblastic structure and banded texture. In bands enriched in mica (Fig. 3.2.22,a) the sizes and the shapes of grains of all minerals are different from the adjacent domains. The grains are smaller in size and show elongated shapes parallel to the orientation of the mica bands.

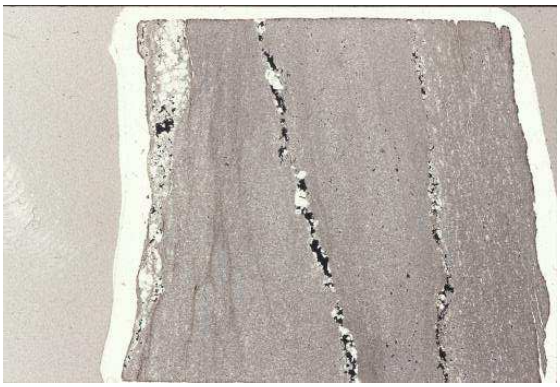

Figure 3.2.21. *Photograph of polished thin section NS-3b*

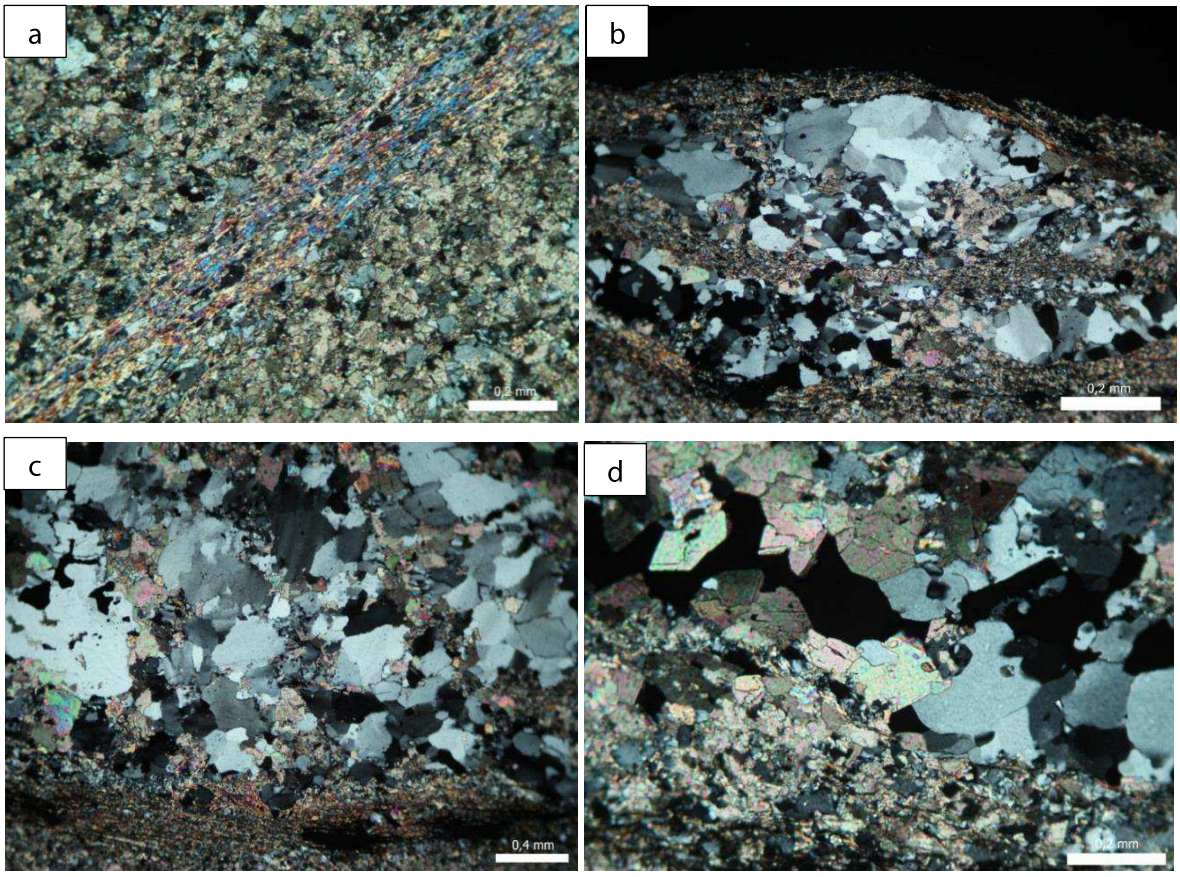

Figure 3.2.22. *Microphotographs taken in XPL: a) mica-rich layer in siltstone; b) sigmoidal shaped aggregate of quartz and carbonate grains in the host rock; c) alternating zones of quartz and carbonate; d) veinlet with quartz and carbonate with copper minerals.*

Quartz occurs as subhedral grains, 0.1 mm – 0.2 mm in diameter. Evidence of deformation are observed (foliation cleavage, sigmoidal shaped quartz aggregates) (Fig.3.2.22,b). Plagioclase occurs as single grains and shows tabular crystal shape, and the size is about 0.1 mm. Carbonate is represented by anhedral and subhedral grains of calcite and dolomite about 0.1 mm – 0.2 mm in diameter.

Quartz from the veinlets occurs as anhedral crystals varying from 0.2 to 2 mm in diameter. Carbonate forms aggregates between quartz grains. Both calcite and dolomite are observed (two varieties of crystals: regular rhomboidal crystals and anhedral fragments). Towards the host rock, the grain size of quartz and carbonate decreases to < 0.2 mm in diameter, and the minerals form recrystallized aggregates (Fig. 3.2.22,c,d). Plagioclase varies in size from 0.5 mm to 1 mm in diameter.

Ore minerals include chalcopyrite, bornite, (neo)digenite, and covellite.

Chalcopyrite is the most abundant ore mineral. Chalcopyrite is concentrated in the veinlets, however, it is also observed in the matrix. Chalcopyrite occurring in the veinlet is represented by big irregular-shaped grains, as well as along microveinlets in bornite. Furthermore, chalcopyrite occurs along the margins of bornite grains. Chalcopyrite commonly shows inclusions of chalcocite and covellite.

Bornite occurs as to 0.2 mm long grains within the host rock, as inclusions in chalcopyrite and in separate large grains in the quartz-carbonate veinlet. Bornite has also formed along fractures in chalcopyrite where it is replaced by (neo)digenite (Fig. 3.2.23, a, b, c, d, e). Sometimes inclusions of chalcopyrite are observed. The size of grains is up to 0.05 mm in diameter. The grains are commonly anhedral, but there are also rounded and tabular-shaped grains.

Bornite occurring in the veinlet always occurs in intergrowth with chalcopyrite, and occasionally it is replaced by covellite. In the veinlet, large grains (up to 0.3 mm in diameter) of elongated shape are observed.

Similar to chalcopyrite and bornite, (neo)digenite occurs both in the matrix and within veinlets. (Neo)digenite has mainly formed at the expense of bornite and chalcopyrite. The size of (neo)digenite grains occurring in the host rock is up to 0.02 mm in diameter, while those in the veinlet is up to 0.05 mm in diameter (Fig. 3.2.23, f).

Grains of covellite, less than 0.03 mm in diameter, are occasionally observed associated with bornite and chalcopyrite.

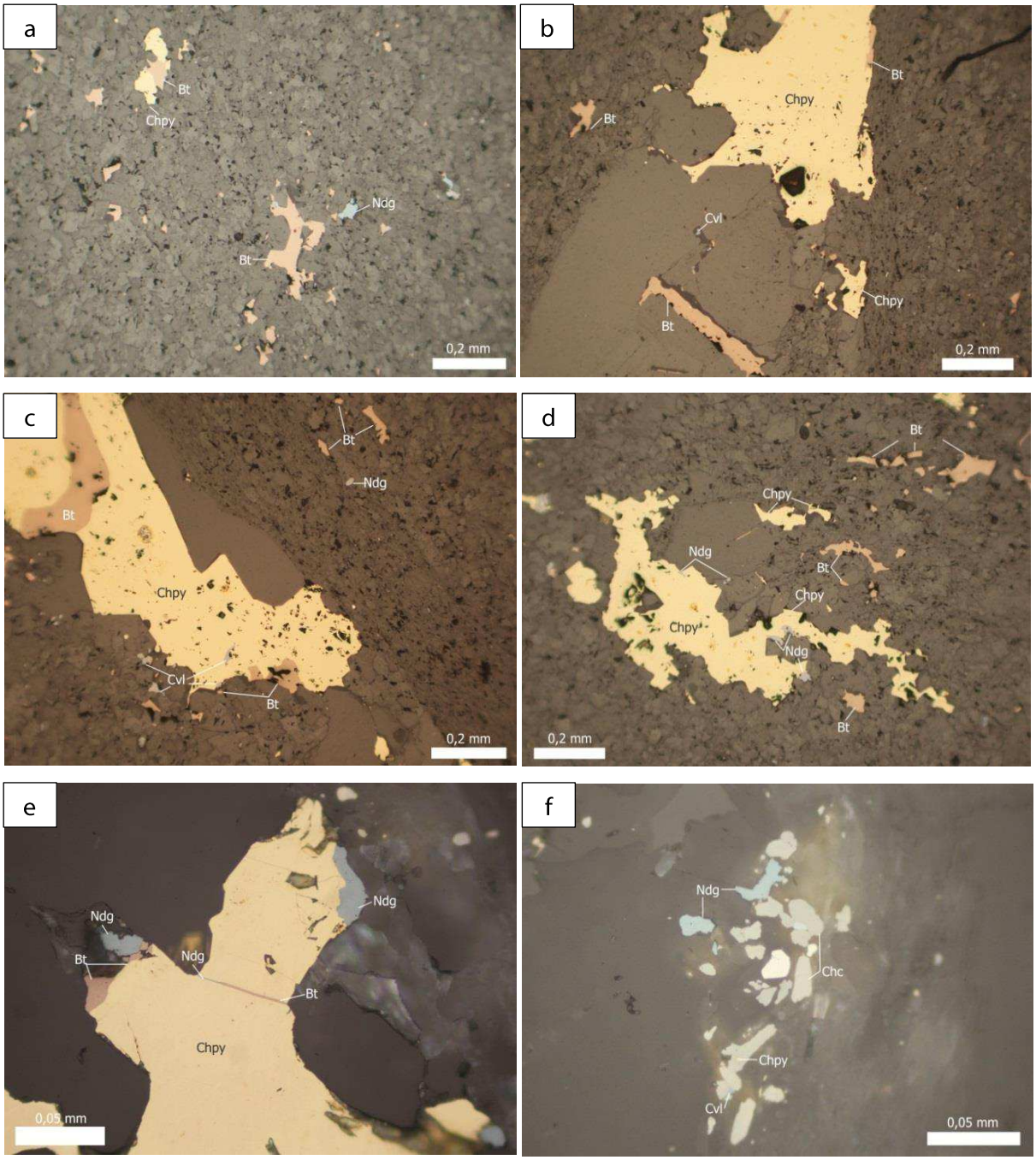

Figure 3.2.23. *Microphotographs in XPL: a) copper mineralization in the host rock (bornite – Bt, chalcopyrite – Chpy, (neo)digenite – Ndg); b) association of chalcopyrite and bornite; c) intergrowth of bornite and chalcopyrite, replacement of chalcopyrite by covellite; (neo)digenite grain in the matrix; d) chalcopyrite grains locally replaced by (neo)digenite; occurrence of bornite nearby; e) bornite occurring along a fracture and the margin of chalcopyrite together with (neo)digenite; f) association of chalcocite, (neo)digenite, and chalcopyrite.*

NS-4 (28.75-28.80m) (Fig.3.2.24,a)

The rock is a mica-rich pelite with fragments of coarse-grained siltstone crosscut by a quartz-carbonate Cu-bearing veinlet. The pelite has nematoblastic structure and banded

texture. The pelite is interlayered with layers of fine-grained quartz and plagioclase. The pelite is enriched in mica (muscovite) (Fig. 3.2.24,b). The amount of muscovite increases towards the veinlet. Carbonate is present in minor amount. Foliation cleavage is observed in pelite.

Quartz occurs as anhedral grains of 0.1 mm – 0.2 mm diameter. Quartz grains form about 0.3 mm thick layers. In the pelite, quartz crystals showing elongated shape are parallel to muscovite-rich layers. Plagioclase (0.2 mm in diameter) shows anhedral shape. Along with quartz, plagioclase is observed in the layers interbedded with the pelite. Carbonate grains (0.1 mm size) show anhedral shape.

The crosscutting veinlets are composed of carbonate, quartz, plagioclase, and copper minerals.

Two types of quartz are present: large elongated grains showing preferred orientation (0.2 mm – 1.5 mm long), and small (≤ 0.1 mm) anhedral-shaped grains representing a mixture between the host rock and the vein (Fig.3.2.24,b,c).

Similar to quartz, carbonate occurs as: 1) elongated grains up to 2 mm in diameter; 2) rhomboidal-shaped crystals, 0.5 mm in length; and 3) fine-grained aggregates showing anhedral shape and 0.05-1 mm in diameter. Polysynthetic twins are observed in carbonate.

In the veinlet, zones of monomineralic carbonate and quartz are observed (Fig. 3.2.24,d,e, f). Elongated grains indicate compressional deformation. Plagioclase occurs as rhomboidal-shaped grains, 0.3 mm in diameter.

Compared to other samples, the highest content of copper minerals is observed in sample NS-4. Observed copper minerals include bornite, chalcopyrite, (neo)digenite, covellite, and chalcocite. The ore minerals are mainly concentrated in the veinlet although large aggregates are also observed in the groundmass.

Chalcopyrite occurs as large anhedral crystals with size ≥1 mm in length. Often, chalcopyrite is intergrown with bornite (Fig. 3.2.25, a) and occurs along the margins of bornite grains and as microfracture fillings in bornite (Fig. 3.2.25, b). Zones of replacement of chalcopyrite by chalcocite, (neo)digenite, and covellite are observed.

Dispersed bornite grains occurring as aggregates of various sizes (up to 0.2 mm in diameter) are observed in the host rock. Covellite has to some extent replaced bornite. Bornite grains, having < 1.5 mm in diameter often occur intergrown with chalcopyrite.

Chalcopyrite being locally replaced by covellite occurs as fracture fillings in bornite. Inclusions of chalcocite are observed in bornite (Fig. 3.2.25, c, d).

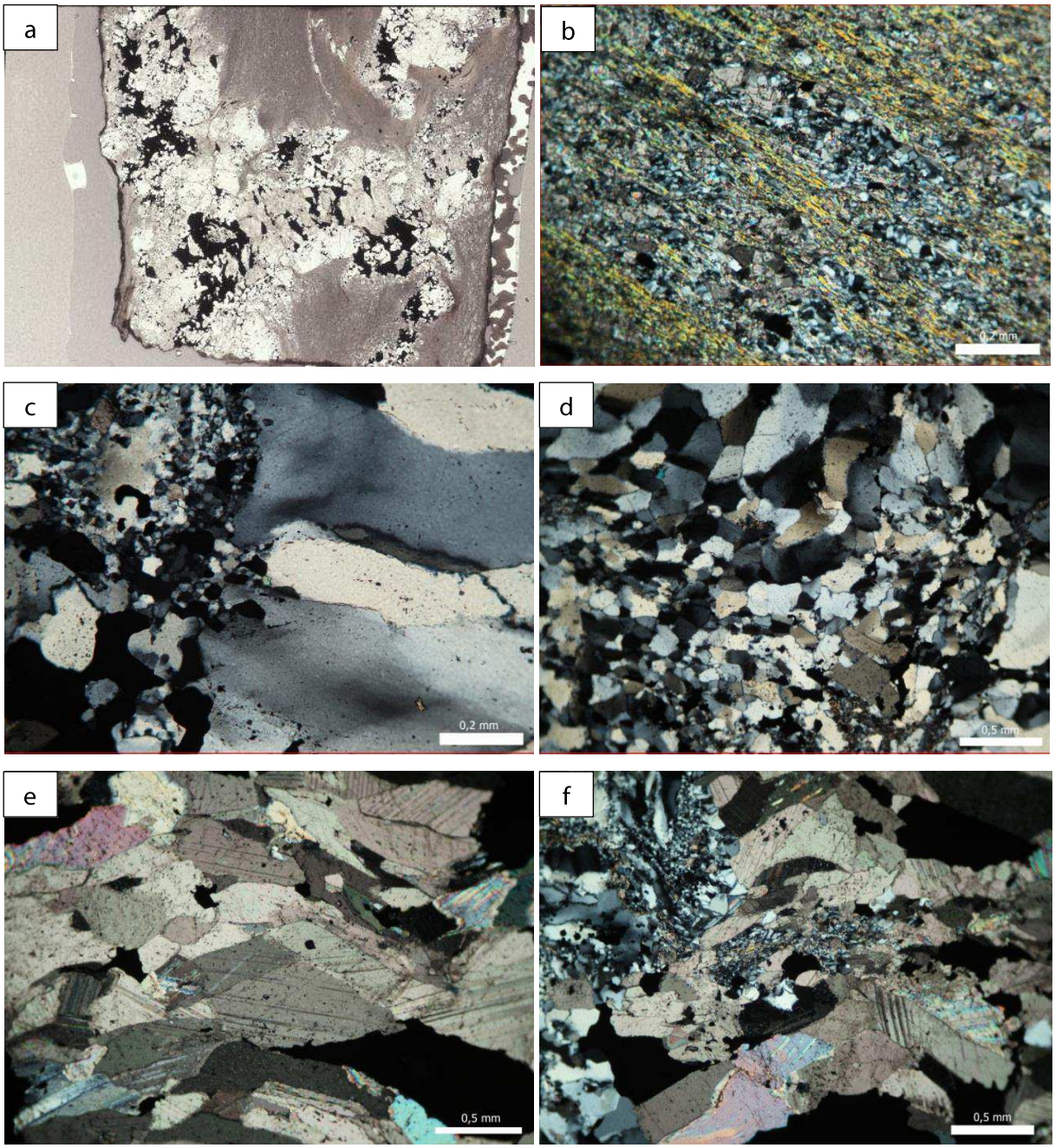

Figure 3.2.24. *a) Photograph of polished thin section; microphotographs (XPL) of: b) interbedding of quartz-carbonate layers with mica-rich layers; c) large elongated shaped quartz grains showing preferred orientation (on the right); d) undeformed quartz grains; e) monomineralic carbonate zone in vein; f) mixture of quartz and carbonate in veinlet.*

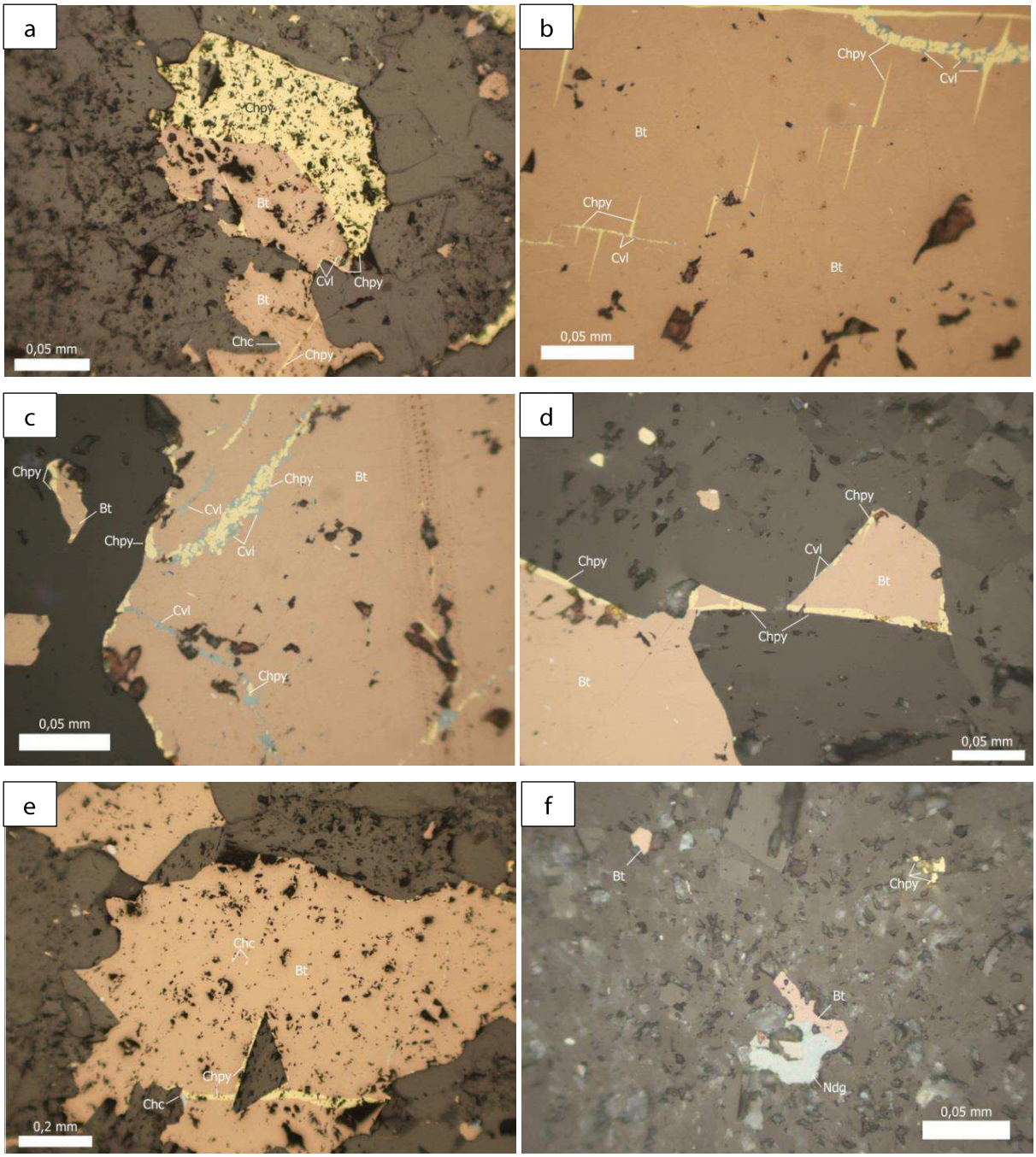

Figure 3.2.25. *a) Intergrowth of chalcopyrite with bornite. Covellite occurs in the contact zone between chalcopyrite and bornite; b), c) chalcopyrite and covellite fill microfracture in bornite; d) chalcopyrite and covellite occur along bornite grain margins; e) inclusions of chalcocite in bornite containing microfracture filled with chalcopyrite.; f) replacement of bornite by chalcopyrite.*

Chalcocite grains, being observed both in the host rock and in the veinlets occur as tabular-shaped grains with lengths of 0.02 mm and larger. Chalcocite is often intergrown with bornite and chalcopyrite (Fig. 3.2.25, e). As mentioned above, covellite mainly occurs as microfracture fillings along with chalcopyrite. Covellite has to some extent replaced

chalcopyrite. Digenite, occurring more often than chalcocite, is observed in contact with bornite (Fig. 3.2.25, f).

NS-5a (28.80-28.92m) (Fig.3.2.26,a)

The rock is a dolomite interlayered with mica-rich bands and crosscut by quartz-carbonate veinlets. The dolomite has a fine-grained structure and shows banded texture.

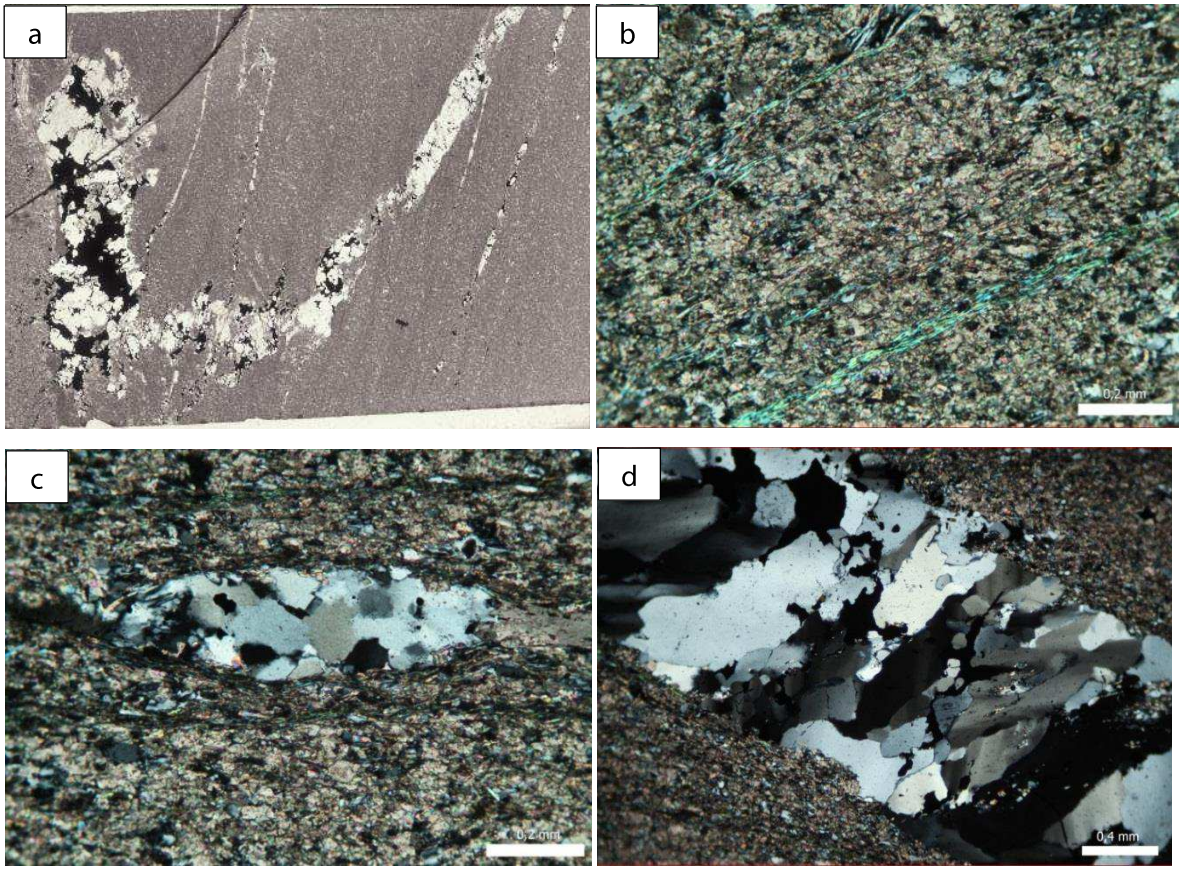

Figure 3.2.26. *a) Photograph of polished thin section NS-5a; Microphotographs taken in XPL: b) dolomite interlayered with mica bands; c) sigmoidal-shaped aggregate of quartz in dolomite; d) quartz-bearing veinlet in the host rock.*

Inclusions of plagioclase and quartz are observed within dolomite. Quartz grains (0.1 mm in diameter) show anhedral shape. Plagioclase occurs as euhedral crystals with size equal to quartz. Bands of mica are observed (Fig. 3.2.26,b). Disseminated quartz-plagioclase aggregates show sigmoidal shape in the dolomite (Fig. 3.2.26,c).

The veinlets consist of quartz, carbonate, and plagioclase. Quartz, being the dominating mineral in the veinlets (Fig. 3.2.26,d), occurs as anhedral large (up to 2.5 mm in length) grains undergone compressional deformation. In the contact zone between the veinlet and the host rock the size of grains decreases showing recrystallized aggregates. Plagioclase occurs as tabular-shaped grains, the size does not exceed 0.5 mm. Carbonate, occurring as recrystallized aggregates, is mainly observed in the contact zones between

the veinlet and the host rock. Carbonate shows rhomboidal-shaped crystals of various sizes (up to 0.3 mm in diameter). Polysynthetic twins are not observed. In the upper part of the thin section, thinning of the veinlet is observed. Here the veinlet shows monomineralic quartz zones. Carbonate occurs locally.

The ore minerals are represented by bornite, chalcopyrite, (neo)digenite, chalcocite, and covellite.

Bornite is the dominating mineral often occurring in intergrowth with chalcocite. Chalcopyrite and covellite occur as fillings in microfractures in bornite grains and along the margins of bornite. The ore minerals in the rock are more abundant than in the samples described above (Fig. 3.2.27, a). Here the aggregates are less abundant, while dispersed fine-grained ore minerals occur. Chalcopyrite, which occurs as aggregates (0.2 mm in diameter) in the host rock is also observed as inclusions in bornite and along the margins of bornite grains. Chalcopyrite is locally replaced by covellite (Fig. 3.2.27, b, c). Covellite occurs in contact with chalcopyrite as a secondary mineral replacing chalcopyrite. The chalcocite of sample NS-5a shows distinct twinning; this feature was not observed in the samples described above. Chalcopyrite occurs as inclusions in chalcocite as well as plates parallel to the twins' margins (Fig. 3.2.27, d).

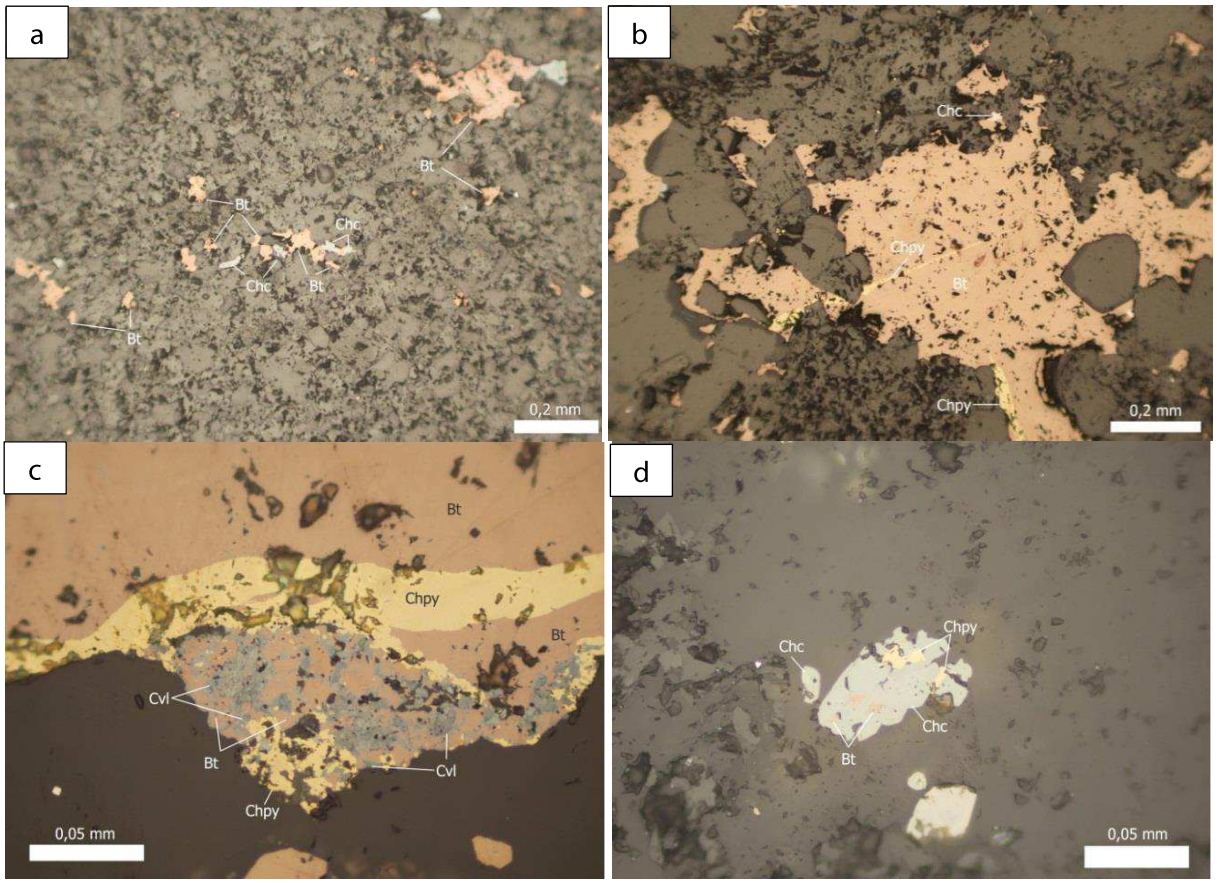

Figure 3.2.27. *a) Grains of chalcocite and bornite in the matrix; b) Chalcopyrite occurring as filling of microfractures in bornite and along the margins of bornite grains; c) decay of bornite-chalcopyrite intergrowth with formation of covellite; d) chalcocite with inclusions of bornite and chalcopyrite. NS-5a.*

NS-5b (28.80-28.92m) (Fig.3.2.28,a)

The rock is represented by pelite and siltstone with quartz-carbonate Cu-bearing veinlets crosscutting them. The structure of the country rock is nematoblastic, and it shows banded texture.

The mica-rich pelite contains inclusions of quartz and carbonate. The amount and size of the carbonate grains increase towards the quartz-carbonate veinlet (Fig. 3.2.28, b). Carbonate occurs as rhomboidal-shaped crystals (≤0.2 mm in diameter), which are oriented parallel to the micaceous layers. Mica-free siltstone (Fig. 3.2.28,c) is crosscut by quartz veinlet containing some carbonate inclusions (Fig. 3.2.28,e,f). Zones of silicification of the siltstone are observed (Fig.3.2.28,d).

The veinlets consist mainly of quartz with inferior amount of carbonate. Carbonate occurs as rhomboidal-shaped grains of 0.5 mm in diameter in the contact zones between the veinlets and the host rock (Fig. 3.2.28,e,f). Quartz grains of 0.1 mm – 1 mm size often form fine-grained aggregates.

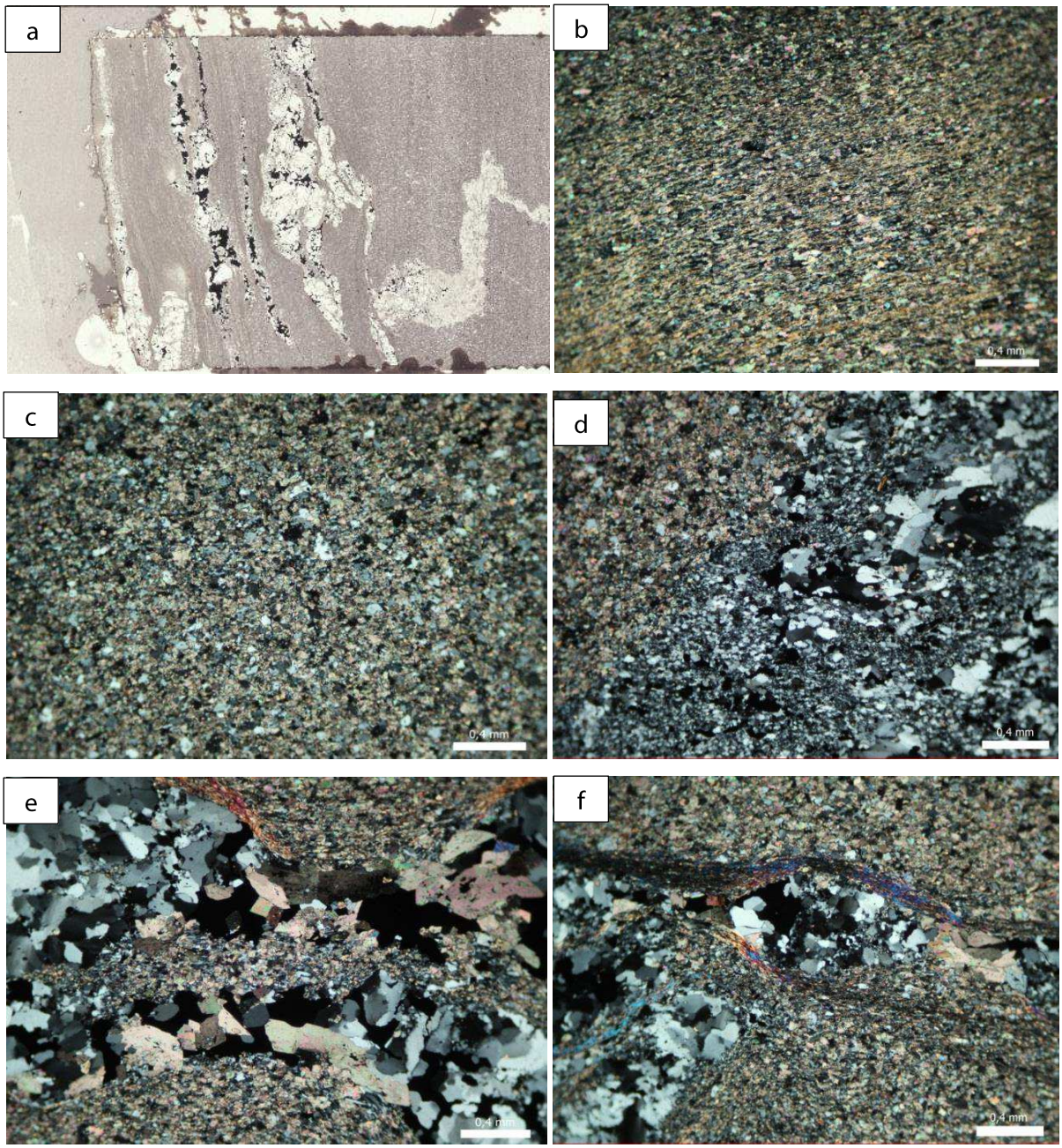

Figure 3.2.28. *Photograph of NS-5b; microphotographs of host rock and crosscutting veins: b) mica-rich pelite; c) mica-free siltstone; d) silicification of siltstone in the contact zone with quartz veinlet; e) contact zone between the quartz-carbonate veinlet and the siltstone; f) mica layers occurring adjacent to the veinlet.*

Ore minerals occurring in the host rock as well as in the veinlets include bornite, chalcopyrite, chalcocite, digenite, galena, and sphalerite. Aggregates of <0.03 mm in diameter composed of chalcopyrite, bornite, and chalcocite are observed in the siltstone and the pelite. Bornite and digenite grains having preferred orientation are observed parallel to mica-rich layers in the pelite. Digenite and chalcocite form aggregates within

the host rock. Digenite and chalcocite have to some extent replaced chalcopyrite because relict disseminated inclusions of chalcopyrite are observed within these minerals (Fig.3.2.29). Bornite and chalcopyrite forming intergrowths are concentrated in the veinlets. Galena occurring together with bornite and covellite shows round-shaped crystals, 0.03 mm in diameter. In addition, sphalerite is also observed (Fig. 3.2.30).

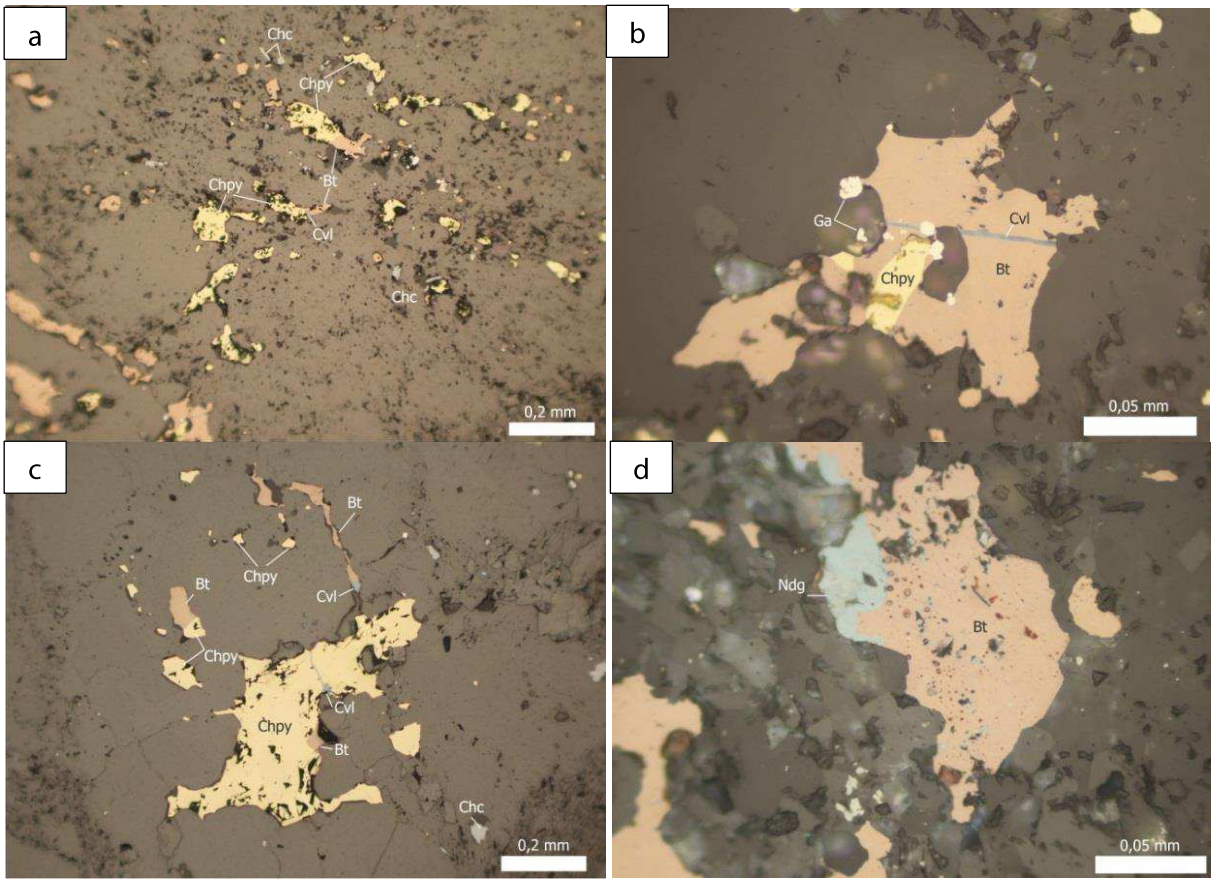

Figure 3.2.29. *Microphotographs taken in reflected light and XPL: a) grains of chalcopyrite, bornite, covellite, and chalcocite disseminated in the pelite; b) chalcopyrite is intergrown with bornite showing microfractures filled by covellite. The grain of galena is in contact with bornite; c) association of bornite and chalcopyrite showing covellite as a microfracture filling; d) (neo)digenite replacing bornite.*

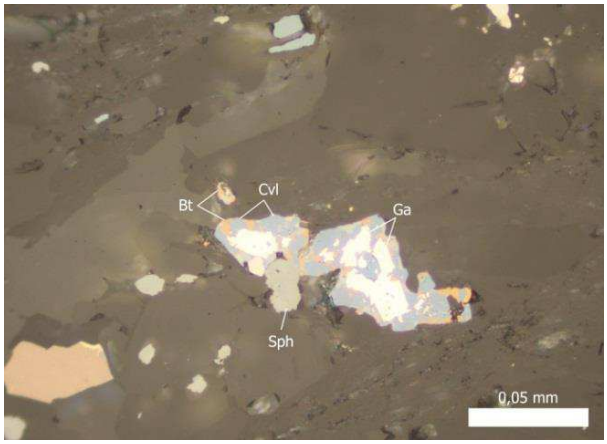

Figure 3.2.30. *Association of galena, bornite, covellite, and sphalerite.*

Appendix 2. To chapter 5.2.

Table 5.2.1. Chemical analysis of chalcopyrite (Ccp) (weight %).

Sample	Lab	Mineral	Fe	As	S	Cu	Zn	Ag	Au	Ni	O	Total
NS-26	UiO	Ccp	26,14	0,02	26,10	44,89	0,02	0,11	0	0	0,01	97,29
NS-4	UiO	Ccp	30,55	0	35,44	33,09	0,11	0	0	0	0	99,15
NS-4	UiO	Ccp	30,41	0,08	35,79	33,31	0	0	0	0	0	99,57
NS-4	UiO	Ccp	29,75	0,01	35,09	34,12	0,02	0,02	0	0	0	98,94
NS-2b	UiO	Ccp	29,93	0,01	33,96	33,26	0,06	0,00	0	0	0	97,16
NS-12	UiO	Ccp	29,77	0	35,41	33,94	0	0,02	0	0	0,01	99,05
NS-12	UiO	Ccp	30,02	0	35,25	34,14	0,08	0,04	0,01	0	0,03	99,47
NS-12	UiO	Ccp	30,32	0,06	35,53	33,95	0,07	0,06	0,06	0	0	100,00
NS-12	UiO	Ccp	30,29	0,00	35,12	33,89	0,10	0	0	0	0	99,24
NS-12	UiO	Ccp	30,83	0,05	36,10	33,69	0,11	0	0,11	0	0,04	100,84
NS-12	UiO	Ccp	30,66	0,04	36,07	33,95	0,12	0,00	0,04	0	0,03	100,89
NS-12	UiO	Ccp	30,94	0,00	35,95	33,95	0,05	0	0,09	0	0,00	100,92
NS-9	UiO	Ccp	30,41	0,07	35,61	34,03	0,07	0,04	0	0	0	100,22
NS-9	UiO	Ccp	29,76	0	34,83	33,75	0,10	0,01	0	0	0,01	98,28
NS-9	UiO	Ccp	30,53	0,04	35,33	33,63	0,12	0,05	0,09	0	0,02	99,74
NS-26	UiO	Ccp	29,52	0	34,59	33,78	0,11	0,06	0,02	0	0,03	97,99
NS-14	UiO	Ccp	29,46	0,05	35,31	34,25	0,01	0,12	0,01	0	0	99,20
NS-14	UiO	Ccp	29,07	0	35,14	34,05	0,06	0,11	0,01	0,01	0	98,45
NS-14	UiO	Ccp	29,68	0,03	35,43	33,29	0	0,05	0,10	0	0	98,53
NS-6	UiO	Ccp	29,79	0,01	34,90	34,24	0,10	0,00	0,01	0	0	99,04
NS-6	UiO	Ccp	29,22	0	35,02	33,39	0,07	0	0,01	0	0	97,66
NS-6	UiO	Ccp	29,86	0	34,89	34,26	0,07	0,04	0,09	0	0	99,18
NS-10	UiO	Ccp	29,91	0,01	34,58	33,75	0,08	0,06	0	0	0	98,33

NS-10	UiO	Ccp	29,83	0,00	34,66	34,10	0,08	0,00	0,01	0	0	98,67
NS-10	UiO	Ccp	30,42	0	35,00	34,30	0,06	0	0	0	0	99,69
NS-10	UiO	Ccp	30,53	0,01	35,21	33,67	0,05	0,04	0,01	0	0	99,51
NS-2b	UiO	Ccp	30,10	0,01	34,10	33,74	0,04	0	0	0	0	97,97
NS-1a	UiO	Ccp	30,02	0,03	34,09	33,55	0,10	0	0	0	0	97,76
NS-5b	UiO	Ccp	29,64	0	34,13	34,03	0	0	0,13	0	0	97,89
NS-26	UiO	Ccp	28,51	0	33,48	35,61	0,08	0,31	0	0	0,03	97,97
NS-26	UiO	Ccp	29,17	0,03	34,43	34,49	0,06	0,25	0,00	0	0,06	98,43
NS-26	UiO	Ccp	29,39	0,02	34,91	34,13	0,13	0,03	0,08	0	0	98,65

Table 5.2.2. Chemical analysis of bornite (Bn) (weight %).

Sample	Lab	Mineral	Fe	As	S	Cu	Zn	Ag	Au	Co	Ni	O	Total
NS-4	UiO	Bn	10,81	0	25,57	58,96	0,09	0	0	0	0	0	95,43
NS-4	UiO	Bn	10,69	0,02	24,97	58,74	0,08	3,70	0	0	0	0	98,11
NS-4	UiO	Bn	11,05	0	26,40	61,36	0,18	0,08	0	0	0	0	99,05
NS-4	UiO	Bn	11,35	0,02	25,90	61,68	0,12	0,31	0,05	0	0	0	99,44
NS-5b	UiO	Bn	10,98	0	25,06	62,09	0,24	0,42	0	0	0	0	98,72
NS-26	UiO	Bn	11,12	0	25,55	62,59	0,14	0,19	0	0	0	0	99,55
NS-16	UiO	Bn	11,20	0,02	26,12	63,72	0,03	0,11	0,03	0	0,00	0	101,21
NS-16	UiO	Bn	11,14	0,01	25,95	63,09	0,07	0,10	0	0,01	0,02	0	100,32
NS-16	UiO	Bn	10,88	0,01	25,68	63,13	0,08	0,10	0	0	0	0	99,85
NS-16	UiO	Bn	11,10	0	25,57	63,37	0,17	0,21	0,07	0	0,02	0	100,52
NS-16	UiO	Bn	10,98	0	25,81	63,13	0,11	0,08	0	0	0	0	100,06
NS-16	UiO	Bn	10,88	0,08	25,12	63,67	0,18	0,13	0,03	0,01	0,02	0	100,13
NS-18	UiO	Bn	10,80	0	25,46	63,22	0,05	0,07	0	0	0	0	99,49
NS-26	UiO	Bn	10,96	0	25,28	62,08	0,08	0,25	0	0	0	0	98,59
NS-26	UiO	Bn	11,13	0,01	25,68	61,83	0,10	0,26	0	0	0	0	98,93
NS-1a	UiO	Bn	11,51	0	25,27	61,36	0,04	0,15	0,01	0	0	0	98,31
NS-26	UiO	Bn	10,78	0	25,21	62,87	0,17	0,22	0	0	0,06	0,06	99,28

NS-26	UiO	Bn	11,01	0,04	25,34	62,80	0	0,50	0,04	0	0	0,03	99,75
NS-1a	IGG	Bn	11,27	0	25,82	63,03	0	0,37	0	0	0	0	100,49

Table 5.2.3. Chemical analysis of digenite (Dg) (weight %).

Sample	Lab	Mineral	Fe	As	S	Cu	Zn	Ag	Au	Co	Ni	Total
NS-5b	UiO	Dg	0	0	22,51	74,99	0,08	0,06	0,01	0	0	97,60
NS-5b	UiO	Dg	0	0,04	22,56	74,50	0,13	0,02	0	0	0	97,20
NS-5b	UiO	Dg	0,03	0	21,60	74,79	0,16	0,81	0	0	0	97,29
NS-16	UiO	Dg	0,06	0	21,50	78,92	0,07	0,04	0,07	0,02	0,01	100,65
NS-16	UiO	Dg	0,04	0	21,54	78,38	0,15	0,06	0	0	0	100,06
NS-16	UiO	Dg	0,12	0	20,90	79,21	0,11	0,17	0	0	0	100,38
NS-16	UiO	Dg	0,18	0	22,46	76,17	0,04	0,14	0	0,02	0,01	98,93
NS-16	UiO	Dg	0,01	0,06	20,83	80,48	0,12	0,21	0,04	0	0,01	101,74
NS-5b	UiO	Dg	0,20	0	22,09	73,30	0,00	1,54	0	0	0	97,09
NS-26	UiO	Dg	0,73	0	22,81	74,09	0,07	0,60	0	0	0	98,19

Table 5.2.4. Chemical composition of chalcocite (Cct) (weight %).

Sample	Lab	Mineral	Fe	As	S	Cu	Zn	Ag	Au	Co	Ni	Total
NS-14	UiO	Cct	0,83	0,02	23,11	75,24	0,06	0,38	0	0,04	0	99,57
NS-16	UiO	Cct	0,00	0	21,11	80,02	0,07	0,15	0	0,01	0	101,15
NS-16	UiO	Cct	0,00	0	21,05	79,84	0,01	0,07	0	0,01	0,03	100,95
NS-26	UiO	Cct	0,35	0	21,90	76,33	0,21	0,52	0,09	0	0	99,38

Table 5.2.5. Chemical composition of covellite (Cv) (weight %).

Sample	Lab	Mineral	Fe	As	S	Cu	Zn	Ag	Co	Total
NS-14	UiO	Cv	11,50	0,06	25,98	62,53	0,07	0,29	0	100,36
NS-14	UiO	Cv	11,30	0	26,07	62,46	0,05	0,09	0,04	99,91
NS-14	UiO	Cv	0,68	0	29,54	67,23	0,08	0,28	0	97,68
NS-16	UiO	Cv	10,72	0,02	25,99	61,77	0,05	0,06	0	98,50
NS-26	UiO	Cv	4,86	0,01	20,73	70,53	0,15	1,00	0	97,10
NS-26	UiO	Cv	11,36	0,05	25,45	62,37	0,11	0,14	0	99,44

Table 5.2.6. Chemical composition of pyrite (Py) (weight %)

Sample	Lab	Mineral	Fe	As	S	Cu	Zn	Ag	Au	Co	Ni	O	Total
NS-24	UiO	Py	46,49	0,12	53,36	0	0,07	0,01	0,06	0	0	0	100,02
NS-25	UiO	Py	46,27	0,07	52,79	0	0	0	0	0	0	0,04	98,91
NS-10	UiO	Py	46,43	0,03	52,09	0	0,06	0	0,08	0,14	0,02	0	98,82
NS-10	UiO	Py	46,84	0,03	52,70	0	0	0,04	0,01	0	0	0	99,45
NS-10	UiO	Py	46,53	0,14	52,11	0	0,04	0,02	0	0	0	0	98,80
NS-10	UiO	Py	45,82	0,08	52,91	0	0	0	0,01	0,50	0	0	99,10
NS-11	UiO	Py	41,20	0,10	41,94	0	0,01	0	0,06	0,69	0,02	0	83,96
NS-11	UiO	Py	44,70	0,07	50,63	0	0,02	0	0,01	0,73	0,66	0	96,80
NS-11	UiO	Py	45,20	0,13	51,35	0	0	0	0,03	0,17	0,08	0	96,87
NS-11	UiO	Py	43,60	0,10	48,85	0,08	0,02	0,03	0,16	0,41	0,03	0	93,28

Table 5.2.7. Chemical composition of galena (Gn) (weight %)

Sample	Lab	Mineral	Fe	As	S	Pb	Cu	Zn	Ag	Au	Total
NS-4	UiO	Gn	0,25	0,01	13,29	86,55	0,04	0	0,02	0,01	100,10
NS-5b	UiO	Gn	0	0,00	12,90	86,17	0	0	0	0	98,88
NS-5b	UiO	Gn	0	0,01	13,19	85,88	0,02	0	0,02	0,04	99,13
NS-1a	UiO	Gn	0,19	0	12,92	86,61	0,13	0,04	0,02	0	99,87
NS-1a	UiO	Gn	0,86	0	13,48	84,81	2,60	0	0,13	0	101,79

Table 5.2.8. Chemical composition of silver minerals (weight %)

Sample	Lab	Mineral	Fe	As	S	Pb	Cu	Ag	Cl	Total
NS-4	UiO	native Ag	0,11	0,03	0,02	0	0,283	99,30	0	99,72
NS-1a	IGG	native Ag	0	0	0,17	0	0,55	97,73	0	98,45
NS-1a	IGG	argentite	0	0	12,36	0	0,31	87,33	0	100
NS-1a	IGG	argentite	0	0	12,98	0	0	87,02	0	100
NS-1a	IGG	*cerargyrite		0	0,81	0	0,28	76,37	8,97	86,42

NS-1a	IGG	stromeyerite	0,41	0	15,12	0	29,33	55,14	0	100
NS-1a	IGG	Stromeyerite		0	15,35	0	33,39	51,26	0	100
NS-1a	IGG	?	0	0	19,72	0	64,01	16,27	0	100
NS-1a	IGG	?	0,06	0	19,88	0	65,72	14,34	0	100
NS-1a	IGG	?	0,29	0	12,47	71,17	6,5	9,57	0	100
NS-1a	IGG	?	0,25	0	12,42	74,11	5,76	7,45	0	100
NS-1a	IGG	?	0,45	0	12,39	71,55	6,68	8,93	0	100

*-Cl is hardly distinguished

Table 5.2.9. Chemical composition of gersdorffite (Gf) (weight %)

Sample	Lab	Mineral	Fe	As	S	Cu	Co	Ni	Total
NS-1a	IGG	Gf	1,55	46,49	18,03	1,49	0,64	31,69	100

Table 5.2.10. Chemical composition of molybdenite (Mol) (weight %)

Sample	Lab	Mineral	S	Mo	Total
NS-1a	IGG	Mol	41,04	58,96	100

Table 5.2.11. Chemical composition of unknown phases (weight %)

Sample	Lab	Mineral	Fe	As	S	Pb	Cu	Zn	Ag	Au	Total
NS-18	UiO	PbSO	0,03	0	1,07	68,56		0,03	0,73	0,07	70,26
NS-2b	UiO	?	1,94	19,66	27,28	0	42,15	6,58	0,16	0	97,70
NS-5b	UiO	?	2,07	34,10	19,58	0	0	0	0	0	55,74
NS-5b	UiO	?	3,09	35,97	19,72	0	0	0	0,02	0,01	58,75

Table 5.2.12. Chemical composition of iron oxides, hydrooxides ** (weight %)

Sample	Lab	Mineral	Fe	As	S	Pb	Cu	Zn	Ag	Au	Ni	O	Total
NS-24	UiO	FeOH	58,66	0,02	0	0	0	0	0	0,09	0,02	19,05	77,58
NS-25	UiO	FeOH	57,40	0,05	0	0,06	0	0,03	0	0,05	0	18,75	76,00
NS-25	UiO	FeOH	59,40	0,07	0	0,02	0	0,02	0,06	0	0	19,22	78,50
NS-14	UiO	FeO	57,25	0,06	0,01	0,07	0	0,01	0,01	0,02	0		57,15
NS-14	UiO	FeO	57,71	0,05	0,00	0	0	0	0	0	0		57,49
NS-14	UiO	FeO	58,41	0,03	0,01	0	0	0,03	0	0,08	0		58,41

NS-14	UiO	FeO	58,39	0,11	0	0	0	0,01	0,03	0,05	0		58,30
NS-14	UiO	FeO	24,05	0	0,01	0,01	0	0,07	0,06	0,01	0		23,31
NS-14	UiO	FeO	45,52	0,01	0	0,01	0,02	1,69	0	0,07	0,02		47,28
NS-14	UiO	FeO	41,95	0	0,00	0,07	0	0,06	0,01	0	0		41,70
NS-14	UiO	FeO	54,77	0,01	0	0,05	0	0,05	0	0	0		54,76
NS-14	UiO	FeO	49,28	0,08	0,01	0,05	0	0,06	0	0	0,04		49,32
NS-20	UiO	FeO	59,56	0,06	0	0	0	0	0,02	0,04	0		59,44
NS-20	UiO	FeO	58,30	0,08	0	0,01	0	0,01	0,04	0,12	0,03		58,29
NS-6	UiO	FeO	63,43	0,06	0	0	0	0	0	0	0,03		63,22
NS-11	UiO	FeO	10,10	0,00	0	0,02	0	0,05	0	0	0,03		10,11

** In the table content of O and H is not given.

Note:

1. Minerals abbreviations are according to Whitney and Evans (2010);
2. UiO – University of Oslo; IGG – Institute on Geology and Geophysics of the Republic of Uzbekistan.
3. ? – unknown mineral.